Living Rev Comput Astrophys (2023) 9:3
https://doi.org/10.1007/s41115-023-00018-w

REVIEW ARTICLE

Computational methods for collisional stellar systems

Rainer Spurzem[1,2,3] · Albrecht Kamlah[1,4]

Received: 30 June 2022 / Accepted: 5 July 2023 / Published online: 6 September 2023

Abstract

Dense star clusters are spectacular self-gravitating stellar systems in our Galaxy and across the Universe—in many respects. They populate disks and spheroids of galaxies as well as almost every galactic center. In massive elliptical galaxies nuclear clusters harbor supermassive black holes, which might influence the evolution of their host galaxies as a whole. The evolution of dense star clusters is not only governed by the aging of their stellar populations and simple Newtonian dynamics. For increasing particle number, unique gravitational effects of collisional many-body systems begin to dominate the early cluster evolution. As a result, stellar densities become so high that stars can interact and collide, stellar evolution and binary stars change the dynamical evolution, black holes can accumulate in their centers and merge with relativistic effects becoming important. Recent high-resolution imaging has revealed even more complex structural properties with respect to stellar populations, binary fractions and compact objects as well as—the still controversial—existence of intermediate mass black holes in clusters of intermediate mass. Dense star clusters therefore are the ideal laboratory for the concomitant study of stellar evolution and Newtonian as well as relativistic dynamics. Not only the formation and disruption of dense star clusters has to be considered but also their galactic environments in terms of initial conditions as well as their impact on galactic evolution. This review deals with the specific computational challenges for modelling dense, gravothermal star clusters.

Keywords Numerical methods · Star clusters · Stellar evolution · Direct N-body simulation

✉ Rainer Spurzem
spurzem@ari.uni-heidelberg.de; spurzem@nao.cas.cn

[1] Astronomisches Rechen-Institut, Zentrum für Astronomie, Mönchhofstr. 12-14, 69120 Heidelberg, Germany

[2] National Astronomical Observatories and Key Laboratory of Computational Astrophysics, Chinese Academy of Sciences, 20A Datun Rd., Chaoyang District 100101 Beijing, China

[3] Kavli Institute for Astronomy and Astrophysics, Peking University, Yiheyuan Lu 5, Haidian Qu, Beijing 100871, China

[4] Max-Planck-Institut für Astronomie, Königstuhl 17, 69117 Heidelberg, Germany

Abbreviations

AC	Ahmad–Cohen neighbour scheme
AGB	Asymptotic giant branch (stellar astrophysics)
AIC	Accretion induced collapse
AMUSE	Astrophysical Multipurpose Software Environment
AR	Algorithmic regularization
ASPS	Advanced stellar population synthesis
AVX	Advanced vector extension
BBGKY	Bogoliubov–Born–Green–Kirkwood–Yvon
BEANS	Software package for big data analysis
BH	Black Hole
BiFROST	Binaries in FROST code
BPS	Binary population synthesis
BSE	Binary Stellar Evolution
CEE	Common envelope (CE) evolution
CMC	Cluster Monte Carlo code
CMD	Colour-magnitude diagram
CMS	Cool luminous stars (stellar astrophysics)
CNO	Carbon nitrogen oxygen burning cycle (stellar astrophysics)
COCOA	Cluster simulation comparison with observations
COWD	Carbon oxygen white dwarf
CPU	Central processing unit
CUDA	Compute unified device architecture
CV	Cataclysmic variable
ECSN	Electron capture (EC) supernova
ELT	Extremely Large Telescope
FITS	Flexible lmage transport system
FP	Fokker–Planck
FROST	Fourth order forward symplectic integrator
FSI	Forward symplectic integrator
FSPS	Flexible stellar population synthesis
GALEV	Galaxy evolutionary synthesis
GC	Globular star cluster
GPU	Graphical processing unit
GR	General relativity, relativistic
GRAPE	Gravity pipeline
HARP	Hermite accelerator pipeline
HB	Horizontal branch (stellar astrophysics)
HDF5	Hierarchical data format V.5
HeWD	Helium white dwarf
HMS	High-mass atars
HOSHI	HOngo Stellar Hydrodynamics Investigator
HRD	Hertzsprung–Russell diagram
HST	Hubble Space Telescope

IBP	Initial binary population
IFMR	Initial final mass relation
IFU	Integral field unit
IMBH	Intermediate-mass black hole
IMF	Initial mass function
IMS	Intermediate-mass stars
JWST	James Webb Space Telescope
KAGRA	Kamioka gravitational wave detector
KH	Kelvin–Helmholtz (stellar astrophysics)
KS	Kustaanheimo–Stiefel regularization
LIGO	Laser Interferometer Gravitational-wave Observatory
LISA	Laser Interferometer Space Antenna
LMS	Low-mass stars
M87	Galaxy Messier catalogue nr. 87
MESA	Modules for Experiments in Stellar Astrophysics
MIC	Merger induced collapse
MLT	Mixing length theory
MOBSE	Massive Objects in Binary Stellar Evolution
MOCCA	Monte Carlo code
MPI	Message passing interface
MS	Main sequence (stellar astrophysics)
MSP	Multiple stellar populations
MSTAR	Minimum spanning tree algorithmic regularization
NGC	New General Catalogue of Nebulae and Clusters of Stars
NS	Neutron star
NSC	Nuclear star cluster
NVlink	NVIDIA high speed GPU interconnect
ONeWD	Oxygen neon white dwarf
P3T	Particle–particle particle-tree
PISN	Pair-instability supernova
PN	Post-Newtonian
pp	Proton proton burning cycle (stellar astrophysics)
PPISN	Pulsational pair-instability supernova
RG	Red giant (stellar astrophysics)
RLOF	Roche-lobe overflow
RSG	Red supergiants (stellar astrophysics)
SDAR	Slow down algorithmic regularization
SEVN	Stellar Evolution for N-body
SIMD	Single instruction multiple data
SISCO	Simulating IFU star cluster observations
SMBH	Supermassive black hole
SN	Supernova
SPMD	Single program multiple data
SSE	Single Stellar Evolution
SSE	Streaming SIMD extension

WD	White dwarf (stellar astrophysics)
WR	Wolf–Rayet (Stars)
ZAMS	Zero-age main sequence (stellar astrophysics)

Contents

1 Astrophysical introduction

Stars play a fundamental role in astronomy—a large piece of information available to us about the Universe we inhabit comes from stars. Coeval associations of stars, also called *star clusters*, are the birth place of most if not all stars. Star clusters form, evolve and "die" by dissolution all across the cosmic time, which is covered in the excellent review "Star Clusters across Cosmic Time" that focuses on the interplay between observations and theoretical knowledge (Krumholz et al. 2019); our review, on the other hand, focuses more on the computational challenges to model a special class of dense star clusters. The term "dense" is not very well defined. We use it here in the sense that both the system should be "gravothermal" and that during at least some phases of the evolution close encounters or even direct collisions between stars or binaries occur. This definition constrains us to globular and young dense star clusters, as well as nuclear star clusters (NSCs). On nuclear star clusters there is another nice review (Neumayer et al. 2020); nuclear star clusters are not in the focus of this work; however, if special computational issues have to be taken into account for nuclear star clusters we may elaborate on them here.

Globular star clusters (GCs) are thought to be the oldest objects in our Galaxy, their age covering a large fraction of the age of the Universe, and they are considered as fossil records of the time of early galaxy formation. GCs of variable age are found near all galaxies (except for the smallest dwarfs) and their specific frequency (number of clusters per galaxy mass unit, see e.g., Harris 1996) differs as a function of galaxy type, highlighting the close relation between cluster and galaxy formation. The approximately 150 globular clusters of our own Milky Way have been studied in much more detail for their proximity. Today, star-by-star observations with the Hubble Space Telescope (HST), and proper motion studies using Gaia with high resolution spectroscopy to determine their stellar velocity dispersions (Bianchini et al. 2013) are possible. Small and big galaxies in the Local Group have systems of GCs, e.g., the Andromeda galaxy and the Magellanic clouds. Globular clusters in huge quantities have been detected around massive galaxies like M87 or other bright central cluster galaxies (Harris et al. 2017) or at sites of star formation near the Antenna galaxies. Still this is—in cosmological scales—our neighborhood. Do clusters form normally following the cosmic star formation history, which peaks at redshifts of around 2 (Reina-Campos et al. 2019)? Or do massive clusters form preferentially as special objects at much higher redshifts (e.g., $z \sim 6$, Boylan-Kolchin 2018)?

Computer simulations of structure formation in the Universe begin to resolve GC scales (Ramos-Almendares et al. 2020), but they cannot compensate the current lack of deep observations. Only recently gravitational lensing from galaxy clusters has helped to identify candidates for proto-GCs at redshifts of $z > 3$ (Vanzella et al. 2017), and more recently even out to $z = 6$ (Vanzella et al. 2019, 2020, 2021). Future instruments such as Extremely Large Telescope (ELT) and others, will improve the situation significantly, while novel instruments such as James Webb Space Telescope (JWST) are already producing ground-breaking results here (Claeyssens et al. 2023; Charbonnel et al. 2023).

We return to the "dense" and "gravothermal" nature of such star clusters. In gravothermal star clusters it is essential to consider the mutual gravitational interactions between many if not all of their stars. The cumulative effect of small angle gravitational deflections (encounters) between distant stars generates transport of heat and angular momentum (relaxation processes connected to these encounters are analogous to heat conduction and viscosity in a gaseous system), and this effect is dominant during certain stages of the star cluster evolution. In order to get the proper time scales connected to such relaxation processes in N-body simulations of star clusters typically a very large number of pairwise distant encounters needs to be followed (which asymptotically results in the computational complexity of all force calculations at a point of time $\approx N^2$, assuming a simple approach without parallelization and hybrid hardware). This physical constraint has led to the use of thermodynamics and statistical mechanics to model gravothermal star clusters (Lynden-Bell and Wood 1968; Hachisu et al. 1978; Hachisu 1979; Spurzem 1991). The star cluster could be modelled using computer codes for the gas dynamical evolution of stars. The relaxation time in a star cluster is *long* compared to the dynamical timescale, while in stars the opposite is true (considering the photon diffusion time as relaxation time). This occurs because the mean free path in stellar systems is much longer than in stellar gaseous matter. Therefore, conductivity and viscosity need to be defined in a different functional form than for the interior of stars (cf. the more detailed discussions in Lynden-Bell and Eggleton 1980; Louis and Spurzem 1991).

An area where observations have picked up greatly through increased angular resolution and sensitivity of spectrographs is the identification of stellar binaries (e.g., Giesers et al. 2018, 2019; Kamann et al. 2020). Binary stars are an extremely important component of star clusters, because they form a dynamically active population which has a dramatic impact on the evolution of the host cluster (e.g., Hénon 1961; Heggie 1975; Elson et al. 1987): for instance stellar exotica observed in clusters (blue stragglers, fast rotating stars, and X-ray binaries) all originate from binary star evolution. The special role that binary stars play in the life cycle of a cluster requires that we pin down as accurately as possible what fraction of stars form in binaries if we are to make progress when predicting the statistics of stellar populations at the later stages of a cluster's evolution. Close stellar encounters, including direct collisions, become a reality in the densest region of dense star clusters. How often these take place, and what the outcomes of such events are remain a puzzle that is only now beginning to be solved. Last, but not least compact objects form in binaries and take part in few-body interactions and stellar evolution of binaries; ultimately, binaries consisting of compact

objects only are possible sources of gravitational waves to be detected by ground-based gravitational wave detectors that are operational today, such as (Advanced) Laser Interferometer Gravitational-Wave Observatory ((a)LIGO) (Aasi et al. 2015; Abbott et al. 2018, 2019), (Advanced) Virgo Interferometer ((a)Virgo) (Acernese et al. 2015; Abbott et al. 2018, 2019) and Kamioka Gravitational Wave Detector (KAGRA) (e.g., Abbott et al. 2018, 2020a; Kagra Collaboration et al. 2019). Note also the next (third) generation space-based detectors in planning—Einstein Telescope (Branchesi et al. 2023) and Cosmic Explorer (Reitze et al. 2019).

The numerical and computational tools to model such dense, massive star clusters are based on either approximate models from statistical physics, or the direct N-body simulation approach. Currently, the latter approach is very dominant since it allows to include details of astrophysics (binaries, stellar evolution, tidal fields) more easily. However, in order to establish the degree of reliability of N-body simulations approximate models have been very important. These are mostly based on the Fokker–Planck approximation in statistical mechanics, and the numerical solution of resulting kinetic equations by using, e.g., Monte Carlo techniques, direct numerical solution, or gaseous and moment models). Since they are important and fundamental to understand results N-body simulations this review contains a basic description of them, too.

GCs and NSCs (dense and gravothermal) are ideal laboratories to examine the theoretical physical processes (heat conduction, angular momentum transport through viscosity) and their influence on the formation and evolution of extreme stellar populations like X-ray binaries or blue stragglers, compact objects (neutron stars, black holes), and are ideal test beds for stellar population synthesis models and stellar evolution.

2 Theoretical foundations

Computational modelling of star clusters requires to follow the complex interplay of thermodynamic processes such as heat conduction and relaxation with the physics of self-gravitating systems, the stochastic nature of star clusters having finite particle number N, and the astrophysical knowledge and models for the evolution of single and binary stars and of external tidal forces. GCs are a very good laboratory for this, because their dynamical and relaxation timescales are well separated from each other and from the lifetime of the cluster and the Universe in its entirety. This article deals with "direct" N-body simulations, which are suitable for systems where the interaction between dynamics and relaxation is important (sometimes also denoted as "gravothermal" systems, Lynden-Bell and Wood 1968). Other kinds of N-body simulations are useful for example for hydrodynamics ("smoothed particle hydrodynamics"), galaxy dynamics ("collisionless systems") or cosmological N-body simulations of structure formation in the Universe, and are not covered here. The main distinction of those from the models presented here, is that the dynamics of systems dominated by two-body relaxation ("collisional systems") require typically very high accuracy (typical energy error per crossing time $\Delta E/E < 10^{-5}$ or smaller) over very long physical integration times (thousands of crossing times). The term "collisional" refers here to elastic gravitational encounters (relaxation encounters),

which drive the "thermal" cluster evolution. Other processes, such as close encounters, encounters involving one or more binaries, and direct collisions also happen in the system.

Let us begin with the definition of some useful time scales. A typical particle crossing time $t_{\rm cr}$ in a star cluster is

$$t_{\rm cr} = \frac{r_{\rm h}}{\sigma_{\rm h}}, \tag{1}$$

where $r_{\rm h}$ is the radius containing 50 % of the (current) total mass and $\sigma_{\rm h}$ is a typical velocity associated with the root mean square random motion (velocity dispersion) taken at $r_{\rm h}$. If virial equilibrium prevails, we have $\sigma_{\rm h}^2 \approx GM_{\rm h}/r_{\rm h}$ (where the sign $\approx$ here and henceforth means "approximately equal" or "equal within an order of magnitude"), thus

$$t_{\rm cr} \approx \sqrt{\frac{r_{\rm h}{}^3}{GM_{\rm h}}}. \tag{2}$$

This relation is equal to the dynamical timescale, which is also used for example in the theory of stellar structure and evolution. Global dynamical adjustments of the system, like oscillations, are connected with this timescale. Taking the square of Eq. (2) yields $t_{\rm cr}^2 \approx r_{\rm h}^3/(GM_{\rm h})$ which is related to Kepler's third law, because the orbital velocity in a Keplerian point mass potential has the same order of magnitude as the velocity dispersion in virial equilibrium. Unlike most laboratory gases stellar systems are not usually in thermodynamic equilibrium, neither locally nor globally. Radii of stars are usually extremely small relative to the average inter-particle distances of stellar systems (e.g. the radius of the sun is $r_\odot \approx 10^{11}$ cm, a typical distance between stars in our galactic neighbourhood is of the order of 10^{18} cm). Only under rather special conditions in the centres of galactic nuclei and during the short high-density core collapse phase of a globular cluster, stellar densities might become large enough that stars come close enough to each other to collide, merge or disrupt each other. Therefore it is extremely unlikely under normal conditions that two stars touch each other during an encounter; encounters or collisions usually are elastic gravitational scatterings. The mean inter-particle distance is large compared to $p_0 = 2Gm/\sigma^2$, which is the impact parameter for a 90° deflection in a typical encounter of two stars of equal mass m, where the relative velocity at infinity is $\sqrt{2}\sigma$, with local 1D velocity dispersion σ. Thus most encounters are small-angle deflections. The relaxation time $t_{\rm rx}$ is defined as the time after which the root mean square velocity increment due to such small angle gravitational deflections is of the same order as the initial velocity dispersion of the system. We use the local relaxation time as defined by Chandrasekhar (1942):

$$t_{\rm rx} = \frac{9}{16\sqrt{\pi}} \frac{\sigma^3}{G^2 m \rho \ln(\gamma N)}. \tag{3}$$

G is the gravitational constant, ρ the mean stellar mass density, σ the 3D velocity dispersion, N the total particle number. This definition was used by Larson (1970); Bettwieser and Spurzem (1986), because it naturally occurs when computing collisional terms (as in Eq. (11)), if the velocity distribution function is written as a series

of Legendre polynomials (Spurzem and Takahashi 1995), with numerical factors being unity (for equipartition terms of lowest order, Spurzem and Takahashi 1995, or only little different from unity, such as 9/10 for the collisional decay of anisotropy (Bettwieser and Spurzem 1986). Other definitions of relaxation can be found frequently, for example in Spitzer (1987). They differ only by numerical factors, except for the so-called Coulomb logarithm $\ln(\gamma N)$, which may take different functional forms. For common forms of the Coulomb logarithms only γ is of order unity, but may take different values (e.g., 0.11, Giersz and Heggie 1994a, or 0.4, Spitzer 1987).

Assuming virial equilibrium a fundamental proportionality turns out:

$$\frac{t_{\rm rx}}{t_{\rm dyn}} \propto \frac{N}{\ln(\gamma N)}. \tag{4}$$

(cf., e.g., Spitzer 1987). As a result, for very large N, dynamical equilibrium is attained much faster than thermodynamic equilibrium. Therefore, even if treated them as "gaseous" spheres, stellar systems evolve qualitatively different from stars; in stars the thermal timescale is short compared to the dynamical timescale (Bettwieser and Sugimoto 1984). Another interesting consequence of the long thermal timescale in star clusters is that anisotropy can prevail for many dynamical times. If one assumes a purely kinetic temperature definition, it ensues that in star clusters the temperatures (or velocity dispersions) can remain different for different coordinate directions over many dynamical times. For example, in a spherical system (using polar coordinates) the radial velocity dispersion of stars ("temperature") σ_r^2 could be different from the tangential one σ_t^2. For the relaxation time above the 3D velocity dispersion $\sigma^2 = \sigma_r^2 + 2\sigma_t^2$ is used. If axisymmetric or triaxial the tangential velocity dispersion can be decomposed into two different dispersions $2\sigma_{\rm t}^2 = \sigma_\theta^2 + \sigma_\phi^2$.

A full account on the relevance of anisotropy for star clusters is beyond the scope of this paper; exemplary we mention here that interest in anisotropy was recently sparked by anisotropic mass segregation in rotating star clusters, both globular and nuclear (Szölgyen and Kocsis 2018; Szölgyen et al. 2019, 2021; Torniamenti et al. 2019; Kamlah et al. 2022b).

3 Direct Fokker–Planck and moment models

Models based on the Fokker–Planck approximation (also denoted as approximate or statistical models) have been designed and implemented in times when it was very difficult to simulate large star clusters directly by N-body simulations. Dramatic development in hardware and software has made now possible direct N-body simulations of up to a million bodies with realistic astrophysics and binaries (Wang et al. 2015, 2016) (`Dragon` simulations). However, the use of the approximate models is very useful to understand the nature of physical processes in star clusters (such as heat conduction or viscosity); by comparison with N-body models they can mutually support each other.

The Fokker–Planck approximation to describe two-body relaxation in spherical star clusters is the foundation for all Monte Carlo models used nowadays (MOCCA

and CMC, see Sect. 4 below). Therefore, it is deemed useful to provide a deeper than usual insight into its theoretical foundations here.

Statistical models have been employed to clarify the physical nature of relaxation processes in star clusters, such as core collapse (Lynden-Bell and Wood 1968), post-collapse evolution due to an energy source from binaries undergoing close encounters with single stars (Inagaki and Lynden-Bell 1983), gravothermal oscillations (Sugimoto and Bettwieser 1983; Bettwieser and Sugimoto 1984; Cohn et al. 1989). These methods have also been important for the study of anisotropy, mass segregation, and rotation later on.

Comparison and mutual adjustment of parameters in order to get agreement between statistical models and direct *N*-body simulations was started by Aarseth et al. (1974) for a first pre-collapse comparison, followed by an extended study using statistical averages of *N*-body simulations to match gaseous models (Giersz and Heggie 1994a, b; Giersz and Spurzem 1994), see also Fig. 1; in Spurzem and Aarseth (1996) it was shown that relaxation processes consistent with theory dominate core collapse in star clusters, and Makino (1996) showed for the first time a signature of gravothermal oscillations in a *N*-body simulation.

Classical models based on the Fokker–Planck approximation use quite strong approximations, like spherical symmetry (in general, with some exceptions allowing axisymmetry), dominance of relaxation encounters, modelling all few-body effects (binary-single and binary-binary close encounters) in a statistical way. A mass spectrum would be modelled by discrete dynamical components with different masses (except Monte Carlo models, see below). With the increasing need to have star cluster models matching detailed observations of star clusters, the use of Fokker–

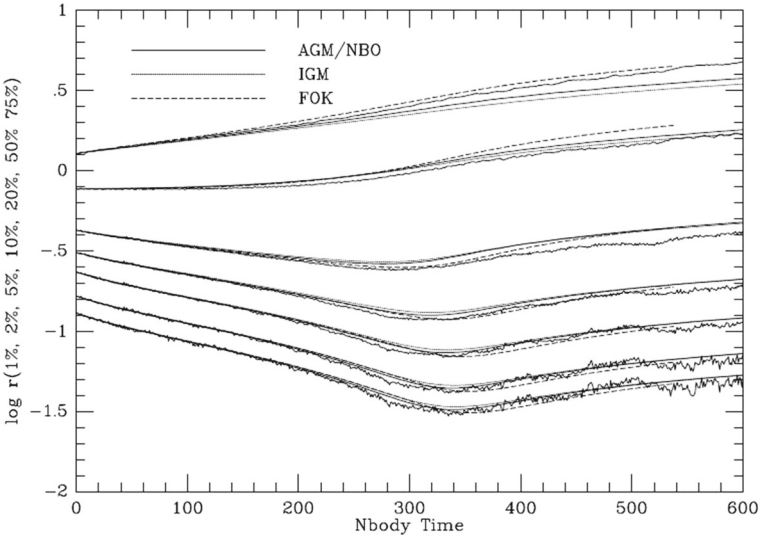

Fig. 1 The time evolution of Lagrangian radii for star clusters modelled by an anisotropic gaseous model (AGM) (Louis and Spurzem 1991), isotropic gas model (Heggie 1984), an isotropic Fokker–Planck model, and direct *N*-body simulation. Image reproduced with permission from Giersz and Spurzem (1994), copyright by RAS; the figure is also included in Chapt. 8 of Binney and Tremaine (2008)

Planck type models was no more practical. That hardware and software developments made more and more realistic particle numbers possible in direct N-body simulations has been another reason for the decline of statistical models.

There is one remarkable exception, the Monte Carlo technique– while it is also based on Fokker–Planck theory it uses a quasi N-body realization and allows state-of-the-art models up to the current time (see Sect. 4). In the following subsections, nevertheless, we will outline the basic theory beneath the statistical models, because in some areas (rotating, flattened star clusters, NSCs, anisotropy) they are still important today in order to analyse results of N-body simulations.

3.1 Fokker–Planck approximation

The Fokker–Planck approximation truncates the so-called BBGKY hierarchy (named after Bogoliubov–Born–Green–Kirkwood–Yvon) of kinetic equations at lowest order assuming that for most of the time all particles are uncorrelated with each other and only coupled via the smooth global gravitational potential (see Chapt. 8.1, Sects. 2 and 3 of Binney and Tremaine 2008; the following paragraph is a summary from their text). We start with most general N-particle distribution function $f^{(N)}$, which depends on positions and velocities $\vec{r}_i, \vec{v}_i$ of a set of N particles and time t:

$$f^{(N)}(\vec{r}_i, \vec{v}_i, i = 1, \ldots, N, t) \tag{5}$$

It provides a probability to find all the particles at their given positions and velocities. In $6N$ dimensional phase space the particles are an incompressible fluid following Liouville's "big" equation

$$\frac{D}{Dt} f^{(N)} = 0 \tag{6}$$

where the derivative is the Lagrangian derivative. If all particles are uncorrelated $f^{(N)} = (f^{(1)})^N$, i.e. the N-particle distribution function is just the N-fold product of a single particle distribution function. That is the case for example in a collisionless stellar system, where all particles just follow their trajectories determined by a global smooth gravitational potential and any direct interaction between two or few particles (stars) is negligible. For collisional stellar systems, however, gravitational encounters (two-body relaxation) change the phase space distribution, particles are not uncorrelated anymore. The theoretical ansatz in that case would be to define a two-body correlation function g by

$$f^{(2)}(\vec{r}_i, \vec{v}_i, i = 1 \ldots 2, t) = f^{(1)}(\vec{r}_1, \vec{v}_1, t) \cdot f^{(1)}(\vec{r}_2, \vec{v}_2, t) + g(\vec{r}_i, \vec{v}_i, i = 1 \ldots 2, t) \tag{7}$$

So, from knowing $f^{(1)}$ and g we get $f^{(2)}$; by using higher order correlation functions one can get from $f^{(n)}$ to $f^{(n+1)}$. Integration of Eq. (6) step-by-step over single particles provides a sequence of equations for $f^{(N-1)}$ to $f^{(1)}$, which is the BBGKY hierarchy. However it is usually not very helpful, because all the correlation functions for $2, \ldots N-1$ need to be known. For practical purposes in collisional stellar systems, where two-body relaxation is important (e.g. open, globular, and nuclear star

clusters), it is sufficient to deal with the two-body correlation, which is done phenomenologically in two different ways for distant and close correlations (encounters and binaries), as described below.

Higher than two-body correlations are rarely important. There could be a relation to Sundmann's famous theorems (Sundman 1907, 1909), which state that in the three-body problem direct three-body collisions occur only with a negligibly small probability; it means whenever three particles get close to each other, there will be always a sequence of separate close two-body encounters, practically never[1] the three bodies will simultaneously get extremely close together. Burrau's three body problem is a nice demonstration of that behaviour (Szebehely and Peters 1967); whether the fundamental assumption of dominance of two-body correlations is in fact realized or not can only be checked computationally by comparison of models based on the Fokker–Planck approximation (such as also Monte Carlo models) with direct N-body simulations. An example for a situation of a very high density in a collapsing core of a star cluster, where higher correlations become important, can be found in Tanikawa et al. (2012).

Instead of determining a general correlation function one resorts to a phenomenological description of the effects of collisions by computing local diffusion coefficients directly from the known solution of the two-body problems. Diffusion coefficients $D(\Delta v_i)$ and $D(\Delta v_i v_j)$ denote the average rate of change of v_i and $v_i v_j$ due to the cumulative effect of many small angle deflections during two-body encounters, at a given radius r (from here assuming spherical symmetry). Let m, $\vec{v}$ and m_f, $\vec{v_f}$ be the mass and velocity of a star from a test and field star distribution, respectively (both distributions can but need not to be the same). In Cartesian geometry (for the local velocities) the diffusion coefficients are defined by

$$D(\Delta v_i) = 4\pi G^2 m_f \ln \Lambda \frac{\partial h(\vec{v})}{\partial v_i}; \quad D(\Delta v_i \Delta v_j) = 4\pi G^2 m_f \ln \Lambda \cdot \frac{\partial^2 g(\vec{v})}{\partial v_i \partial v_j} . \tag{8}$$

Local means here that we do not explicitly consider the dependence of f on the spatial coordinate. g, h are the Rosenbluth potentials defined in Rosenbluth et al. (1957)

$$h(\vec{v}) = (m + m_f) \int \frac{f(\vec{v}_f)}{|\vec{v} - \vec{v}_f|} d^3 \vec{v}_f; \quad g(\vec{v}) = m_f \int f(\vec{v}_f) |\vec{v} - \vec{v}_f| d^3 \vec{v}_f . \tag{9}$$

Note that provided the distribution function f is given in terms of a convenient polynomial series as in Legendre polynomials the Rosenbluth potentials can be evaluated analytically to arbitrary order, as was seen already by Rosenbluth et al. (1957), see for a modern re-derivation and its use for star cluster dynamics (Giersz and Spurzem 1994; Spurzem and Takahashi 1995; Schneider et al. 2011). With these results we can finally write down the local Fokker–Planck equation in its standard form for the Cartesian coordinate system of the v_i:

[1] Meaning the set of initial conditions, which lead to a triple collision is mathematically of measure zero compared to the general space of initial conditions; in physical language: what is needed is that three bodies have in total zero angular momentum with respect to their center of mass.

$$\frac{\partial f}{\partial t} + \vec{v}_i \frac{\partial f}{\partial \vec{r}_i} + \vec{v}_i \frac{\partial f}{\partial \vec{v}_i} = \left(\frac{\delta f}{\delta t}\right)_{\text{enc}}, \tag{10}$$

$$\left(\frac{\delta f}{\delta t}\right)_{\text{enc}} = -\sum_{i=1}^{3} \frac{\partial}{\partial v_i}\left[f(\vec{v}) D(\Delta v_i)\right] + \frac{1}{2}\sum_{i,j=1}^{3} \frac{\partial^2}{\partial v_i \partial v_j}\left[f(\vec{v}) D(\Delta v_i \Delta v_j)\right]. \tag{11}$$

The subscript "enc" should refer to encounters, which are the driving force of two-body relaxation. Still Eq. (10) is a six-dimensional integro-differential equation; its direct numerical simulation in stellar dynamics can presently only be done by further simplification. If the encounter term is zero, Eq. (10) is transformed into Liouville's equation for a collisionless system. For a self-gravitating system Eqs. (10) and (11) are not sufficient, since the knowledge of the gravitational potential Φ is necessary. This can be seen above from the $\vec{v}_i$ term—its computation requires to know the gravitational force. In moment or gas models described below (for spherical symmetry) Poisson's equation takes the simple form Eq. (28); for orbit averaged Fokker–Planck or Monte Carlo models (see Sects. 3.3 and 4.2) the gravitational potential enters directly into the energy as constant of motion (cf. Eq. (30)).

3.2 Moment or gas models

The local Fokker–Planck equation (10) is utilized in another way for gaseous or conducting gas sphere models of star clusters. Integrating it over velocity space with varying powers of the velocity coordinates yields a system of equations in the spatial coordinates; the local approximation is used in the sense that the orbit structure of the system is not taken into account, diffusion coefficients and all other quantities are assumed to be well defined just as a function of the local quantities (density, velocity dispersions and so on). The system of moment equations is truncated in third order by a phenomenological equation of heat transfer. Such an approach has been suggested by Lynden-Bell and Eggleton (1980); Heggie (1984) and generalized to anisotropic systems by Bettwieser (1983); Bettwieser and Spurzem (1986); Louis and Spurzem (1991). In the following the derivation of the model equations is described.

3.2.1 The "left-hand sides"

In spherical symmetry, polar coordinates r θ, ϕ are used and t denotes the time. The vector $\vec{v} = (v_i), i = r, \theta, \phi$, denotes the velocity in a local Cartesian coordinate system at the spatial point r, θ, ϕ. In the interest of brevity $u = v_r$, $v = v_\theta$, $w = v_\phi$ is used. The distribution function f, which due to spherical symmetry is a function of r, t, u, $v^2 + w^2$ only, is normalized according to

$$\rho(r,t) = \int f(r, u, v^2 + w^2, t) du\, dv\, dw, \tag{12}$$

where $\rho(r,t)$ is the mass density; if m denotes the stellar mass, we get the particle density $n = \rho/m$. Then

$$\bar{u} = \int uf(r,u,v^2+w^2,t)du\,dv\,dw, \tag{13}$$

is the bulk radial velocity of the stars. Note that for the analogously defined quantities $\bar{v}$ and $\bar{w}$ we have in spherical systems $\bar{v} = \bar{w} = 0$ (rotating, axisymmetric systems: $\bar{w} \neq 0$). In order to go ahead to the anisotropic gaseous model equations we now turn back to the left-hand side of the Fokker–Planck equation (10), which is the collisionless Boltzmann or Vlasov operator. For practical reasons we prefer for the left-hand side local Cartesian velocity coordinates, whose axes are oriented towards the r, θ, ϕ coordinate space directions. With the Lagrange function

$$\mathcal{L} = \frac{1}{2}\left(\dot{r}^2 + r^2\dot{\theta}^2 + r^2\sin^2\theta\,\dot{\phi}^2\right) - \Phi(r,t) \tag{14}$$

the Euler–Lagrange equations of motion for a star moving in the cluster potential Φ become:

$$\dot{u} = -\frac{\partial\Phi}{\partial r} + \frac{v^2+w^2}{r}\,; \quad \dot{v} = -\frac{uv}{r} + \frac{w^2}{\tan\theta}\,; \quad \dot{w} = -\frac{uw}{r} - \frac{vw}{r\tan\theta}\,. \tag{15}$$

The complete local Fokker–Planck equation, derived from Eq. (10), attains the form

$$\frac{\partial f}{\partial t} + u\frac{\partial f}{\partial r} + \dot{u}\frac{\partial f}{\partial u} + \dot{v}\frac{\partial f}{\partial v} + \dot{w}\frac{\partial f}{\partial w} = \left(\frac{\delta f}{\delta t}\right)_{\mathrm{enc}} \tag{16}$$

where the term subscribed by "enc" denotes the terms involving diffusion coefficients as in Eq. (11). Moments $\langle i,j,k\rangle$ of f are defined in the following way (all integrations range from $-\infty$ to ∞):

$$\langle 0,0,0\rangle := \rho = \int f du dv dw\,; \quad \langle 1,0,0\rangle := \bar{u} = \int uf du dv dw \tag{17}$$

$$\langle 2,0,0\rangle := p_r + \rho\bar{u}^2 = \int u^2 f du dv dw \tag{18}$$

$$\langle 0,2,0\rangle := p_\theta = \int v^2 f du dv dw\,; \quad \langle 0,0,2\rangle := p_\phi = \int w^2 f du dv dw \tag{19}$$

$$\langle 3,0,0\rangle := F_r + 3\bar{u}p_r + \bar{u}^3 = \int u^3 f du dv dw \tag{20}$$

$$\langle 1,2,0\rangle := F_\theta + \bar{u}p_\theta = \int uv^2 f du dv dw \tag{21}$$

$$\langle 1,0,2\rangle := F_\phi + \bar{u}p_\phi = \int uw^2 f du dv dw\,. \tag{22}$$

Note that the definitions of p_i and F_i are such that they are proportional to the random motion of the stars. Due to spherical symmetry we have $p_\theta = p_\phi =: p_t$ and $F_\theta = F_\phi =: F_t/2$. By $p_r = \rho\sigma_r^2$ and $p_t = \rho\sigma_t^2$ the random velocity dispersions are

given, which are closely related to observables in GCs and galaxies. It is convenient to define velocities of energy transport by

$$v_r = \frac{F_r}{3p_r} + u\,; \quad v_t = \frac{F_t}{2p_t} + u\,. \tag{23}$$

By multiplication of the Fokker–Planck equation (16) with various powers of u, v, w we get up to second order the following set of moment equations for $\bar{u}$ dropped in the following):

$$\frac{\partial \rho}{\partial t} + \frac{1}{r^2}\frac{\partial}{\partial r}\left(r^2 u\rho\right) = 0 \tag{24}$$

$$\frac{\partial u}{\partial t} + u\frac{\partial u}{\partial r} + \frac{GM_r}{r^2} + \frac{1}{\rho}\frac{\partial p_r}{\partial r} + 2\frac{p_r - p_t}{\rho r} = 0 \tag{25}$$

$$\frac{\partial p_r}{\partial t} + \frac{1}{r^2}\frac{\partial}{\partial r}\left(r^2 u p_r\right) + 2p_r\frac{\partial u}{\partial r} + \frac{1}{r^2}\frac{\partial}{\partial r}\left(r^2 F_r\right) - \frac{2F_t}{r} = \left(\frac{\delta p_r}{\delta t}\right)_{\mathrm{enc,bin3}} \tag{26}$$

$$\frac{\partial p_t}{\partial t} + \frac{1}{r^2}\frac{\partial}{\partial r}\left(r^2 u p_t\right) + 2\frac{p_t u}{r} + \frac{1}{2}\frac{1}{r^2}\frac{\partial}{\partial r}\left(r^2 F_t\right) + \frac{F_t}{r} = \left(\frac{\delta p_t}{\delta t}\right)_{\mathrm{enc,bin3}}. \tag{27}$$

The terms labeled with "enc" and "bin3" symbolically denote the collisional terms resulting from the moments of the right hand side of the Fokker–Planck equation (Eq. (11)) and an energy generation by formation and hardening of three body encounters. Both will be discussed below. With the definition of the mass M_r contained in a sphere of radius r

$$\frac{\partial M_r}{\partial r} = 4\pi r^2 \rho \tag{28}$$

the set of Eqs. 25–27 is equivalent to gas-dynamical equations coupled with Poisson's equation. Since moment equations of order n contain moments of order $n+1$, it is necessary to close the system of the above equations by an independent closure relation. Here we choose the heat conduction closure, which consists of a phenomenological Ansatz in analogy to gas dynamics. It was first used (restricted to isotropy) by Lynden-Bell and Eggleton (1980). It is assumed that heat transport is proportional to the temperature gradient, where we use for the temperature gradient an average velocity dispersion $\sigma^2 = (\sigma_r^2 + 2\sigma_t^2)/3$ and assume $v_r = v_t$ (this latter closure was first introduced by Bettwieser and Spurzem 1986). Therefore, the last two equations to close our model are

$$v_r - u + \frac{\lambda}{4\pi G\rho t_{\mathrm{rx}}}\frac{\partial \sigma^2}{\partial r} = 0\,; \quad v_r = v_t\,. \tag{29}$$

With Eqs. (25)–(27), (28), and (29) we have now seven equations for our seven dependent variables M_r, ρ, u, p_r, p_t, v_r, v_t.

3.2.2 The "right-hand sides"

All right-hand sides of the moment equations (25)–(27) are calculated by multiplying the right-hand side (the encounter term) of the Fokker–Planck equation as it occurs in Eq. (11) with the appropriate powers of u, v and w and integrating over velocity space. Since the diffusion coefficients in Eq. (8) also contain the distribution function f, the equation depends non-linearly on it. That has led in the early papers to a simplification by using an isotropized background distribution function f_b inside the diffusion coefficients, different from the actual one (Larson 1970; Cohn 1980). in Bettwieser and Spurzem (1986); Einsel and Spurzem (1999); Schneider et al. (2011) there is always full consistency between the background and the actual distribution function.

3.3 Orbit averaged Fokker–Planck models and rotation

The direct solution of the six-dimensional integro-differential equations (Eqs. (10) and (11)) is generally not possible. To have numerical solutions of the Fokker–Planck equation directly one applies Jeans's theorem and transforms f into a function of the classical integrals of motion of a particle in a potential under the given symmetry, as e.g., energy E and modulus of the angular momentum J^2 in a spherical potential or E and z-component of angular momentum J_z in axisymmetric coordinates. Thereafter, the Fokker–Planck equation can be integrated over the accessible coordinate space for any given combination of constants of motion and the orbit-averaged Fokker–Planck equation ensues. By transformation from v_i to E and J and via the limits of the orbital integral the potential enters both implicitly and explicitly. In a two-step scheme alternatively solving the Poisson- and Fokker–Planck equation a direct numerical solution is obtained for spherical systems in 1D (using E only [Cohn (1980)]), or in 2D (using both E and J^2 [Cohn (1979); Takahashi (1995, 1996, 1997)]).

One of the main uncertainties in this method is that for non-spherical mass distributions the orbit structure in the system may depend on unknown non-classical third integrals of motion which are neglected. First 2D models of axisymmetric, rotating globular star clusters (Einsel and Spurzem 1999) used initial models obtained published earlier (Goodman 1983a; Lupton and Gunn 1987; Longaretti and Lagoute 1996), which are generalizations of the standard King models (King 1966), using its dimensionless central potential value W_0 and a new dimensionless rotation parameter ω_0. These models have a rigid rotation in the core, maximum of the rotation curve around the half-mass radius and a differentially decreasing rotation in the halo. They are still mainly supported by "thermal" pressure (velocity dispersions), the rotational energy provides a smaller part of the energy. Typical initial data for $W_0 = 6$ and different rotation parameters are seen in Table 1: the ratio of total rotational to total kinetic energy, dynamical ellipticity, ratios of tidal and half-mass radii to initial core radii, the central relaxation time and finally the half-mass relaxation time in system units are given (for definitions see Einsel and Spurzem 1999).

Table 1 Initial conditions of rotating King models from Einsel and Spurzem (1999) with $W_0 = 6$

ω_0	$T_{\rm rot}/T_{\rm kin}$ (%)	$e_{\rm dyn}(0)$	$r_{\rm tid}/r_{\rm c}(0)$	$r_{\rm h}/r_{\rm c}(0)$	$\tau_{\rm rc}(0)$	$\tau_{\rm rh}(0)$
0.00	0.00	−0.001	18.72	2.70	19.24	91.88
0.05	0.23	0.002	18.61	2.70	19.23	91.77
0.10	0.89	0.013	18.25	2.68	19.22	90.80
0.20	3.38	0.051	16.83	2.66	19.20	89.71
0.30	7.00	0.105	14.99	2.62	19.21	87.73
0.40	11.23	0.165	13.08	2.55	19.22	84.12
0.50	15.61	0.224	11.46	2.48	19.27	80.49
0.60	19.81	0.278	9.94	2.39	19.40	76.32
0.70	23.71	0.327	8.77	2.30	19.50	71.78
0.80	27.18	0.368	7.69	2.20	19.71	67.37
0.90	30.25	0.403	6.88	2.12	19.86	63.24
1.00	32.99	0.433	6.22	2.04	20.02	59.63

$T_{\rm rot}/T_{\rm kin}$ is the ratio of bulk rotational energy to total kinetic energy in percent, $e_{\rm dyn}(0)$ is the dynamical ellipticity, $r_{\rm tid}/r_{\rm c}(0)$ is the ratio of the tidal radius to core radius, $r_{\rm h}/r_{\rm c}(0)$ is the ratio of the half-mass radius to core radius, $\tau_{\rm rc}(0)$ is the central relaxation timescale and $\tau_{\rm rh}(0)$ is the half-mass relaxation timescale. All of these quantities are shown for $t = 0$ of system time units. Table data are from Einsel and Spurzem (1999), but note that in this paper the per cent sign (%) in the header for $T_{\rm rot}/T_{\rm kin}$ had been omitted erroneously

Fokker–Planck models showed that in presence of rotation there is an effective viscosity transporting angular momentum outwards and accelerating cluster evolution significantly as compared to a spherical cluster (see Fig. 2 and Einsel and Spurzem 1999). A series of follow-up papers include post-collapse and multi-mass models (Kim et al. 2002, 2004, 2008) and found an accelerated rotation in the core for heavy masses sinking to the core—as it was predicted by the combined gravogyro and gravothermal "catastrophes" predicted by Hachisu (1979); Akiyama and Sugimoto (1989). One rotating model included in the `Dragon` simulations (Wang et al. 2016), however, did not show accelerated evolution. Whether this is due to heavy mass loss by stellar evolution (not included in earlier papers) or due to a small deviation from the proper initial model is not clear. There is an urgent need for more coverage of rotating stellar clusters by direct *N*-body simulations, see some first progress (Tiongco et al. 2022; Livernois et al. 2022; Kamlah et al. 2023). The initial models of Table 1 are still in frequent use, in particular if realized as *N*-body configurations for *N*-body models (Hong et al. 2013; Tiongco et al. 2017, 2022; Livernois et al. 2022; Kamlah et al. 2023). Notice also the alternative rotating models of Varri (Varri and Bertin 2012; Varri et al. 2018), which are more suitable with regard to the outer cluster zones under influence of tidal fields.

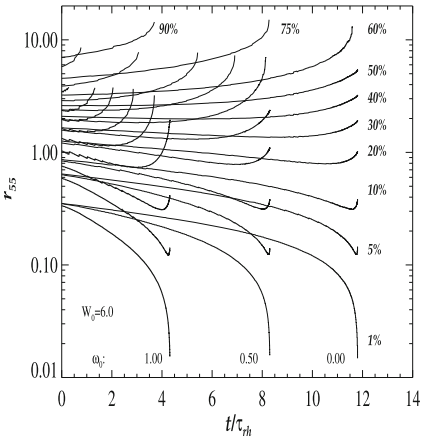

Fig. 2 Evolution of mass shells (Lagrange radii r_{55}) for models with King central potential parameter $W_0 = 6$, and three different dimensionless rotation parameters (see Table 1) $\omega_0 = 0.0, 0.3, 0.6$ as indicated. Shown are the radii for mass columns containing the indicated percentage of total initial mass in the direction of the $\theta = 54°.74$ angle. Image reproduced with permission from Einsel and Spurzem (1999), copyright by RAS

4 Monte Carlo models

Monte Carlo models of star clusters are the only ones which are still intensively used up to the present time, even though they are based on the Fokker–Planck approximation, in the same way as Fokker–Planck or gaseous/moment models. Sometimes this may not be clear to every reader of current papers using Monte Carlo models, because they provide data equivalent to *N*-body simulations—particles with masses, positions and velocities at certain times. Astrophysics (stellar single and binary evolution, stellar collisions, relativistic binaries...) has been included very much like in *N*-body models. This review is not about Monte Carlo models, but a brief summary of their history and entry points to the current literature should be given.

4.1 Hénon and Spitzer type method

As the name suggests, Monte Carlo models are based on the principle that stars have an orbit in a known self-consistent potential; random perturbations are applied, which model the effect of relaxation by distant gravitational encounters. Spitzer's method follows the orbits of stars in the global potential of the cluster and randomly applies kicks in velocity to the stars; at the end of a long series of papers they included binaries and a mass spectrum (Spitzer and Hart 1971a, b; Spitzer and Shapiro 1972; Spitzer and Thuan 1972; Spitzer and Chevalier 1973; Spitzer and Shull 1975a, b; Spitzer and Mathieu 1980).

Hénon's method is using the phase space of constants of motion of a star in a spherically symmetric potential, energy and angular momentum. Deflections are selected randomly, and their effect on angular momentum and energy computed and applied (Hénon 1971). The method was extended to include astrophysical effects, including binaries and stellar evolution (Stodołkiewicz 1982, 1986). These models still allowed for "superstars", i.e., one particle in the Monte Carlo model could represent many real stars.

Current Monte Carlo models are based on Hénon's method, but restricted to star-by-star modelling (much like *N*-body), where every star is a particle in the Monte Carlo simulation. This only made it possible to include all astrophysical effects in the same way than it is done in *N*-body simulations. This new line of Monte Carlo models was initiated by Giersz (1998) (code name MOCCA) and the Northwestern team (Joshi et al. 2000) (code name CMC).

4.2 MOCCA and CMC

The Monte Carlo codes based on the Hénon scheme use constants of motion (specific energy E, specific angular momentum L) as basic variables, properties of stars in the simulation. If the spherically symmetric gravitational potential $\Phi(r)$ is known, the pericenter $r_{\min}$ and apocenter $r_{\max}$ of the orbit are known. At every point of the orbit r the radial velocity is known from

$$v_r = \pm\sqrt{2\Big(E - \Phi(r)\Big) - \frac{L^2}{r^2}}. \tag{30}$$

The orbital integral defines the orbital time τ by

$$\frac{\tau}{2} = \int_{r_{\min}}^{r_{\max}} \frac{dr}{v_r}. \tag{31}$$

With $p(r) = (2/\tau)\cdot(dr/v_r)$ one gets a probability distribution function, used to randomly pick a radial position r_i for the star on its orbit (which should be distributed according to $p(r)$). Let m_i be the stellar mass of stars ($i = 1, \ldots, n$), then the spherically symmetric gravitational potential can be computed according to Hénon (1971)

$$\Phi(r) = G\left(-\frac{1}{r}\sum_{i=1}^{k} m_i - \sum_{i=k+1}^{n}\frac{m_i}{r_i}\right). \tag{32}$$

In addition to that two angles θ and ϕ are randomly picked, so as to have a three dimensional position of the star. Velocities are obtained from E, L, and $U(r_i)$ (one more random number needed). In that way a model star cluster is produced whose data structure is three dimensional—equivalent to that of an *N*-body simulation. To model the relaxation effect, two neighbouring stars are selected and a mean squared deflection angle chosen, which is proportional to the time-step over the relaxation time. Using this angle changes in E and L are computed. Binaries and close encounters between them have been first modelled completely stochastically as well (using random impact parameters, and using random realization of known cross sections). More recently a few-body integration is done in both MOCCA and CMC codes. This is a very rough account of Monte Carlo principles, the reader interested in more details is referred to the papers cited in the next paragraphs.

An account of the state of the MOCCA code and comparison with *N*-body simulations is published in Giersz et al. (2013, 2015). Recently, it has been used for a large number of simulations of Galactic and extragalactic clusters, the MOCCA Survey

Database has been published (Hong et al. 2020; Leveque et al. 2021, 2022a, 2023). The CMC code (Rodriguez et al. 2021b) has been developed in parallel, with matching models to observations (Rui et al. 2021), and an overview of the current state of the code (Rodriguez et al. 2022). Examples of current use of this code focus on compact remnants and their gravitational wave emission, such as e.g., Rodriguez et al. 2021a; Kremer et al. 2021; Ye et al. 2022.

Both Monte Carlo codes have been very successful in terms of generating a large amount of cluster simulations to be compared with observational data and also to follow the evolution of special objects. However, one should not forget their serious limitations:

- if we have a number of massive objects in a central high density region—the assumption of a smooth spherically symmetric potential breaks down;
- at high densities and if many binaries are present, the assumption that there are uncorrelated two-body relaxation encounters and close few-body encounters, which can be clearly separated, breaks down.
- Taking into account external tidal fields is quite difficult, though in simple cases not impossible, due to the strictly spherical cluster centered gravitational potential.

The bottom line is that Monte Carlo models have to be used in order to get an overview of large parameter ranges of star cluster evolution, but in many cases a check by comparison with direct N-body simulations is desirable. They do not suffer from all the problems mentioned above; however, also direct numerical solutions of the N-body problem have certain issues, see Sect. 5.4. A nice overview of current Monte Carlo models is in Vasiliev (2015), who also present a somewhat restricted Monte Carlo code for rotating systems (see Sect. 6.4.6).

5 Direct N-body simulations—methods and algorithms

To integrate the orbits of particles in time under their mutual gravitational interaction the total gravitational potential at each particle's position is required. Poisson's equation in integral form gives the potential Φ generated at a point in coordinate space $\vec{r}$ due to a smooth mass distribution $\rho(\vec{r})$

$$\Phi(\vec{r}) = -G \int \frac{\rho(\vec{r}')}{|\vec{r}' - \vec{r}|} d^3\vec{r}'. \tag{33}$$

A discrete particle distribution in N-body simulations is given by

$$\rho(\vec{r}) = \sum_{i=1}^{N} m_i \, \delta(\vec{r} - \vec{r}_j) \tag{34}$$

with N particles of mass m_i distributed at positions $\vec{r}_j$. Putting this into the integral Poisson equation (33) we get Newton's law for point masses:

Table 2 Table showing important algorithmic, hardware and software development stepping stones in the development of direct *N*-body codes

Year	Keyword	Reference
1961 .	Force polynomial	Aarseth (1963)
	Individual time steps	Aarseth (1963)
	Gravitational softening	Aarseth (1963)
1966 .	Spherical harmonics	Aarseth (1967)
1969 .	Two-body KS regularization	Kustaanheimo and Stiefel (1965)
1972 .	Three-body regularization	Aarseth and Zare (1974)
1973 .	Global regularization	Heggie (1974)
	AC neighbor scheme	Ahmad and Cohen (1973)
1978 .	Co-moving coordinates	Aarseth (1979)
1979 .	Regularized AC	Aarseth (1985a)
1980 .	Planetary formation	Lecar and Aarseth (1986)
1986 .	Hierarchical block-time steps	Hut and McMillan (1986)
1989 .	Chain regularization	Mikkola and Aarseth (1990)
1990 .	Particle in box scheme	Aarseth et al. (1993)
1991 .	Collisional tree code	McMillan and Aarseth (1993)
1992 .	Chain *N*-body interface	Aarseth (1994)
1993 .	Hermite integration	Makino (1991b); Makino and Aarseth (1992)
1995 .	Synthetic stellar evolution	Tout et al. (1997)
	Tidal circularization	Mardling (1995a, 1995b)
	Slow chain regularization	Mikkola and Aarseth (1998)
1996 .	Hierarchical stability	Mardling and Aarseth (1999)
1998 .	Evolution of hierarchies	Mardling and Aarseth (1999)
	Stumpff KS method	Mikkola and Aarseth (1998)
1999 .	HARP-6 procedures	Aarseth (1999a)
	Symplectic integrators	Mikkola and Tanikawa (1999a, 1999b)
	NBODY6++ SPMD / MPI acceleration	Spurzem (1999)
2000 .	Single stellar evolution (SSE)	Hurley et al. (2000)
2002 .	Binary stellar evolution (BSE)	Hurley et al. (2002)
2003 .	GRAPE-6 procedures	Makino et al. (2003)
2006 .	2.5PN in NBODY5	Kupi et al. (2006)
2007 .	Direct *N*-body GPU acceleration	Portegies Zwart et al. (2007)
2008 .	AR with PN terms	Mikkola and Merritt (2008)
2010 .	Updated AR for few-body problems	Hellström and Mikkola (2010)
2012 .	NBODY codes GPU acceleration	Nitadori and Aarseth (2012)
2013 .	MPI acceleration on GPU clusters / PHIGPU	Berczik et al. (2013)
	3.5PN in NBODY6	Brem et al. (2013)
2015 .	SSE/AVX acceleration on GPU clusters	Wang et al. (2015)
2017 .	Forward symplectic integrators (FSI)	Dehnen and Hernandez (2017)
2020 .	P^3T with SDAR in PETAR	Wang et al. (2020c)
		Wang et al. (2020a)

Table 2 continued

Year	Keyword	Reference
2021 .	Minimum spanning tree MSTAR/BIFROST	Rantala et al. (2021, 2023)

The table is adapted from Aarseth (1999a), corrected in some places, but expanded to more recent developments. The abbreviations used are as follows: - KS: Kustaanheimo–Stiefel - AC: Ahmad–Cohen - HARP-6 / GRAPE-6: special-purpose computers named Hermite AcceleratoR Pipeline-6 / GRAvity piPE-6 - PN: Post-Newtonian - SPMD / MPI: Single Program Multiple Data scheme/Message Passing Interface. - AR: Algorithmic chain - GPU: graphics processing unit - SSE / AVX: Advanced Vector Extension/ Streaming SIMD (Single Instruction, Multiple Data) Extension for vectorization in the CPU (central processing unit). - P^3T / SDAR: particle-particle particle-tree/Slow-Down Agolrithmic chain - MSTAR / BiFrost: Minimum spanning tree + algorithmic chain / Binaries in Frost

$$\Phi(\vec{r}) = -G\sum_{j=1}^{N}\frac{m_j}{|\vec{r}-\vec{r}_j|}. \tag{35}$$

5.1 NBODY—the growth of an industry

It was already discovered by Sebastian von Hoerner in the earliest published *N*-body simulations that the relaxation time (Chandrasekhar 1942) is relevant for star cluster evolution and that the formation of close and eccentric binaries occurs as the rule rather than as an exception. It was particularly difficult to accurately integrate them, effectively the simulation would be stopped if close binaries demanded too small time-steps (von Hoerner 1960, 1963).

About at the same time a young postdoc—Sverre Aarseth—in Cambridge developed a direct *N*-body integrator for galaxy clusters with gravitational softening, thereby avoiding von Hoerner's problems with tight binaries (Aarseth 1963). His code was based on Taylor series evaluation of the gravitational force up to its second derivative. Eight years later regularization methods (Kustaanheimo and Stiefel 1965) were implemented in Aarseth's direct *N*-body code (Aarseth 1971). This allowed to proceed past the binary deadlock detected in von Hoerner's models.

Another direct *N*-body code by Roland Wielen appeared on the market, and in a seminal paper (Aarseth et al. 1974) fair agreement was shown between Aarseth's and Wielen's codes and a Monte Carlo code by Lyman Spitzer (see above Sect. 4.1). However, only at the turn of the century Aarseth and von Hoerner could compare their codes, and von Hoerner published a remarkable account on "how it all started" (von Hoerner 2001).

Already in 1985, the code NBODY5 (Aarseth 1985a) had become a kind of "industry standard", attaining world wide use. It employed Taylor series using up to the third derivative of the gravitational force, in a divided difference scheme based on four time points, with individual particle time-steps. Also there were regularizations for more than two bodies, such as the classical chain regularization (Mikkola and Aarseth 1990), and the Ahmad–Cohen (Ahmad and Cohen 1973) neighbour scheme already in NBODY5. The advent of vector and parallel computers demanded an optimization towards hierarchically blocked time-steps and the Hermite

Table 3 Comparison of the code versions

	ITS	ACS	KS	HITS	PN	AR	CC	MPI	GPU
NBODY1	✓								
NBODY2		✓		✓					
NBODY3	✓		✓						
NBODY4			✓	✓			✓		
NBODY5	✓	✓	✓		(✓)		✓		
NBODY6		✓	✓	✓	r		✓		
NBODY6GPU		✓	✓	✓	✓		✓		✓
NBODY6++		✓	✓	✓			✓	✓	
NBODY6++GPU		✓	✓	✓	r		✓	✓	✓
NBODY7		✓	✓	✓	✓	✓			✓

✓: Included in standard version of that level

ITS: Individual time-steps (Aarseth 1985a)

ACS: Ahmad–Cohen neighbour scheme (Ahmad and Cohen 1973)

KS: KS–regularization of few-body subsystems (Kustaanheimo and Stiefel 1965)

HITS: Hermite scheme integration method combined with hierarchical block time-steps (Makino and Aarseth 1992)

PN: Post-Newtonian (Kupi et al. 2006; Mikkola and Merritt 2008; Aarseth 2012)

r: restricted PN, only orbit-averaged energy loss by gravitational radiation (Rizzuto et al. 2021, 2022; Arca-Sedda et al. 2021)

(✓): only included in special version of the code (Kupi et al. 2006)

AR: Algorithmic regularization (Mikkola and Merritt 2008)

CC: Classical chain regularization (Mikkola and Aarseth 1998)

MPI: Message Passing Interface, multi-node multi-CPU parallelization (Spurzem 1999)

GPU: use of GPU acceleration (Nitadori and Aarseth 2012) (if also MPI: multi-node many GPU, Berczik et al. 2013)

scheme (Sect. 5.2.1) (Hut and McMillan 1986; Makino and Aarseth 1992), because it used only two time points, which made memory management easier. This became known as NBODY6.

The growth of the "industry" (Aarseth 1999a) included further improvements in the regularization techniques (Mikkola and Aarseth 1996, 1998; Aarseth 1999b) and a comprehensive book summary (Aarseth 2003). Table 2 summarizes the main algorithmic, hardware and software development stepping stones in the direct *N*-body community up until today.

5.2 The NBODY6 scheme

In the following, the NBODY6 integrator is described in some more detail (note that NBODY7 already contains parallelization through GPU acceleration and will be treated in the next section). NBODY6 and its parallelized and GPU accelerated offspring (NBODY6++, NBODY6GPU, NBODY6++GPU, NBODY7, see Table 3) is still the most

widely used method for direct N-body simulations, but recently also new approaches have been published (cf. Sect. 5.5).

5.2.1 The Hermite scheme

The Hermite scheme and NBODY6 go back to Makino and Aarseth (1992); in conjunction with a hierarchically blocked time-step scheme (see below and Hut and McMillan 1986) it improved the performance on vector computers and turned out to be efficient for all of recent parallel and innovative hardware (general and special purpose parallel computers, GRAPE and GPU). Assume a set of N particles with positions $\vec{r}_i(t_0)$ and velocities $\vec{v}_i(t_0)$ $(i = 1, \ldots, N)$ is given at time $t = t_0$, and let us look at a selected test particle at $\vec{r} = \vec{r}_0 = \vec{r}(t_0)$ and $\vec{v} = \vec{v}_0 = \vec{v}(t_0)$. Note that here and in the following the index i for the test particle i and also occasionally the index 0 indicating the time t_0 will be dropped for brevity; sums over j are to be understood to include all j with $j \neq i$, since there should be no self-interaction. Accelerations $\vec{a}_0$ and their time derivatives $\dot{\mathbf{a}}_0$ are calculated explicitly:

$$\vec{a}_0 = \sum_j G m_j \frac{\vec{R}_j}{R_j^3}\,; \quad \vec{a}_0 = \sum_j G m_j \left(\frac{\vec{V}_j}{R_j^3} - 3(\vec{V}_j \cdot \vec{R}_j) \frac{\vec{R}_j}{R_j^5} \right), \tag{36}$$

where $\vec{R}_j := \vec{r} - \vec{r}_j$, $\vec{V}_j := \vec{v} - \vec{v}_j$, $R_j := |\vec{R}_j|$, $V_j := |\vec{V}_j|$. By low order predictions,

$$\vec{x}_p(t) \& = \frac{1}{6}(t - t_0)^3 \vec{a}_0 + \frac{1}{2}(t - t_0)^2 \vec{a}_0 + (t - t_0)\vec{v} + \vec{x}, \tag{37}$$

$$\vec{v}_p(t) = \frac{1}{2}(t - t_0)^2 \vec{a}_0 + (t - t_0)\vec{a}_0 + \vec{v}\,, \tag{38}$$

new positions and velocities for all particles at $t > t_0$ are calculated and used to determine a new acceleration and its derivative directly according to Eq. (36) at $t = t_1$, denoted by $\vec{a}_1$ and $\vec{a}_1$. On the other hand $\vec{a}_1$ and $\vec{a}_1$ can also be obtained from a Taylor series using higher derivatives of $\vec{a}$ at $t = t_0$:

$$\vec{a}_1 = \frac{1}{6}(t - t_0)^3 \vec{a}_0^{(3)} + \frac{1}{2}(t - t_0)^2 \vec{a}_0^{(2)} + (t - t_0)\vec{a}_0 + \vec{a_0}\,, \tag{39}$$

$$\vec{a}_1 = \frac{1}{2}(t - t_0)^2 \vec{a}_0^{(3)} + (t - t_0)\vec{a}_0^{(2)} + \vec{a}_0\,. \tag{40}$$

If $\vec{a}_1$ and $\vec{a}_1$ are known from direct summation (from Eq. (36) using the predicted positions and velocities) one can invert the equations above to determine the unknown higher order derivatives of the acceleration at $t = t_0$ for the test particle:

$$\frac{1}{2}\vec{a}^{(2)} = -3\frac{\vec{a}_0 - \vec{a}_1}{(t - t_0)^2} - \frac{2\vec{a}_0 + \vec{a}_1}{(t - t_0)} \tag{41}$$

$$\frac{1}{6}\vec{a}^{(3)} = 2\frac{\vec{a}_0 - \vec{a}_1}{(t-t_0)^3} - \frac{\vec{a}_0 + \vec{a}_1}{(t-t_0)^2}\,, \tag{42}$$

This is the Hermite interpolation, which finally allows to correct positions and velocities at t_1 to high order from

$$\vec{x}(t) = \vec{x}_p(t) + \frac{1}{24}(t-t_0)^4\vec{a}_0^{(2)} + \frac{1}{120}(t-t_0)^5\vec{a}^{(3)}\,, \tag{43}$$

$$\vec{v}(t) = \vec{v}_p(t) + \frac{1}{6}(t-t_0)^3\vec{a}_0^{(2)} + \frac{1}{24}(t-t_0)^4\vec{a}_0^{(3)}\,. \tag{44}$$

Taking the time derivative of Eq. (44) it turns out that the error in the force calculation for this method is $\mathcal{O}(\Delta t^4)$, as opposed to standard leap-frog scheme, which has a force error of $\mathcal{O}(\Delta t^2)$ (but see new developments in Sect. 5.5). Additional errors induced by approximate potential calculations (particle mesh or TREE) create potentially even larger errors than that. In Fig. 3, however, it is shown that the above Hermite method used for a real N-body integration sustains generally an error of $\mathcal{O}(\Delta t^4)$ for the entire calculation.

5.2.2 Time-step choice

Aarseth (1985a) provides an empirical time-step criterion

$$\Delta t = \sqrt{\eta\frac{|\vec{a}||\vec{a}^{(2)}| + |\vec{a}_0|^2}{|\vec{a}_0||\vec{a}^{(3)}| + |\vec{a}^{(2)}|^2}}. \tag{45}$$

The error is governed by the choice of η, which in most practical applications is taken

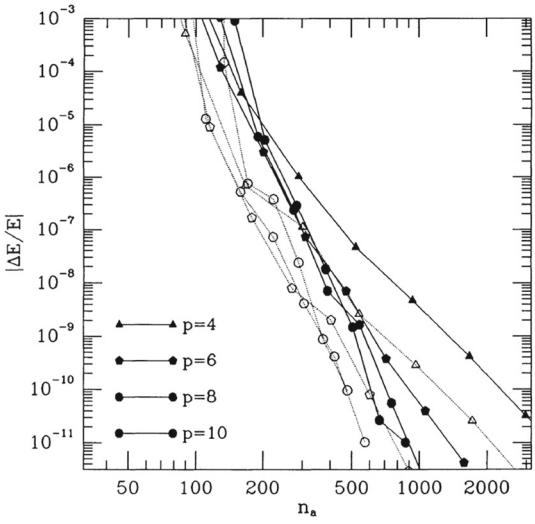

Fig. 3 The relative energy error as the function of the number of steps. A time-step criterion using differences between predicted and corrected values is used, different from Eq. (45). Dotted curves are for Hermite schemes, solid curves for Aarseth schemes. The step number p denotes the order of the integrator. Image reproduced with permission from Makino (1991b), copyright by AAS

to be $\eta = 0.01 - 0.04$. It is instructive to compare this with the inverse square of the curvature κ of the curve $\vec{a}(t)$ in coordinate space

$$\frac{1}{\kappa^2} = \frac{1 + |\vec{a}_0|^2}{|\vec{a}^{(2)}|^2} \,. \tag{46}$$

Clearly, under certain conditions the time-step choice of Eq. (45) becomes similar to choosing the time-step according to the curvature of the acceleration curve; since it was determined just empirically, however, it cannot generally be related to the curvature expression above. In Makino (1991b) a different time step criterion has been suggested, which appears simpler and more straightforwardly defined, and couples the time-step to the difference between predicted and corrected coordinates. The standard Aarseth time-step criterion from Eq. (45) has been used in most N-body simulations so far, because it seems to achieve an optimal step better than (on average) the mathematically more sound Makino step (see the time-step related discussion in Sweatman 1994).

Since the position of all field particles can be determined at any time by the low-order prediction from Eq. (38), the time-step of each particle (which determines the time at which the corrector of Eq. (44) is applied) can be freely chosen according to the local requirements of the test particle; the additional error induced due to the use of only predicted data for the full N sums of Eq. (36) is negligibly small, for the benefit of not being forced to keep all particles in lockstep. Such an individual time-step scheme is in particular for non-homogeneous systems very advantageous, as was quantitatively pointed out by Makino and Hut (1988). Particles in the high density core of a star clusters need to be updated much more often than particles on orbits very far from the centre. They show that the gain in computational speed due to the individual time-step scheme (as compared to a lockstep scheme where all particles share the minimum required time-step) is of the order $N^{1/3}$ for homogeneous and N^1 for strongly spatially structured systems (Makino and Hut 1988).

For the purpose of vectorization and parallelization it is better not to have the particles continuously distributed on a time axis. Consequently, Makino (1991a) uses a hierarchical scheme, still on the basis of Eq. (45); but a change of the time-step is considered only if that equation yields a variation of Δt compared to the last step by more than a factor of 2 (increase or decrease). If this is the case a variation by 2 is applied only. Thus in model units all time-steps are selected from the set $\{2^{-i} | i = 0, ...i_{\max}\}$ with $k = i_{\max}$ determined by the condition that $\Delta t_{\min} > 2^{-i_{\max}}$ for the minimum time-step $\Delta t_{\min}$ determined from Eq. (45). For core collapse simulations of star clusters of a few ten thousand particles $i_{\max}$ goes up to about 20; empirically and theoretically (Makino and Hut 1988) $\Delta t_{\min} \propto N^{-1/3}$, so for large N $i_{\max}$ becomes larger, however, on the other hand, how large $i_{\max}$ grows for fixed N depends on the selected criteria for so-called KS regularisation of perturbed two–body motion (see below). The implementation of the block step scheme indeed uses an even stronger condition than the above described one, it is demanded that not only the time-steps, but also the individual accumulated times of each particles are commensurate with the time-step itself. This ensures that for any particle i and any time $T_i = t_i + \delta t_i$ *all* particles with $\delta t_j < \delta t_i$ have for their own time $T_j = t_j + \delta t_j = T_i$, where the last

equality is the non–trivial one. Such procedure is important for the parallelization of the algorithm. For example it has as a consequence that at the big time-steps always huge groups of particles are due for correction, sometimes even all particles (at the largest steps).

5.2.3 Ahmad–Cohen neighbour scheme

Another refinement of the Hermite or Aarseth "brute force" method is the two-time-step scheme, denoted as neighbour or Ahmad–Cohen scheme (Ahmad and Cohen 1973). For each particle a neighbour radius is defined, and $\vec{a}$ and $\vec{a}$ are computed due to neighbours and non-neighbours separately. Similar to the Hermite scheme the higher derivatives are computed separately for the neighbour force (irregular force) and non-neighbour force (regular force). Computing two time-steps, an irregular small $\Delta t_{\rm irr}$ and a regular large $\Delta t_{\rm reg}$, from these two force components by Eq. (45) yields a time-step ratio of $\gamma := \Delta t_{\rm reg}/\Delta t_{\rm irr}$ being in a typical range of 5–20 for N of the order 10^3 to 10^4. The reason is that the regular force has much less fluctuations than the irregular force. The Ahmad–Cohen neighbour scheme is implemented in a self-regulated way, where at each regular time-step a new neighbour list is determined using a given neighbour radius r_{si} for each particle. If the neighbour number found is larger than the prescribed optimal neighbour number, the neighbour radius is increased or vice versa. In Aarseth (1985a); Makino and Hut (1988) more complicated algorithms to adjust the neighbour radius are described. Over a wide range of particle numbers (ranging from 10^4 to 1.6×10^7) the neighbour number has to be varied only slightly (from 50–400). It has been published for runs with up to a million bodies in Huang et al. (2016) and will be published soon for the larger particle numbers. Generally, the neighbour number is a choice for optimization and can be chosen relatively freely without problems for the accuracy. This is in conflict with earlier claims that the optimal neighbour number should be adjusted as $N_{n,opt} \propto N^{3/4}$ (Makino and Hut 1988). The reason is that by using special purpose machines or parallelization for parts of the code, an optimal neighbour number is not well defined, so the neighbour number can be selected according to accuracy and efficiency requirements. After each regular time-step the new neighbour list is communicated along with the new particle positions to all processors of the parallel machine, thus making it possible to do the irregular time-step in parallel as well.

Using a two-time-step or neighbour scheme again increases the computational speed of the entire integration by a factor of at least proportional to $N^{1/4}$ (Makino 1991b). Both the regular and irregular time-steps are arranged in the hierarchical, commensurable way.

5.2.4 Regularizations

As the relative distance r of the two bodies becomes small, their time-steps are reduced to prohibitively small values, and truncation errors grow due to the singularity in the gravitational potential. Such a close encounter is characterised by

an impact parameter p and a relative velocity at "infinity" (in practice some distance inside the cluster) v_∞. A close encounter is characterized by

$$p < p_{90} = 2G(m_1 + m_2)/v_\infty^2, \tag{47}$$

where p_{90} is the impact parameter related to a 90 degree deflection in a two-body problem; G, m_1, m_2, v_∞ are the gravitational constant, the masses of the two particles and their relative velocity at infinity. In the cluster centre, it is very likely that two stars come very close together in a hyperbolic encounter. So, if the separation of two particles gets smaller than p_{90} they are candidates for regularization. To be actually regularized, the two particles have to fulfil two more sufficient criteria: that they are approaching each other, and that their mutual force is dominant. These sufficient criteria are defined as

$$\mathbf{R} \cdot \mathbf{V} > 0.1\sqrt{(G(m_1 + m_2)R}$$
$$\gamma := \frac{|\mathbf{a}_{\rm pert}| \cdot R^2}{G(m_1 + m_2)} < 0.25$$

Here, $\mathbf{a}_{\rm pert}$ is the vectorial differential force exerted by other perturbing particles onto the two candidates, R, $\mathbf{R}$, $\mathbf{V}$ are scalar and vectorial distance and relative velocity vector between the two candidates, respectively. The factor 0.1 in the upper equation allows nearly circular orbits to be regularized; $\gamma < 0.25$ demands that the relative strength of the perturbing forces to the pairwise force is one quarter of the maximum. These conditions describe quantitatively that a two-body subsystem is dynamically separated from the rest of the system, but not necessarily unperturbed.

The idea is to take both stars out of the main integration cycle, replace them by their centre of mass (c.m.) and advance the usual integration with this composite particle instead of resolving the two components. The internal motion of the two members of the regularized pair (henceforth KS pair, for **K**ustaanheimo and **S**tiefel, Kustaanheimo and Stiefel 1965) is done in a separate coordinate system. However, as was already noted by Aarseth (1971) there is no need for the perturbation of the KS pair from other stars to be small.

The internal motion of a KS pair is integrated in a 4D vector space obtained from a combined canonical and time transformation of relative Cartesian positions and velocities. The coordinate transformation goes back to Levi-Civita in 2D (Levi-Civita 1916). A full generalization to higher dimensions is only possible over the mathematical object of a field, the next one to be quaternions in 4D. Kustaanheimo and Stiefel found a way to transform forward from 3D to 4D and back from 4D to 3D by working over a skewed field of quaternions (sacrificing some commutativity rules; their mathematical language was different though). A modern theoretical approach to this subject can be found e.g. in Neutsch and Scherer (1992); the complete formalism including also the time transformation can be found in Mikkola (1997a). Aarseth uses this method to integrate the KS pairs in 4D space, and when using the back-transformation automatically returning to Cartesian 3D space (Aarseth 1971). The KS transformation converts the motion in a singular Newtonian gravitational potential into a harmonic oscillator in 4D space, which has no singularity. Since the

harmonic potential is regular, numerical integration with high accuracy can proceed with much better efficiency, and there is no danger of truncation errors for arbitrarily small separations. The internal time–step of such a KS–regularized pair is independent of the eccentricity and of the order of some 50–100 steps per orbit.

While regularization can be used for any analytical two–body solution even across a mathematical singularity (collision), it is practically applied to perturbed pairs only. Once the perturbation γ falls below a critical value of $\approx 10^{-6}$, a KS pair is considered unperturbed, and the analytical solution for the Keplerian orbit is used instead of doing numerical integration. The two-body KS regularization occurs in the code either for short-lived hyperbolic encounters or for persistent binaries.

Close encounters between single particles and binary stars are also a central feature of cluster dynamics. The chain regularization (Mikkola and Aarseth 1998) is invoked if a KS pair has a close encounter with another single star or another pair. Especially, if systems start with a large number of primordial (initial) binaries, such encounters may lead to stable (or quasi-stable) hierarchical triples, quadruples, and higher multiples. They are treated by using special stability criteria (Mardling and Aarseth 2001).

Every subsystem—KS pair, chain or hierarchical subsystem - could be perturbed by other single stars. Perturbers are typically those objects that get closer to the object than $R_{\rm sep} = R/\gamma_{\rm min}^{1/3}$, where R is the typical size of the subsystem; for perturbers, the components of the subsystem are resolved in their own force computation as well. Algorithmic regularization is a relatively recent method based on a time transformed leap-frog method (Mikkola and Merritt 2008); it does not employ the KS transformation. See for its use and application the next subsection.

5.3 Parallel and GPU computing and NBODY

A fundamental problem was raised by Daiichiro Sugimoto about 30 years ago (Sugimoto et al. 1990)—direct numerical simulations of globular star clusters—with order of a million stars in direct N-body—could not be completed for decades if extrapolating the standard evolution of computational hardware at that time (Moore's law) for the future. Therefore astronomers in the Department of Astronomy at Tokyo University started wire-wrapping and designing a new integrated circuit, a special purpose computer chip named GRAPE (=**GRA**vity **P**ip**E**). The work was continued with great success by the team of Junichiro Makino, the GRAPE chips were finally assembled into GRAPE accelerator mainboards containing several chips (such as HARP, GRAPE-4, GRAPE-6) (Makino et al. 1993, 1997; Makino and Taiji 1998; Makino et al. 2003).

The GRAPE chip is an application specific integrated circuit (ASIC), which could only compute gravitational forces between particles (it also computed the time derivative of the force, to be directly applicable to the Hermite scheme of NBODY6). A GRAPE board is a multi-core (multi-chip) parallel computing device (e.g., GRAPE-4 board contained 48 chips with shared memory, each chip contained one pipeline for force calculation; the GRAPE-6 chip contained 6 force pipelines, Makino et al. 2003).

Custom built computing clusters using GRAPE were built outside of Japan, e.g., in Rochester and Heidelberg (Harfst et al. 2007). In the following years, graphical processing units (GPU) widely replaced GRAPE; direct *N*-body implementations were done on GPU clusters (Portegies Zwart et al. 2007; Schive et al. 2008). Interfaces have been written such that GRAPE users could right away also use GPU with the newly invented programming language CUDA (Yebisu, Nitadori and Makino 2008; Sapporo, Gaburov et al. 2009; Kirin, Belleman et al. 2008, 2014). Still somewhat state of the art is NBODY6GPU, which includes GPU acceleration of NBODY6 using CUDA kernels for single node servers (Nitadori and Aarseth 2012). Many of these kernels written by Keigo Nitadori are still in current use, even for the massively parallel programs such as NBODY6++GPU, see below.

At the same time another development started, parallelization of NBODY6 with the (at that time) new standard MPI (message passing interface). NBODY6++ (Spurzem 1999) uses the SPMD (Single Program Multiple Data) scheme to run many instances of the code in parallel, while distributing force computations for different particles to the processors of a massively parallel computer. From time to time data transfers using MPI communication routines are necessary, to make sure all processors are synchronous. Systems with hundreds of processing units were used at the time (e.g. CRAY T3E), which demanded efficient coding of the communication scheme. Copy and ring algorithms were developed, and asynchronous data transfer and computation implemented (Makino 2002; Dorband et al. 2003).

A copy algorithm keeps always a complete copy of all particle data on every parallel process; parallelization is over groups of particles due for the correction step; communication sends around all new particle positions and velocities in the Hermite scheme to all other processes. In contrast the ring algorithm uses a domain decomposition, every process has its specific set of particles (at least for some time), and instead of communicating particle positions and velocities partial gravitational forces and their time derivatives are communicated. A copy algorithm has been implemented by Spurzem (1999); Hemsendorf et al. (2002) for NBODY6++, and a ring algorithm is used in PHIGRAPE (Harfst et al. 2007). All these communication algorithms have been implemented long time ago using the ‚PI_SENDRECV routine in a cyclic fashion—for p processes $p-1$ communication steps are needed.[2] Every process simultaneously sends data to its next neighbour and receives data from its other neighbour, in a ring structure. Therefore these algorithms are also denoted as systolic communication algorithms (both copy and ring). Nowadays MPI_ALLGATHER or MPI_ALLREDUCE may be used, but their implementations are not transparent and vary; the latter would normally use a TREE-based implementations (instead of systolic)—the number of communication steps is then only $\log_2(p)$ (while our systolic algorithm needs $\mathcal{O}(p)$ steps). It can be shown that asymptotically (for large data chunks and low latency) both algorithms are equivalent with regard to the total time required, because the TREE based algorithm uses increasingly large data packages, while in systolic algorithms every step communicates the same amount of data (Dorband et al. 2003). Hence, currently still the systolic communication with a

[2] p is the number of processing elements running an MPI process, typically one multi-core CPU runs 1–4 MPI processes per node, across several nodes; each of them is connected to GPUs on the node.

copy algorithm is used in NBODY6++GPU. If going to ten or hundred million bodies the copy algorithm may become too large for system memories, and should be updated to the ring algorithm with domain decomposition, which is not a fundamental problem (already used in the PHIGRAPE code, which is a simple variant of the Hermite scheme with blocked hierarchical time steps). While both ring and copy algorithms scale linearly with p a hypersystolic algorithm exists which scales only with $\sqrt{n_p}$ (Lippert et al. 1996, 1998). For GRAPE a special implementation of a hypersystolic algorithm for 2D meshes of processing elements has been proposed (Makino 2002). Hypersystolic and other TREE based communication algorithms can play out their strengths in case of a huge number of processes (as in case of GRAPE for example) with relatively modest computational load on every process. On the contrary the current NBODY6++GPU algorithm requires modest numbers of processes (order 10–100 with current particle numbers of up to around a million, may be more in the future), which have big computing loads and very large data chunks to communicate.

NBODY6++ (Spurzem 1999) parallelizes both force loops with MPI, for the regular and the neighbour force in the Ahmad–Cohen scheme.

A ring communication algorithm with domain decomposition in the future would also help for situations when there are many small block time-steps with few particles to integrate. The current code NBODY6++ (and its successors NBODY6++GPU using GPU) only invoke parallel MPI execution if the number of particles in a time block is large enough (like e.g. 50–100, best value has to be tested for every hardware). For smaller blocks all processors are redundantly computing everything without communication, to avoid the overhead connected with MPI. Since the special hierarchical time-step scheme of NBODY6 favours time blocks with many particles this is for usual globular cluster simulations no bottleneck. However, in case of very high central density, like in nuclear star clusters with central supermassive black hole (see Sect. 7) the parallel performance gets degraded.

With the advent of clusters, where nodes would be running MPI, and each node having a GPU accelerator, NBODY6++GPU was created – on the top level MPI parallelization is done for the force loops (coarse grained parallelization) and at the bottom level each MPI process calls its own GPU to accelerate the force calculation (Berczik et al. 2013), using Nitadori's Yebisu library (Nitadori and Makino 2008) for the regular force only. Secondly, an AVX/SSE implementation accelerates prediction and neighbour (irregular) forces, and also a number of other features had been severely optimized and improved (such as particle selection at block times) (Wang et al. 2015). This code currently keeps the record of the largest direct N-body simulation of a globular cluster with all required astrophysics (single and binary stellar evolution, stellar collisions, tidal field), simulated over 12 Gyrs (Wang et al. 2016).

In recent years, inspired also by LIGO/Virgo/KAGRA gravitational-wave detections (Abbott et al. 2016), numerous current updates have been made with regard to stellar evolution of massive stars in singles and binaries (Kamlah et al. 2022b), and with regard to collisional build up of stars (mass loss at stellar collisions allowed) and intermediate-mass black holes (Rizzuto et al. 2021, 2022; Arca-Sedda

et al. 2021). The current code is available via GitHub.[3] Note that a different service is provided by Long Wang, quoted in Varri et al. (2018). That alternative version of NBODY6++GPU has been recently used by the Padova team, replacing the older SSE/BSE stellar evolution by MOBSE (see e.g., Di Carlo et al. 2021).

Star clusters with primordial (initial) binaries inevitably lead to binaries of black holes. If two black holes get close enough to each other, either during a hyperbolic encounter or due to close Newtonian three-body or four body interactions, Post-Newtonian corrections have to be taken into account. They take the form of an expansion of the relative acceleration between the two bodies in terms of $(v/c)^{2i}$, denoted as PNi-terms. PN1, PN2, and PN3 are conservative, producing periastron shifts of orbits, while PN2.5 and PN3.5 provide the energy and angular momentum loss due to gravitational radiation. The first implementation was done in NBODY5 up to PN2.5 (Kupi et al. 2006); and for NBODY7 (Aarseth 2012). Also relativistic spin-spin and spin-orbit interactions of orders PN1.5, PN2.0, PN2.5 have been recently included (Brem et al. 2013). The most recent version of NBODY7 (Banerjee et al. 2020) includes also the full PN terms by using the ARChain (algorithmic regularization chain) method (Mikkola and Merritt 2008). NBODY7 is GPU accelerated, but has not yet the MPI parallelization of NBODY6++ and NBODY6++GPU. Generally binary evolution governed by Post-Newtonian terms has been compared with full numerical solutions of general relativity; deviations between fully relativistic and Post-Newtonian evolution only occur during the final period of merger, in a time span usually negligible for astrophysical purposes. The reader interested in the original citations with regard to the derivation and justification of Post-Newtonian terms is referred to Kupi et al. (2006); Mikkola and Merritt (2008); Brem et al. (2013) for further references therein.

When black holes merge they experience a kick due to asymmetric gravitational wave emission, see e.g., the MOCCA implementation (Morawski et al. 2018); a similar model is already used in NBODY7 (Banerjee et al. 2020), and this is a field where NBODY6++GPU is currently lagging behind, current work is ongoing on it. The following Table 3 gives a summary of the features of different variants of the NBODY codes.

Table 4 shows for NBODY6++GPU a model fit, obtained from a number of simulations using a range of particle numbers N and MPI process number N_p, where each MPI process also uses a GPU (Huang et al. 2016). Eight different pieces of the code have been profiled as indicated. The fit shows the following key information:

1. regular and irregular force computation are very well parallelized ($\propto N_p^{-1}$);
2. regular force computation still scales with approximately N^2, but with a very small factor in front, due to the fast GPU processing.
3. MPI communication and synchronization provide a bottleneck, no further speedup possible for more than 8–16 MPI processes.
4. Also prediction and sequential parts on the host are bottlenecks if going for large N, because they scale approximately with $N^{1.5}$, and do not scale down with processor number.

[3] https://github.com/nbody6ppgpu.

Table 4 Profiling model developed for NBODY6++GPU, details explained in main text

Description	Timing variable	Expected scaling N	N_p	Fitting value [sec]
Regular force computation	$T_{\rm reg}$	$\mathcal{O}(N_{\rm reg} \cdot N)$	$\mathcal{O}\left(N_p^{-1}\right)$	$(2.2 \cdot 10^{-9} \cdot N^{2.11} + 10.43) \cdot N_p^{-1}$
Irregular force computation	$T_{\rm irr}$	$\mathcal{O}(N_{\rm irr} \cdot \langle N_{nb} \rangle)$	$\mathcal{O}\left(N_p^{-1}\right)$	$(3.9 \cdot 10^{-7} \cdot N^{1.76} - 16.47) \cdot N_p^{-1}$
Prediction	$T_{\rm pre}$	$\mathcal{O}\left(N^{kn_p}\right)$	$\mathcal{O}\left(N_p^{-kp_p}\right)$	$(1.2 \cdot 10^{-6} \cdot N^{1.51} - 3.58) \cdot N_p^{-0.5}$
Data moving	$T_{\rm mov}$	$\mathcal{O}\left(N^{kn_m}1\right)$	$\mathcal{O}(1)$	$2.5 \cdot 10^{-6} \cdot N^{1.29} - 0.28$
MPI communication (regular)	$T_{\rm mcr}$	$\mathcal{O}\left(N^{kn_{cr}}\right)$	$\mathcal{O}\left(kp_{cr} \cdot \frac{N_p-1}{N_p}\right)$	$(3.3 \cdot 10^{-6} \cdot N^{1.18} + 0.12)\left(1.5 \cdot \frac{N_p-1}{N_p}\right)$
MPI communication (irregular)	$T_{\rm mci}$	$\mathcal{O}\left(N^{kn_{ci}}\right)$	$\mathcal{O}\left(kp_{ci} \cdot \frac{N_p-1}{N_p}\right)$	$(3.6 \cdot 10^{-7} \cdot N^{1.40} + 0.56)\left(1.5 \cdot \frac{N_p-1}{N_p}\right)$
Synchronization	$T_{\rm syn}$	$\mathcal{O}\left(N^{kn_s}\right)$	$\mathcal{O}\left(N_p^{kp_s}\right)$	$(4.1 \cdot 10^{-8} \cdot N^{1.34} + 0.07) \cdot N_p$
Sequential parts on host	$T_{\rm host}$	$\mathcal{O}\left(N^{kn_h}\right)$	$\mathcal{O}(1)$	$4.4 \cdot 10^{-7} \cdot N^{1.49} + 1.23$

Table reproduced with permission from Huang et al. (2016), copyright by NAO/CAS/IOP

The timing model is already a few years old, the current code version has made progress in MPI parallelization of prediction (pos. 3). To improve the communication scaling faster MPI or NVLink[4] communication hardware will be beneficial (pos. 5, 6). Note that all numerical factors in the fit dependent on the specific hardware used —CPUs, GPUs, communication lines between CPU nodes and between CPU and GPU.

Figure 4 shows in principle similar information as Table 4, but here the eye should inspect the relative weight of the different components, when increasing the number of MPI processes. The coloured fields correspond to the code parts discussed above, but a little more segmented:

a. Reg. and Irr. correspond to regular and irregular force computation in Table 4;
b. Pred. is prediction;
c. Move is data moving;
d. Comm.R, Send.R., Comm.I. and Send.I is MPI communication (regular, irregular)
e. Barr. is synchronization
f. Init.B., Adjust, KS, refer to sequential parts on the host.

[4] NVIDIA High Speed GPU Interconnect.

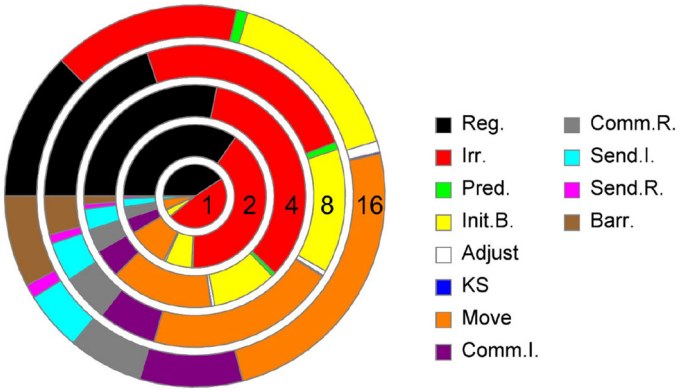

Fig. 4 Pie chart showing the time fraction spent in different parts of the NBODY6++GPU code for a one million body simulation without initial (primordial) binaries. Different rings show different number of MPI processes N_p (inside to outside 1, 2, 4, 8 and 16.). Colours are explained in the main text

The bottom line to stress from these results is that even for one million bodies the bottleneck of the parallel code is *NOT* the regular force (which would be extremely dominant in a sequential processing), so it is *NOT* the stumbling block for going to much higher particle number, these are prediction and communication.

There are also PHIGPU (Berczik et al. 2013), PHIGRAPE (Harfst et al. 2007), and HIGPU (Capuzzo-Dolcetta et al. 2013; Spera 2014). All of them are using the Hermite scheme with hierarchically blocked time-steps, and are fully parallelized and GPU accelerated. There is no Ahmad–Cohen neighbour scheme and no regularization, which means that on a serial computer they would be much slower than e.g. NBODY6++GPU. But with a very efficient parallelization and GPU acceleration this is partly compensated; they have been used for astrophysical problems where star-by-star modelling could be neglected, such as e.g. galactic nuclei and galaxy mergers with supermassive black holes (cf., e.g, Zhong et al. 2014, 2015; Li et al. 2017, 2019; Bortolas et al. 2018).

An interesting feature is that these codes implement higher order Hermite integration schemes (in PHIGPU 4th, 6th, or 8th order can be chosen, HIGPU uses 6th order. There is another 6th and 8th order Hermite integrator (Nitadori and Makino 2008); so far these higher order integrators have seen relatively little use, consistent with the conclusion that the 4th order integrator is an optimal choice for performance and accuracy (Makino 1991b).

5.4 Are *N*-body simulations reliable?

At this point the reader may expect that direct N-body simulation turn out to be the most reliable (although computationally most expensive) way to simulate the dynamical evolution of a gravitating system consisting of N point masses. It does not involve any serious approximations and assumptions, as e.g., the Fokker–Planck approximation and the Monte Carlo codes. By reducing the η-values in the time-step (Eq. (45)) any accuracy can be achieved in principle, as long as machine accuracy

permits it. Usually for accuracy and time-step choice globally conserved quantities are used, such as energy and angular momentum, and center of mass conservation (position and velocity).

However, for a system with N particles phase space has $6N$ dimensions, and a check of say energy, angular momentum, and center of mass alone only checks whether the numerically calculated system remains within an allowed $6N-9$ dimensional hypervolume. There is no a priori information how "exact" the "true" individual trajectories are reproduced in the simulation within this hypervolume. It was early pointed out that, due to repeated close encounters occurring between particles, initial configurations that are very close to each other, quickly diverge in their evolution from each other (Miller 1964). In that work it was shown that the separation in phase space of two trajectories increases exponentially with time, or with other words, the evolution of the configuration is extremely sensitive to initial conditions (particle positions and velocities). The timescale of exponential instability is as short as a fraction of a crossing time, and the accurate integration of a system to core collapse would require of order $\mathcal{O}(N)$ decimal places (Goodman et al. 1993; Kandrup et al. 1994). These papers argue that the problem is caused by two-body encounters, but chaotic orbits in non-integrable potentials can be a source of exponential instability and thus cause unreliable numerical integrations as well.

However, the situation is not as bad as it seems. N-body simulations of star clusters or galactic nuclei do not always exploit the detailed configuration space of all particles. Quantities of interest are global or somehow averaged quantities, like Lagrangian radii or velocity dispersions averaged in certain volumes. As it was nicely demonstrated in a pioneering series of papers (Giersz and Heggie 1994a, b, 1996, 1997) such results are not sensitive to small variations of initial parameters. They took statistically independent initial models (positions and velocities at the beginning selected by different random number sets) and showed that the ensemble average of the dynamical evolution of the system always evolved predictably and in remarkable accord with results obtained from the Fokker–Planck approximation. The method was also partly and successfully used in Giersz and Spurzem (1994), which focused on the evolution of anisotropy and comparisons with the anisotropic gaseous models of the author of this paper, or in more recent examples (Rizzuto et al. 2021, 2022) where the formation of intermediate mass black holes was analyzed over a large set of N-body simulations, using statistically independent initial models.

As a consequence, it should be remembered, however, that great care has to be taken when interpreting results of N-body simulations on a particle by particle basis, for example determining rates of specific types of encounters, which could produce mergers in a large direct N-body model.

The long-term behaviour of dynamical systems as the solar system are being studied by N-body simulations as well, but clearly there are much higher requirements on the accuracy of the individual orbits in contrast to the star cluster problem. Therefore for the solar system dynamics symplectic methods, using a generalized leap-frog, like the widely used Wisdom–Holman symplectic mapping method (Wisdom and Holman 1991) are the standard integration method. Symplectic mapping methods do not show secular errors in energy and angular momentum.

However, in their standard implementation they require a constant time-step (but see recent new developments described in the following subsection). A generalization using a time transformation simultaneously with the generalized leap-frog has been suggested which can cope with variable time-steps (Mikkola 1997b).

It has been proposed to reduce secular errors in Hermite schemes and direct *N*-body simulations to a level comparable with symplectic methods by using a time-symmetric scheme. A small variation in the Hermite corrector is needed, which allows to iterate to convergence (few iterations usually enough) and individual time-steps made reversible through another iteration (Hut et al. 1995; Funato et al. 1996; Makino et al. 1997). How well this generally works and its relation to symplectic schemes is presently not clear. But it has been well used for direct *N*-body simulations of planet formation and planetary systems (Kokubo et al. 1998; Makino et al. 1997). These codes though are still on the level of NBODY4, because they do not use the Ahmad–Cohen neighbour scheme—even in the smallest steps full force calculations over all *N* particles are needed. NBODY6++ has been similarly improved using an extended Hermite scheme to allow iteration, for a hybrid *N*-body and Fokker–Planck simulation of planetesimal growth in protoplanetary disks (Glaschke et al. 2014; Amaro-Seoane et al. 2014) (no GPU implementation with NBODY6++GPU yet).

In Mikkola and Aarseth (1998) it is stressed that even with a newly applied classical method secular errors in the integration of close binaries can be strongly reduced. One should keep in mind though, that the *N*-body integration schemes discussed in this paper yield excellent results in the star-cluster research (see Sect. 4) but are unsuitable for long-term solar system studies, because they generally have secular errors, although small. Due to the inherently physically chaotic nature of star clusters remaining small secular errors can usually be tolerated. It means that the solution found in the computer always stays near a permitted solution of the underlying Hamiltonian, even if it does not stay on the one trajectory which belongs to the initial conditions (Quinlan and Tremaine 1992). But a recent dynamical study has reiterated that it may not be sufficient just to check a few globally conserved quantities, because that could be dominated by a few high energy objects (binaries) and could cover up errors in other parts of the system (Wang and Hernandez 2021).

As outlined above in star cluster simulations the secular errors are being kept small relative to typical values of energy and angular momentum and an accurate reproduction of all individual stellar orbits is not generally required.

5.5 New approaches

A completely new code, called PETAR has been introduced (Wang et al. 2020a). It is a hybrid *N*-body code, which combining the P^3T (particle-particle particle-tree) method (Oshino et al. 2011; Iwasawa et al. 2015, 2016, 2017) and a slow-down time transformed symplectic integrator (SDAR) (Wang et al. 2020c). The latter is mathematically similar to a KS (Kustaanheimo and Stiefel 1965) regularization, using a time transformation in a similar way (based on the Poincaré transform of the Hamiltonian, Preto and Tremaine 1999; Mikkola and Merritt 2008), but regarding the

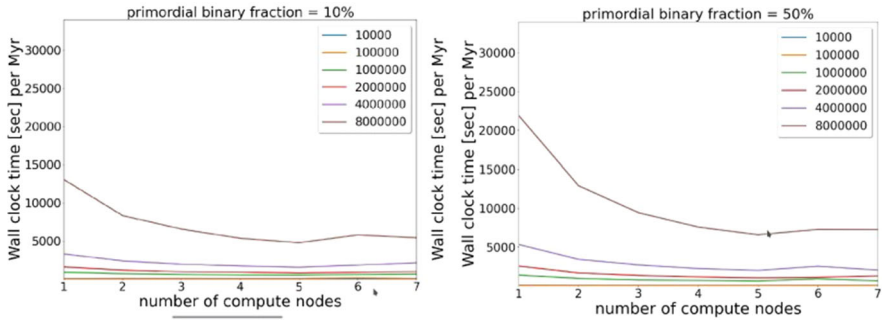

Fig. 5 Strong scaling of the novel PeTar code Wang et al. (2020a), showing wall clock times obtained on the Juwels-Booster as a function of number of compute nodes, for particle numbers up to eight million and binary fractions of up to 50%. The benchmarks have been done by Qi Shu, and will be published in Spurzem et al. (2022)

canonical coordinate transformation it uses an extended classical phase space rather than the 4D KS space. Both regularization methods also employ a slow-down procedure. PETAR uses the parallelization framework for developing particle simulation codes (FDPS, Iwasawa et al. 2016, 2020) to manage the particle-tree construction and long-range force calculation. For single and binary stellar evolution the standard SSE and BSE packages are used as in e.g. MOCCA (Hurley et al. 2005; Banerjee et al. 2020; Kamlah et al. 2022b).

The code is conceptually ahead of NBODY6++GPU in several respects; parallelization of a large number of hard binaries is included and a domain decomposition makes it easier to go to particle numbers much larger than 10^6, as well as the use of the TREE scheme for distant groups of particles, rather than the Ahmad–Cohen neighbour scheme in NBODY6++GPU. We show in Fig. 5 its excellent strong scaling obained on the Juwels Booster supercomputer in Germany (Jülich Supercomputing Centre 2021).

In Wang et al. (2020a, the paper about the PETAR code) performance comparisons with NBODY6++GPU seem too pessimistic in comparison with benchmarks published in Huang et al. (2016) and further recent tests done with up to 1.6×10^7 particles to be published soon. Undoubtedly, PETAR is ahead in terms of parallelization of binaries, but also in NBODY6++GPU regularized binaries can and will be parallelized soon. Also the paper presents a couple of convincing comparisons between both codes, but a real long time model comparison with many binaries is still work in progress. The problem is, that the single and binary stellar evolution in NBODY6++GPU has a much stronger coupling to the dynamical evolution of binaries and close encounters – that is from a programmer's viewpoint a trouble (as stated in Wang et al. 2020a), but it is important when following very hard and relativistic binaries (Rizzuto et al. 2021, 2022). Even the TREE algorithm is not really essential—inherently it can be much faster than the direct Hermite scheme (even with Ahmad–Cohen neighbour scheme), but it depends on the accuracy required. By comparison of NBODY6++GPU with the BONSAI TREE code (Bédorf et al. 2012) it has been shown that if same accuracy is required, performance difference is not significant (Huang et al. 2016).

This can be also seen in Sect. 5.3 from the performance analysis of NBODY6++GPU—even for more than a million bodies the regular distant forces are not the bottleneck, they have been effectively parallelized.

Another novel approach is based on forward symplectic integrators (FSI) (Chin 1997; Chin and Chen 2005; Chin 2007; Dehnen and Hernandez 2017). It is called BIFROST (Rantala et al. 2021, 2023), uses MPI parallelization and GPU acceleration and shows competitive benchmarks for very large N (million and more). The authors note that the FSI approach has hardly been used in the community, even though it generates very accurate orbital integrations. However, as discussed above, for most star cluster simulations orbit integration with maximum machine precision is not really needed; however, for the innermost regions of nuclear star clusters, with stellar orbits around supermassive black holes, this will be important and FROST may turn out to be excellently suited for such environment. On the other hand the planetary system and protoplanetary disk simulation community regularly uses either symplectic schemes or the improved iterated Hermite schemes (see above Sect. 5.3). A very significant innovation in FROST is MSTAR—a fast parallelized algorithmically regularized integrator. Instead of classical and algorithmic chains, which assemble their particles linearly (in a chain), MSTAR uses a minimum spanning TREE, so the chain can have branches. That leads to smaller average distances within chain particles as before, reduces computing time and errors. Such an algorithm could be as well used for the other chain regularizations.

Finally, hybrid codes have been constantly designed and used for a while to amend the direct N-body for a large number of distant particles. It started already with NBODY5 which was coupled to a TREE scheme (McMillan and Aarseth 1993); NBODY6++ has been hybridized with a series expansion code (Hemsendorf et al. 2002) (sometimes also called self-consistent field (Hernquist and Ostriker 1992), SCF). Last, but not least there is a new hybrid code ETICS (Meiron et al. 2014), which has been coupled with PHIGRAPE, and applied to the loss cone problem in a nuclear star cluster around a binary supermassive black hole (Avramov et al. 2021).

6 Astrophysics in star clusters

6.1 Single stellar evolution

In realistic star cluster simulations all stars undergo stellar evolution as time proceeds, see e.g., Church et al. (2009) and therefore, a large array of stellar evolutionary processes must be considered. We briefly outline the fundamentals of single stellar evolution (Sect. 6.1) because it is essential to understand the complexities that need to be modelled before we move on to an area, in which collisional N-body simulations find some of their strongest applications, which is binary stellar evolution (Sect. 6.2) in dense star clusters. The discussion in this Sect. 6.1 is primarily based on Kippenhahn et al. (2012), but a more recent review may also be found in Salaris and Cassisi (2017).

A star is a self-gravitating object of a hot plasma, which emits energy at the surface in form of photons (and from the inner regions in the form of neutrinos). Furthermore, it is spherically symmetric in the absence of rotation, magnetic fields and a sufficiently close companion or multiple companion stars that induce interior oscillations and bulges through tidal interaction or deform the star through mass transfer. These are typical assumptions in 1D modelling of single stars and they yield four fundamental structure equations that govern stellar evolution under the assumption of hydrostatic equilibrium. Any deviation from hydrostatic equilibrium will become increasingly important in harder binary stars.

Energy transport in a star is either radiative or convective (where convective transport can also include some conduction, which is not that important). Whether it is one or the other is given by the Schwarzschild stability criterion, which compares the temperature gradient in the radiative case with the temperature gradient by an adiabatic movement of matter elements: $\nabla_{\rm rad} < \nabla_{\rm ad}$. The less practical Ledoux criterion also takes into account a possible gradient in the density and chemical composition of a star. If some matter is unstable according to the Ledoux criterion, then convection will set in and will mix the material until stellar homogeneity. This process will diminish these gradients. Therefore, in practice the Schwarzschild criterion is more commonly used.

Radiative energy transport is commonly described using a diffusion equation. For convection, on the other hand, there is a convective gradient and since no complete theory of convection exists, the problem is approximated using mixing-length theory (MLT). MLT describes the convective temperature gradient $\nabla_{\rm c}$ surprisingly well despite a large number of unrealistic assumptions, e.g., all convective "bubbles" are assumed to travel the same distance due to buoyancy forces until they disappear leading to the dispersion of all their energy to the next level. MLT is parameterised globally by $\alpha_{\rm MLT}$, which is the ratio of the mixing length to the pressure scale height. $\alpha_{\rm MLT}$ is around 2 for Solar models. Since in deep stellar interiors, convection is very efficient and thus the "blobs" move adiabatically, it is $\nabla_{\rm c} \simeq \nabla_{\rm ad}$. In the outermost layers (low densities), however, convection is not so efficient, a lot of energy is lost by a blob moving up and the energy transport is super-adiabatic even approaching the radiative gradient in the extreme: $\nabla_{\rm rad} > \nabla_{\rm c} > \nabla_{\rm ad}$.

The chemical composition of a star changes with time due to nuclear reactions in its interior. It can also be subject to convective mixing, sedimentation, rotation (angular momentum transport) and hydrodynamical instabilities. The inclusion of all of these effects is difficult, because it requires 3D treatment; but most currently used stellar evolution codes, such as Modules for Experiments in Stellar Astrophysics (MESA) (Paxton et al. 2011, 2013, 2015, 2016, 2018, 2019) or HOngo Stellar Hydrodynamics Investigator (HOSHI) (Takahashi et al. 2016, 2018, 2019; Yoshida et al. 2019) are 1D.

6.1.1 Two fundamental principles of stellar evolution

The general evolution of a star following the assumptions above is governed by two fundamental principles: the first one is the virial theorem (gravitational energy $E_{\rm g} =$

$-2E_{\rm i}$ total internal energy), which follows from the assumption of hydrostatic equilibrium in the star that is represented by a self-gravitating sphere (Sect. 6.1). The virial theorem implies that on contraction of a star that is modelled as an ideal gas, half of the liberated energy is radiated away and the other half is used to increase the internal energy, which means that the star is heating up. In other words, if stars lose energy from the surface, the star must contract overall and heat up, which is a consequence of its negative heat capacity. That does not mean that some parts like the stellar envelope are not expanding over the star's evolution, but what is certain that the largest part of the star is contracting over the life-time and heating up. Interestingly, massive stars, which are radiation pressure dominated, approach the limit of an unbound structure, which is one of the reasons why they lose mass much more easily.

The second fundamental principle is the Coulomb repulsion, which determines the sequence of nuclear burning phases. Due to the virial theorem above that leads to a general increase in the interior stellar temperature, nuclear burning phases follow a sequence of light to heavier elements, i.e. they start with hydrogen (H) burning (the main sequence (MS) phase), followed by helium (He) burning (horizontal branch (HB) phase), the carbon (C) burning phase and so on. This burning sequence stops when an iron (Fe) core is reached, because any further nuclear fusion is endothermic. We reach an "onion-like" stellar structure: in the outer layers original stellar material is still processing (H fusing to He), while at the centre an Fe and Nickel (Ni) core forms simultaneously if the stellar mass is large enough.

6.1.2 Timescales, energy conservation and homology

The following timescales are extremely useful in characterising the evolution of stars:

1. hydrostatic timescale $\tau_{\rm hydro}$: let us assume that the internal stellar forces are not balanced and the star is not in hydrostatic equilibrium anymore. The timescale to return to hydrostatic equilibrium is: $\tau_{\rm hydro} \simeq \frac{1}{2}(G\bar{\rho})^{-1/2}$. It is extremely short, on the order of seconds for White Dwarfs (WDs), of minutes for the Sun and of the order of days for Red Giants (RGs).
2. Kelvin–Helmholtz (thermal) timescale $\tau_{\rm KH}$: it is defined as the timescale during which the entire internal energy of star would be radiated away by its current luminosity. For the Sun it is on the order of 10 million years.
3. nuclear timescale $\tau_{\rm nuc}$: let us assume that the whole luminosity comes only from the nuclear energy reservoir within the star and that the luminosity stays constant at the current state for the duration of the thought experiment. For the Sun this the emission of all nuclear energy as radiation is on the order of 70 billion years.

In most phases of stellar evolution, we have $\tau_{\rm hydro} \ll \tau_{\rm KH} \lessapprox \tau_{\rm nuc}$ and mostly also even $\tau_{\rm KH} \ll \tau_{\rm nuc}$ for MS and core He burning (CHeB) stars. In late stellar evolution phases $\tau_{\rm KH}$ can approach $\tau_{\rm nuc}$.

If we look at the global energy conservation in stellar evolution, we arrive at the homology ("similarity") relations for stars. From these we can derive a mass-luminosity relation that is very fundamental in stellar physics. For MS stars, the homology analysis yields $L \simeq \mu^4 M^3$, where μ is the mean molecular weight

($rT \sim \mu m$). This relation implies that the luminosity does not directly depend on energy generation; also the proportionality factor predominantly depends on the opacity of the stellar material, which in turn is determined by its chemical composition. If the energy generation in the star changes, it will adjust itself such that is has the same luminosity as before.

Furthermore, a mass-radius (M–R) relation is derived from the homology relations for stars. The relation now depends on the energy generation too in contrast with the mass-luminosity (M–L) relation. For the two main nuclear cycles on the MS, we get for the CNO-cycle $R \sim \mu^{0.61} M^{0.78}$ and for the pp-cycle we obtain $R \sim \mu^{0.125} M^{0.5}$.

The M–L relation, the M–R relation and the Stefan–Boltzmann law for black-body radiation leads to the equation for the MS in the Hertzsprung–Russell diagram (HRD): $\log(L) = 8 \times \log(T_{\text{eff}}) + \text{const.}$ and also to lines of constant radius in the HRD, which follow $\log(L) = 4 \times \log(T_{\text{eff}}) + \text{const.}$.

The lifetime of stars is derived from the M–L relation and $\tau_{\text{nuc}} \sim E_{\text{nuc}}/L \sim M/L$ to get $\tau_{\text{nuc}} \sim M^{-2}$. This means that more massive stars are brighter, but have shorter lifespans. In phases beyond the MS, the nuclear reaction energy release is smaller and the luminosities are generally larger, which leads to shorter lifetimes. Consequently, the total lifetime of a single star is dominated by its time spent on the MS.

Through the homology relations values of the central temperature T_{c}, central pressure P_{c}, and central density ρ_{c} of a star on the MS are obtained, which all depend on the stellar mass and the nuclear energy generation. Increasing stellar mass along the MS leads to: (1) increase of central temperature T_{c}; (2) decrease of central density ρ_{c} if the CNO-cycle ($1\,M_{\odot} \lessapprox M$) is the dominant nuclear burning mechanism, while ρ_{c} increases if the pp-cycle ($M \lessapprox 1\,M_{\odot}$) dominates; (3) decrease of the central pressure. Hence, with increasing mass, stars along the MS are hotter and radiation pressure becomes increasingly dominant until it dominates completely for very high-mass stars.

Finally, we discuss the homologous contraction of a gaseous sphere. This analysis yields a relation between the central temperature and central density. For ideal gases, the contraction thereof leads to heating of the gas and for non-relativistic strongly degenerate gases, this contraction leads to cooling in a transition from non-degenerate to strongly degenerate region. This means that low mass stars will never ignite certain elements, because at some stage they become degenerate in the core and the central temperature drops upon further contraction.

6.1.3 Fundamental parameters-mass and composition

While they are incredibly useful to understand fundamental relations in stellar astrophysics, the homology relations (see Sect. 6.1.2) cannot be applied over the full evolution of the star and are typically only applied to MS stars. We need other ways to describe the full evolution of a star. In general, the fundamental parameters of stellar evolution are the zero-age MS (ZAMS) mass and the (homogeneous) chemical composition.

Other very important parameters independent of mass and composition are rotation and magnetic fields. Rotation can lead to additional interior mixing, which

changes the chemical composition of the star. Magnetic fields may influence the pressure balance and interact with convection and rotation, which is probably most important for massive stars.

6.1.4 Mass change of stars—stellar winds

The masses of all stars change throughout their lives through winds, parameterised by a stellar mass loss rate $\dot{M}$. Stellar winds are the outflows of matter leaving the stellar surface with an energy sufficient to escape from the star's gravity. The main question is what the nature of the force is that is powerful enough to overcome the star's gravity. Different types of stars have different winds. Recently, excellent reviews of the winds of lower mass stars were written by Decin (2020) and similarly of high-mass stars by Vink (2021).

1. Hot luminous stars (HMSs), such as massive MS or evolved stars ($R \sim 10\,R_\odot$), have strong and *fast* (terminal wind velocities of $v_\infty \sim 2000$–$3000\,\mathrm{km\,s^{-1}}$) stellar winds powered by radiative line driving (radiative forces that are exerted on atomic lines, such as ionized C, N, O or Fe-group elements; resonance lines in optically think regions just a couple of $R_\odot$ around the HMS). These have very high-mass loss rates $\dot{M}$ of 10^{-8}–$10^{-4}\,M_\odot/\mathrm{yr}$.
2. Cool luminous stars (CMSs), such as AGB intermediate mass stars (IMS) ($R > 100\,R_\odot$) have strong and *slow* ($v_\infty \leq 25\,\mathrm{km\,s^{-1}}$) stellar winds that are pulsation-driven. These two have very high-mass loss rates $\dot{M}$ of 10^{-8}–$10^{-4}\,M_\odot/\mathrm{yr}$. The fact the CMSs are cool, it is believed that close to the stellar atmosphere, these stars can form dust grains, because the pulsations from the star can form regions of large density just above the stellar atmosphere. The dust grains absorb momentum and collide with surrounding gaseous species and thus you get a launch of a stellar wind.
3. Solar-type stars (LMSs) have hot surrounding coronae and have a *weak* stellar wind that is a pressure-driven coronal wind of intermediate speeds ($v_\infty \leq 400$–$800\,\mathrm{km\,s^{-1}}$). They have very low mass loss rates $\dot{M}$ of $10^{-14}\,M_\odot/\mathrm{yr}$.

Many stellar evolution models used inside N-body codes express wind acceleration by a Γ factor. Γ is defined as the ratio of radiative over gravitational acceleration. Radiative acceleration is due to radiative pressure and introduces an extra force acting on a spherically symmetric, isothermal wind. It is related to electron scattering Γ_e or dust scattering Γ_d, for example. These quantities are introduced into the momentum equation of an isothermal, spherically symmetric stellar wind, which leads to an effective gravitational acceleration $g_\mathrm{eff}(r)$. Using $g_\mathrm{eff}(r)$, we can calculate the escape velocities and these are lower by the introduction of the extra force. However, it depends very strongly on the distance to the stellar surface, where this additional force is introduced; the farther out it occurs, the less impactful it becomes on the overall stellar mass loss rate. Therefore, since dust grains form very *close* to the star (e.g. in CMSs), these are very impactful on the mass loss rate. In red

supergiants (RSGs), on the other hand, these grains form much farther out and therefore, dust-driven winds are generally not relevant here.

Moreover, radiation transport and the chemistry in the wind are both essential to a full modelling of a stellar wind. It is important to state that in general, there is no full theory of stellar winds available (Decin 2020). Furthermore, the layperson is overwhelmed by the large number of mass loss rate prescriptions derived predominantly from observations, which differ enormously in magnitude and slope (Decin 2020). The choice of mass loss recipe has an enormous impact on the outcome of realistic *N*-body simulations and the dynamics of the star cluster as described in this review. As an astrophysical community, we are just at the beginning of unravelling the complexities of specific stellar winds, such as Wolf–Rayet (WR) stars (Sander and Vink 2020) or the impact of pulsations and variability on winds in AGB and post-AGB stars (Trabucchi et al. 2019) before a fully self-consistent theory can be envisioned.

6.1.5 Formation of compact objects and their natal masses, kicks and spins

Depending on the progenitor star core mass, a compact object such as a white dwarf (WD), neutron star (NS) or black hole (BH) may form. Oftentimes binary processes are involved (Willems et al. 2005; Fragos et al. 2009; Wong et al. 2012, 2014), but these are discussed in the next sub-chapter. The following processes apply to all single stars in the relevant mass ranges. The formation of a compact object is associated with a natal remnant mass, a natal kick and a natal spin, which are all subject to significant theoretical and observational uncertainty. Nevertheless, it is important to model these as accurately as possible, because the global dynamical evolution of a collisional stellar system critically depends on these. The natal mass depends on a number of factors and we will only focus now on the collapse mechanism and its associates fallback and not the mass loss in the progenitor star, although it is also instrumental. The impact of the mass loss has been discussed already in a previous section. Traditionally, the natal masses of the WDs (and their three main types HeWDs, COWDs, ONeWDs) and their dependence on the progenitor masses are modelled by Hurley et al. (2000); Hurley and Shara (2003). For NSs a maximum mass of around $2.5\,M_{\odot}$ (Linares 2018, 2020) and the relationship follows typically (Hurley et al. 2000), but the exact masses are unknown because of the large uncertainties mainly in the internal structure of a NS (Lattimer and Prakash 2004; Lattimer 2012). In addition to Hurley et al. (2000), the possibility of a so-called electron-capture SNe (ECSNe) that leads to the formation of a NS (Nomoto 1984, 1987; Podsiadlowski et al. 2004; Kiel et al. 2008; Ivanova et al. 2008; Leung et al. 2020b), which has very important properties that are discussed below, has been included in many codes (Belczynski et al. 2008; Banerjee et al. 2020; Kamlah et al. 2022a). Most attention has arguably been paid to the remnant BH masses (Eldridge and Tout 2004; Belczynski et al. 2008; Fryer et al. 2012) and a number of collapse mechanisms for certain mass ranges have been proposed. In simulations, the most popular prescriptions are the rapid or delayed core-collapse SNe models by Fryer et al. (2012) in combination with various (pulsational) pair instability SNe ((P)PISNe) stellar evolution recipes (Fryer et al. 2001; Yoshida et al.

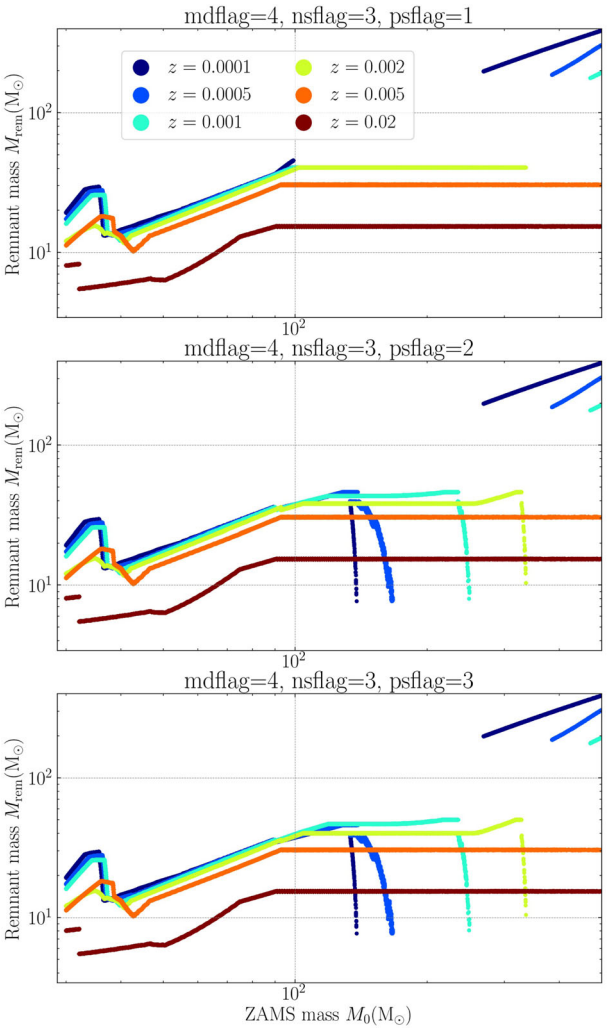

Fig. 6 Initial-final-mass-relations (IFMRs) of the black holes (BHs) from MCLUSTER samples ($N = 2.5 \times 10^4$ single ZAMS stars) depending on six different metallicities ranging from $Z = 0.0001$ to Solar metallicity at $Z = 0.02$. The MCLUSTER version uses `level C` stellar evolution (Kamlah et al. 2022a). Shown are the recipes for the "strong" (`psflag=1`) on top (Belczynski et al. 2016), "weak" (`psflag=2`) in the middle (Leung et al. 2019, 2020a) and the "moderate" (`psflag=3`) (P)PISNe on the bottom (Leung et al. 2019, 2020a). The ZAMS stars suffer wind mass loss via metallicity-dependent winds (`mdflag=4`) (no bi-stability jump) from Belczynski et al. (2010) and the core-collapse SNe are set to "rapid" (Fryer et al. 2012). Image reproduced with permission from Kamlah et al. (2022a), copyright by the author(s)

2016; Spera and Mapelli 2017; Woosley 2017; Woosley and Heger 2021; Belczynski et al. 2016; Leung et al. 2019, 2020a). Figure 6 shows a suite of small simulations when MCLUSTER (Kuepper et al. 2011; Kamlah et al. 2022a; Leveque et al. 2022b) is used as a population synthesis tool with `level C` stellar evolution Kamlah et al.

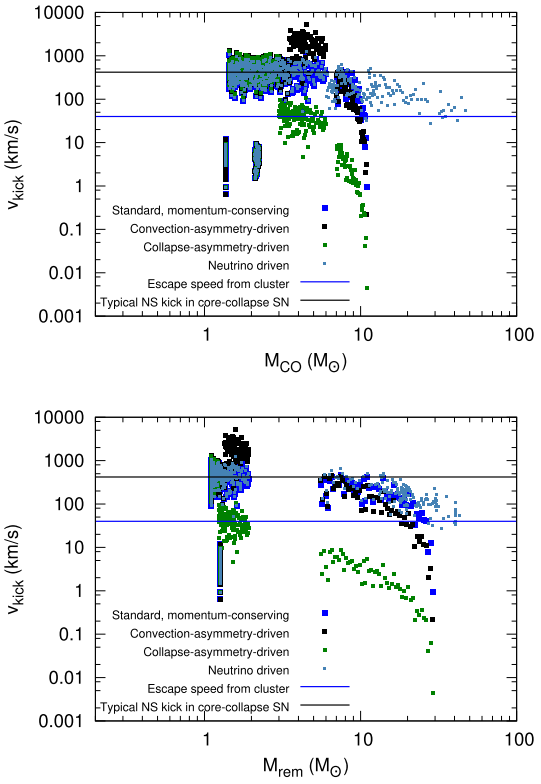

Fig. 7 Plot showing natal kick prescriptions, v_{kick} (all of them are at least also available in NBODY6++GPU, MOCCA, MCLUSTER and PETAR), as generated by NBODY7 in Banerjee et al. (2020). A metallicity of Z=0.0001 is assumed here. The models feature rapid core-collapse SNe from Fryer et al. (2012) and strong (P)PISNe from Belczynski et al. (2016). Due to the logarithmic vertical axis, direct-collapse BHs with a fallback fraction, $f_{fb} = 1$ and $v_{kick} = 0$ are not shown in these panels. The sharp drop in v_{kick} with increasing m_{CO} or m_{rem} is the approach towards direct collapse. The typical v_{esc} for the $M_{cl}(0) \simeq 5.0 \times 10^4\, M_\odot$ and $r_h(0) \simeq 2$ pc clusters considered here (blue, solid line). The velocity dispersion of the Maxwell distribution from all the kick models are scaled is $265.0\,\mathrm{km\,s^{-1}}$ from Hobbs et al. (2005). It is apparent that for these settings the collapse asymmetry driven kicks will produce most (stellar mass) BHs below v_{esc} of the cluster. Image reproduced with permission from Banerjee et al. (2020), copyright by ESO

(2022a). It shows all relevant remnant mass phases, which can be sub-divided into a core-collapse SNe, PPISNe, PISNe and a direct collapse phase in increasing ZAMS mass (this is an extension of the core-collapse SNe models for ZAMS masses above which PISNe is ineffective; in our case an extension of the rapid SNe models by Fryer et al. 2012). Two interesting conclusions can immediately be drawn here: first, the metallicity is incredibly important for the production of high-mass BHs, because progenitor stars with high metallicities will contain more metal lines for radiative wind mass loss. Secondly, the (P)PISNe prescriptions available from theory can have an enormous impact on the abundance of BHs. This might particularly important in Population III (Pop-III) star clusters, where intermediate mass black hole (IMBH)

progenitor stars are postulated to have large enough masses and crucially also low enough metallicities from birth to evolve by (P)PISNe from interior evolution alone (e.g., Kamlah et al. 2023; Wang et al. 2022 for recent *N*-body simulations of these clusters; see Sect. 6.4.3 for a more general discussion of Pop-III stars in the initialisation of star cluster simulations).

The magnitude of natal kicks results, broadly speaking, from an inherent asymmetry in the SNe process and generally their magnitude is rather uncertain (Hansen and Phinney 1997; Hobbs et al. 2005). They affects the dynamical stability of a binary (if one of the binary stars is forming a compact object) and are even able to disrupt a binary completely. This also implies that a large amount of gravitational binding energy in binaries may be removed from the cluster in this way and this will consequently impact the global cluster evolution. WDs are associated with low velocity kicks of the order of $10^0\,\mathrm{km\,s^{-1}}$ (Fellhauer et al. 2003), while neutron stars may reach kicks above even $10^3\,\mathrm{km\,s^{-1}}$ except in the case in which they form as a result of an electron-capture SNe (ECSNe). Here they receive then kicks of order of only $10^0\,\mathrm{km\,s^{-1}}$ (Gessner and Janka 2018) meaning that they can be retained in a star cluster (simulation) (Clark 1975; Abbott et al. 2017, 2020c; Manchester et al. 2005; Kamlah et al. 2022a). Natal kicks for BHs and NSs, which do not undergo an ECSNe (or AIC or MIC, see next chapter), receive kicks traditionally scaled by fallback during the SNe in simulations (Belczynski et al. 2008; Fryer et al. 2012). The more fallback of stellar material there is onto the proto-remnant core, the lower the resulting kick is. Furthermore, in simulations, it is typically assumed that the asymmetry is produced by a dominant process (Banerjee et al. 2020; Banerjee 2021): convection-asymmetry driven kicks (Scheck et al. 2004; Fryer and Young 2007; Scheck et al. 2008), collapse-asymmetry driven kicks (Burrows and Hayes 1996; Fryer 2004; Meakin and Arnett 2006, 2007) or neutrino-driven natal kicks (Fuller et al. 2003; Fryer and Kusenko 2006; Banerjee et al. 2020; Banerjee 2021). These lead to different retention fractions of BHs in star cluster simulations (Banerjee et al. 2020), which can be seen in Fig. 7 for a sample of NBODY7 simulations from Banerjee et al. (2020). It is apparent that for these settings the postulated collapse asymmetry driven kicks will produce most (stellar mass) BHs below v_{esc} of the cluster.

The natal spins of compact objects are important in general binary evolution and can also have significant impact on the mergers of compact objects, for example in a BH-BH merger (Morawski et al. 2018, 2019). In the following, we focus on BHs, but the same arguments can be extended to NSs and WDs and the discussion is largely taken from Kamlah et al. (2022a). In general, the spin angular momentum of the parent star does not necessarily translate directly into the natal spin angular momentum of the BH upon collapse. To quantify the spin, Kerr (1963) define a dimensionless parameter a_{spin} that accounts for the natal spin angular momentum. Banerjee (2021) assumes that the magnitude of a_{spin} for the BHs is set directly at the moment of birth without any related mass accretion of GR coalescence processes.

In the following, we highlight three natal spin models that are available now in NBODY7, NBODY6++GPU, MCLUSTER, PETAR and MOCCA, see also Kamlah et al. (2022a). The simplest model of BH natal spins, the `Fuller` model, produces zero natal spins (Banerjee 2021) as here the Tayler-Spruit magnetic dynamo can essentially extract all

of the angular momentum of the proto-remnant core, leading to nearly non-spinning BHs (Spruit 2002; Fuller and Ma 2019; Fuller et al. 2019). The second spin model is the `Geneva` model (Eggenberger et al. 2008; Ekström et al. 2012; Banerjee 2021). The basis for this model is the transport of the angular momentum from the core to the envelope. This is only driven by convection, because the `Geneva` code does not have magnetic fields in the form of the Taylor–Spruit magnetic dynamo. This angular momentum transport is comparatively inefficient and leads to *high* natal spins for low to medium mass parent O-type stars, whereas for high-mass parent O-type stars, the angular momentum of the parent star may already have been transported away in stellar winds and outflows and thus the natal BH spins may be low. The third and last spin model is the `MESA` model, which also accounts for magnetically driven outflows and thus angular momentum transport (Spruit 2002; Paxton et al. 2011, 2015; Fuller et al. 2019; Banerjee 2021). This generally produces BHs with much *smaller* natal spins than the `Geneva` model described above. The `Geneva` and the `MESA` models and their metallicity dependence are shown in Fig. 8.

6.2 Binary stellar evolution

In addition to the astrophysical processes that affect all stars in isolation, the proximity (orbital period $P_{\rm orb} \leq 10^4$ days (Eggleton 1996) to another star or compact object through the frequent encounters in collisional stellar systems or through intrinsic binary evolution, can affect the individual stars or compact objects dramatically and we need to account for these in the simulations. A population synthesis code should include them all (Eggleton 2006).

6.2.1 Stellar spin and orbital changes due to mass loss or gain

If two stars are in a binary, they can transfer mass via stellar winds and therefore also transfer angular momentum even if they are not yet undergoing Roche-lobe overflow (RLOF) (Hurley et al. 2002; Eggleton 2006; Tout 2008). If a secondary star accretes mass by passing through the wind of the primary star, it is spun up intrinsically by a fraction of the spin angular momentum that is lost by the donor star. The accretion rate is traditionally modelled by Bondi and Hoyle (1944), which depends on the wind velocity $v_{\rm W}$. This quantity is observationally difficult to determine (Decin 2020) and should be proportional to the escape velocity from the stellar surface of the star (Hurley et al. 2002).

The mass variations between companion stars also changes the orbital parameters of the binary star. In general, the eccentric orbit is circularised as a result of mass transfer being more effective at periastron than apastron. Additionally, the accretor star is slowed down by the drag induced by the wind it passes through and this dissipates angular momentum away from the system. The orbital circularisation timescale $\tau_{\rm circ}$ as result of mass transfer is orders of magnitudes larger than the equivalent timescale caused by tidal friction for the same binary star system (see Sect. 6.2.2).

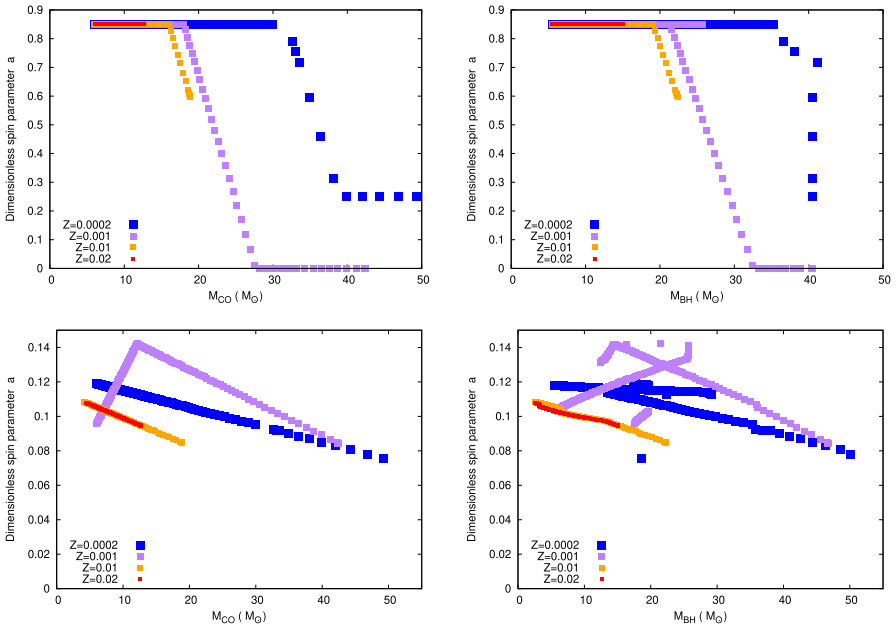

Fig. 8 Plot showing the magnitude of dimensionless spin parameter, $a_{\rm spin}$, of stellar-remnant BHs at birth (i.e., of BHs that have not undergone any mass accretion or GR coalescence after their formation) as a function of the progenitor star's carbon-oxygen core mass, $M_{\rm CO}$ (left column), and the BH mass, $M_{\rm BH}$ (right columnn; all of them are at least also available in NBODY6++GPU, MOCCA, MCLUSTER and PETAR), as generated by NBODY7 in Banerjee (2021). Top panels: the *N*-body models corresponding to these panels employ the "Geneva model" of Belczynski et al. (2020) for BH spin and comprise only single stars initially, whose ZAMS masses range from (0.08-−150.0) $M_\odot$ and which are distributed according to a standard Kroupa IMF (Kroupa 2001). The models feature rapid core-collapse SNe from Fryer et al. (2012) and strong (P)PISNe from Belczynski et al. (2016). The models are shown for four metallicities, Z= 0.0002, 0.001, 0.01, and 0.02 as indicated in the legends. Bottom panels: the *N*-body models corresponding to these panels employ the "MESA model" of Belczynski et al. (2020) for BH spin. The other model characteristics are the same as those in the top panels except that the "weak" PPISNe mass prescription (Leung et al. 2019) is utilized (resulting in the non-monotonic behaviour with respect to $M_{\rm BH}$, which, here, extends up to $\simeq 50\,M_\odot$ as opposed to the models in the top panels, where $M_{\rm BH}$ is capped at $\simeq 40.5\,M_\odot$ due to the use of Belczynski et al. (2016). Image reproduced with permission from Banerjee (2021), copyright by the author(s)

6.2.2 Effects of tidal damping

Observations show that the rotation of close binary stars is synchronised with the orbital motion without any dynamical mass transfer having taken place (Lurie et al. 2017; Mazeh 2008; Meibom and Mathieu 2005). Therefore, there must exist a torque that transfers angular momentum between the stellar spin and the orbit in such a way that the binary approaches the observed equilibrium state that is characterised by corotation (spin-orbit synchronisation timescale $\tau_{\rm sync}$) and a circular orbit (circularisation timescale $\tau_{\rm circ}$) (Zahn 1977; Hut 1981; Hurley et al. 2002; Tout 2008).

Alternatively, dissipation of energy might also lead to an accelerated in-spiral of the binary stars (Hut 1980; Rasio et al. 1996; Tout 2008).

When two binary star members are detached but sufficiently close, tidal interaction between them becomes important. The mere presence of a companion star causes a tidal force that elongates a star along the line between the centres of mass, thereby resulting in tidal bulges (see e.g., Hurley et al. 2002).

When the binary component rotates uniformly with a circular orbital motion, then the tidal bulges on its stellar surfaces are steady and the stars are in hydrostatic equilibrium. In such a scenario, we also speak of equilibrium tides. However, when this condition no longer holds, the hydrostatic equilibrium is disrupted and the star undergoes forced stellar oscillations. This scenario is described by a combination of equilibrium and now also dynamical tides, the latter of which produce much smaller tidal bulges than the former and they can also take any orientation (Eggleton et al. 1998; Eggleton 2006; Hurley et al. 2002; Zahn 1970, 1974, 1975, 1977; Siess et al. 2013). Dissipative processes within a star cause the tides to be misaligned with the line of centres. This results in a torque that transfers angular momentum between the stellar spin and the orbit (Hurley et al. 2002). This dissipation is non-conservative and happens on relatively long timescales (Eggleton 2006).

The dissipative processes within a star depend on the stellar structure. Typically, a distinction is made between stars with appreciably deep convective envelopes and stars with radiative envelopes. The tides dissipate energy and the binary system approaches an equilibrium state that is characterised by a circular orbit and corotation (Zahn 1977; Hut 1981; Hurley et al. 2002; Tout et al. 2008).

In stars with appreciably deep convective envelopes, turbulent viscosity that acts on equilibrium tides (the same effect on dynamical tides is negligible, Zahn 1975, 1977) is the most efficient form of dissipation (Kopal 1978; Hut 1981; Hurley et al. 2002). The dissipation takes shorter than the nuclear burning timescale $\tau_{\rm nuc}$ (see Sect. 6.1.2) (Zahn 1989, 1991; Hurley et al. 2002).

In stars with radiative envelopes, radiative dissipation near the surface of the star causes an asymmetry in the internal stellar oscillations induced by tides and the tidal field itself. This leads to a torque that is necessary for the binary system to approach the equilibrium state (Zahn 1977, 1989, 1992; Hurley et al. 2002) and in sufficiently close binaries this happens on shorter timescales than the nuclear burning timescale $\tau_{\rm nuc}$ (Zahn 1975). This radiative damping on the dynamical tides is the most efficient process to achieve the equilibrium state in binary stars with member stars that do not have an outer convective zone. However, if they do then the aforementioned turbulent friction on the equilibrium tides provides the primary torquing (Zahn 1975, 1977, 1989).

$\tau_{\rm sync}$ and $\tau_{\rm circ}$ in binary stars with convective envelopes are typically orders of magnitude smaller than those with radiative envelopes (Zahn 1977; Hurley et al. 2002). $\tau_{\rm sync}$ and $\tau_{\rm circ}$ are generally not equal except in a limiting case (Zahn 1977).

If the stars are degenerate but have sufficient stellar structure, i.e. WDs and NSs, then the above two dissipative mechanisms cannot be used as the stellar structure is significantly different. WDs will have very low spins, because the progenitor AGB star has already spun down in its expansion. Furthermore, in WD-WD binaries, the

orbit will already be circularised (in the absence of WD natal kicks, Fellhauer et al. 2003) due to the stellar wind mass and thus angular momentum loss. For this reason only the synchronisation timescale $\tau_{\rm sync}$ due to degenerate damping is of importance here and it is only applicable for close systems. $\tau_{\rm sync}$ in WD-WD, WD-NS and NS-NS binaries could exceed the age of the Universe (Campbell 1984).

6.2.3 Dynamical mass transfer and its stability

Apart from mass transfer through stellar winds, mass transfer can also happen via RLOF. This happens when the primary star fills it RL as a result of stellar expansion or in-spiral. The subsequent mass transfer then happens through the innermost Lagrange point. Typically, this process depends strongly on the mass ratio of the binary (Eggleton 1983) and happens in corotating, circularised binaries but in some instances, it can also occur in highly eccentric binaries, that are a result of tidal capture.

In the RLOF mass transfer, also angular momentum is transferred. The stability of the mass transfer traditionally determined by three logarithmic derivatives of radii with respect to the mass of the RL-filling star following Webbink (1985, 2003): the derivative describing the rate of change of the RL radius $R_{\rm L}$ for conservative mass transfer (total mass and angular momentum conservation) $\zeta_{\rm L}$ (Eggleton 2006), the derivative at constant entropy s and composition of each isotope $X_{\rm i}$ throughout the star $\zeta_{\rm ad}$ and a third derivative that describes the rate of change of the radius of the primary with mass in equilibrium $\zeta_{\rm eq}$. The mass transfer rate $\dot{M}$ depends on the relative values of these derivatives (Tout 2008):

1. $\zeta_{\rm ad} < \zeta_{\rm L} \rightarrow \dot{M}$ increases rapidly, there is positive feedback and the mass transfer is unstable, the secondary star cannot accrete at such a high rate and it expands $\rightarrow$ formation of a common envelope (CE) around the two stars (Paczynski 1976; Ivanova et al. 2013; Ivanova 2019).
2. $\zeta_{\rm eq} < \zeta_{\rm L} < \zeta_{\rm ad} \rightarrow \dot{M}$ decreases in its immediate response, but then expands on a thermal timescale.
3. $\zeta_{\rm L} < \zeta_{\rm ad}$ & $\zeta_{\rm L} < \zeta_{\rm eq} \rightarrow \dot{M}$ decreases initially, because the stellar radius decreases. RLOF happens again, when the primary fills it RL again.

On these basis of these exponents alone, it is possible to make a number of arguments on the evolution of Cataclysmic Variables (CVs), Algols and other exotic binary stars.

6.2.4 Common-envelope evolution

The process of CE evolution (CEE) is instrumental in compact binary and close binary formation. Ivanova et al. (2013); Ivanova (2016, 2018, 2019); Paczynski (1976). A CE is the outcome when $\zeta_{\rm ad} < \zeta_{\rm L}$ in RLOF or when two stars collide, where one of the stars has a dense core. Generally, CEE occurs when the primary star transfers more mass on dynamical timescales than secondary can accept. It strongly

depends on the instabilities in the RLOF preceding the formation of a CE (Olejak et al. 2021). The CE expands and thus rotates more slowly than the orbit of the secondary and primary star. This causes friction, the binary spirals in and transfers orbital energy to the envelope. Either so much energy in this process is transferred that the envelope is expelled completely leaving behind a close binary in corotation or in the process of in-spiral the binaries coalesce (Eggleton 2006; Hurley et al. 2002; Tout et al. 1997).

The CE is traditionally modelled with the "$\alpha\lambda$" energy-formalism (Webbink 1984; Tout et al. 1997; Hurley et al. 2002), which assumes energy is conserved and where α ($\alpha < 1$ if no other energy sources other than the binding and orbital energy are present; it can be as high as $\alpha = 5$ otherwise, Fragos et al. 2019) is the "efficiency" of the energy re-use and λ is a measure of the binding energy between the envelope and the core of the donor star and should depend on the type of the star, its mass and its luminosity (Dewi and Tauris 2000; Claeys et al. 2014; Ivanova 2019; Olejak et al. 2021). This picture is very simplistic and does not take into account the myriad of processes that go on during CEE, which are also not fully understood yet (Ivanova et al. 2013; Ivanova and Nandez 2016; Ivanova 2019; Ivanova et al. 2020). On the other hand, the $\alpha\lambda$ energy-formalism is computationally very efficient and therefore it is widely used in population synthesis codes that require fast and robust stellar evolution computations (Hurley et al. 2002; Belczynski et al. 2008; Claeys et al. 2014; Eldridge et al. 2017; Mapelli 2018; Breivik et al. 2020; Kamlah et al. 2022a). Some of these also allow for recombination energy of hydrogen in the cool outer layers of the CE being transferred back into the binding energy of the CE.

Recently, a new formalism has been developed by Trani et al. (2022), which solves a binary orbit under gas friction with numerical integration. This means that the authors do not approximate CE as an instantaneous process, unlike in many binary population synthesis (BPS) codes around. The new formalism, which can be easily implemented in BPS codes, provides a significant upgrade, which can explain observations of post-CE binaries which non-zero eccentricities (Kruckow et al. 2021).

In a binary consisting of a NS or a BH and a giant star, after the CE has been ejected and if the binary survives this phase, the H-rich envelope of giant stars might be stripped completely off. Now, the binary consists of a BH or a NS orbiting a naked He star. There might now be subsequent mass transfer from the naked He star to the NS of BH. This post-CE RLOF mass transfer leaves behind a so-called "ultra-stripped" He star that explodes in an ultra-stripped SNe (Tauris et al. 2013; Tauris 2015; Tauris et al. 2017). This type of SNe is significantly different from the typical core-collapse SNe and the process of ultra-stripping leads to a significant decrease in BH-NS and BH-BH mergers and a slight increase in NS-NS mergers (Schneider et al. 2021).

6.2.5 Mergers and general relativistic merger recoil kicks

An outcome of CEE may be the coalescence of the two stars. The subsequent merger product depends on the relative compactness of the two stars and thus it depends on the stellar evolutionary stage (Tout et al. 1997; Hurley et al. 2002). If similar in stellar

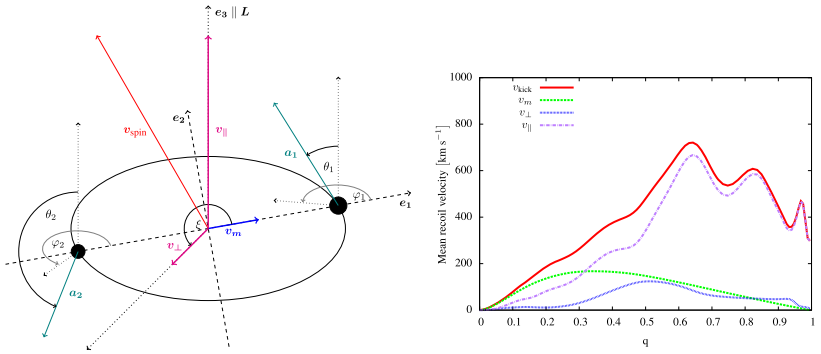

Fig. 9 *Left-hand side:* Conceptual picture presenting components of the recoil velocity. Dashed lines represent a Cartesian coordinate system in the orbital plane: $\mathbf{e_1}$ and $\mathbf{e_3}$. A vertical dotted line is a line perpendicular to orbital plane ($\mathbf{e_3}$, parallel to orbital angular momentum). The red vector is the kick component related to spin asymmetry, and magenta vectors are its projections on the plane and parallel to $\mathbf{e_3}$. The blue vector represents the mass inequality contribution. The black filled circles represent a pair of BHs, their spins and orientation in a spherical coordinate system are illustrated. This drawing also reflects typical proportions between recoil velocity components. *Right-hand side:* Example of how each recoil velocity component depends on mass ratio q for a metallicity dependent spin vector from Belczynski et al. (2017). q is the only variable for the determination of v_m. Other components and the overall kick velocity depend also on spin magnitudes and orientations, in this case the mean value is plotted. As we can see, the major component is almost always $v_\parallel$, others only play a role for low q. Images reproduced with permission from Morawski et al. (2018), copyright by the author(s)

type, then the two stars mix completely. If one is much more compact than the other, then the more compact core sinks to the centre and the other mixes with the envelope. An unstable Thorne–Żytkow object is created if the merger involves a NS or a BH (Thorne and Zytkow 1977). Detailed calculations on the merger outcomes following coalescence and collisions, which are less likely than coalescence, but still relevant in star clusters (e.g., Rizzuto et al. 2021, 2022), depending on the initial stellar types have been tabulated in Hurley et al. (2002). A coalescence for our purposes here means that at least one of the members is a star with a core and that the binary has a circular orbit before merging, while a collision means an actual physical collision, where none of the binary members is an evolved stellar type, but the member can also be a compact object. Generally, the mixing and the final masses of the merger products are highly uncertain and only approximations can be made according to our current knowledge (Olejak et al. 2020; Kamlah et al. 2022a). There are recent attempts to unravel the masses and compositions of merger products of massive stars with hydrodynamical codes (Costa et al. 2022; Ballone et al. 2023) and they can be used to give approximate formulae for N-body or BPS codes in the future.

The merger of compact objects is associated with a general relativistic (GR) merger recoil kick due to the asymmetry in the GW (see also Kamlah et al. 2022a for a brief discussion with respect to NBODY6++GPU and MOCCA). The recoil velocity in this process depends on the mass ratio of the two compact objects and their spin vectors (Lousto et al. 2012) and can reach several hundreds km s^{-1} on average (Morawski et al. 2018, 2019), which is much larger than typical star cluster escape

speeds. Figure 9 (from Morawski et al. 2018, 2019) shows a conceptual picture of the geometry of a GR merger recoil kick in a BH-BH merger and the dependence of the mean recoil velocity on the mass ratio q of the two BHs for a metallicity dependent spin model from Belczynski et al. (2017). It can be seen that q has a huge impact on whether a GR merger recoil kick velocity exceeds the escape speed of the surrounding stellar (and gaseous) material or not. Equal mass mergers might be retained in nuclear star clusters (Schödel et al. 2014) and extreme mass ratio mergers might theoretically even be retained in open clusters (although IMBHs will probably not form there) (Baker et al. 2007, 2008; Portegies Zwart et al. 2010; Baumgardt and Hilker 2018). For (nearly) non-spinning BHs (FULLER model, Fuller and Ma 2019), the kick velocity is smaller than for high spins. For non-aligned natal spins and small mass ratios, the asymmetry in the GW may produce GR merger recoils that reach thousands of $\mathrm{km\,s^{-1}}$ (Baker et al. 2008; van Meter et al. 2010). The calculation of the mass ratio is straightforward and the spins may be calculated from, e.g., Hoffman and Loeb (2007) or Jiménez-Forteza et al. (2017).

Generally, the orbital angular momentum of the BH-BH dominates the angular momentum budget that contributes to the final spin vector of the post-merger BH and therefore, within limits, the final spin vector is mostly aligned with the orbital momentum vector (Banerjee 2021). In the case of physical collisions and mergers during binary-single interactions, the orbital angular momentum is not dominating the momentum budget and thus the BH spin can still be low. Banerjee (2021) also includes a treatment for random isotropic spin alignment of dynamically formed BHs. Additionally, Banerjee (2021) assumes that the GR merger recoil kick velocity of NS-NS and BH-NS mergers (Arca Sedda 2020; Chattopadhyay et al. 2021) to be zero but assigns merger recoil kick to BH-BH merger products from numerical-relativity fitting formulae of van Meter et al. (2010) (which is updated in Banerjee 2022). The final spin of the merger product is then evaluated in the same way as a BH-BH merger.

The inclusion of these kicks in direct N-body simulations is still unusual (e.g., Di Carlo et al. 2019, 2020a, b, 2021; Rizzuto et al. 2021, 2022; Kamlah et al. 2022a, b all do not include these in addition to missing PN terms), but it is worth mentioning Arca-Sedda et al. (2021) do include the GR merger recoil kicks by posterior analysis. NBODY7 (Aarseth 2012; Banerjee et al. 2020; Banerjee 2021) on the other hand does include GR merger recoil kicks based on Lousto et al. (2012); Hoffman and Loeb (2007). In MOCCA numerical relativity (NR) models (Campanelli et al. 2007; Rezzolla et al. 2008; Hughes 2009; van Meter et al. 2010; Jiménez-Forteza et al. 2017) have been used to formulate semi-analytic descriptions for MOCCA and NBODY codes (Morawski et al. 2018, 2019; Banerjee 2021; Belczynski and Banerjee 2020; Arca-Sedda et al. 2021; Banerjee 2022). Recently, GR merger recoil kicks have also been added to NBODY6++GPU (Arca Sedda et al. 2023a) following Campanelli et al. (2007); Jiménez-Forteza et al. (2017) and with this code version, the whole kick process can be followed self-consistently.

6.2.6 Accretion or merger induced collapse

In sufficiently close double degenerate COWD-COWD, ONeWD-ONeWD or COWD-ONeWD binary stars, sufficiently high and dynamically stable RLOF mass accretion of hot CO-rich matter may lead to a heating of the outer layers of the secondary, which will result in the ignition of nuclear burning (Saio and Nomoto 2004). If carbon burning is ignited in the COWD envelope, the heat will be transported the stellar core by conduction and then the secondary will evolve into an ONeWD (Saio and Nomoto 1985, 1998), which will eventually collapse into a NS if the critical mass of the ONe core is surpassed ($M_{\rm ecs} = 1.38\,M_\odot$) (Nomoto 1984, 1987; Belczynski et al. 2008). This ONeWD collapse is referred to as accretion induced collapse (AIC). If, on the other hand, the ignition happens in the centre then the star will undergo a SN-Ia explosion, which leaves no remnant behind.

Double degenerate COWD binaries may also coalesce without undergoing dynamically stable mass transfer. During this process the less massive forms a thick, turbulent accretion disk and the more massive COWD will accrete matter close to the Eddington limit. Here the carbon will be ignited on the envelope of the secondary and thus the outcome will be a ONeWD and no SN-Ia will happen (Saio and Nomoto 2004). Again, if the ONe core mass surpasses $M_{\rm esc}$, then the ONeWD will collapse into a NS and this is known as a merger-induced collapse (MIC). Other pathways for MIC are mergers of a ONeWD with any type of WD companion if the resulting merger mass surpasses the critical mass for NS formation (Saio and Nomoto 1998; Belczynski et al. 2008).

The distinction between AIC and MIC is made, because the former may be observed already through their stable mass transfer phase or in low-mass X-ray binary stars and the latter may be observed through gravitational waves observed with the Laser Interferometer Space Antenna (LISA, Ruiter et al. 2019).

6.2.7 Gravitational radiation and magnetic braking

Gravitational radiation emitted from sufficiently close binary stars ($P \leq 0.6$ days) transports angular momentum away from the system and drives it to a mass transfer state that might result in coalescence (Peters and Mathews 1963; Hurley et al. 2002; Eggleton 2006). The effect this radiation has on the orbit of the binary (excluding PN terms) may be obtained by averaging the rates of energy loss and angular momentum loss over an approximately Keplerian orbit (Peters 1964; Eggleton 2006). Gravitational radiation will circularise the orbit on the same timescale as the orbit shrinks until coalescence.

In co-rotating and sufficiently close binary stars, magnetic braking slows down the rotation of the individual star with a convective envelope, but also drains angular momentum from the orbit of the binary star, because tidal friction between the stars may conserve co-rotation (Mestel 1968a, b; Mestel and Spruit 1987; Eggleton 2006). As a result, this process will force a close binary to a state of RLOF within Hubble time. In some situations, this process is dominating binary evolution, such as in CVs above the orbital period gap (Schreiber et al. 2016; Zorotovic et al. 2016; Belloni

et al. 2018). In spin-spin period evolution ($P - \dot{P}$) of pulsars this process is also important (e.g., Kiel and Hurley 2006, 2009). Both processes outlined above are non-conservative.

6.3 Combining stellar evolution with collisional N-body codes

There are two main methods that stand out in practice concerning the integration of the complicated stellar evolution into *N*-body codes. Both of these, interpolation between tables or approximation of stellar evolution data by some interpolation (fitting) formulae as functions of mass, age and metallicity, has unique advantages and disadvantages that have been known for a long time (Eggleton 1996). As it stands now, the two approaches are not in competition, but rather complement one another (Hurley et al. 2000).

6.3.1 Interpolation between tables

This method calculates stellar parameters from detailed evolutionary tracks (e.g., Pols et al. 1998). These evolutionary tracks are derived from 1D stellar evolution codes and are in tabular format. They are necessarily rather large and therefore, this approach has historically been limited by memory availability on hardware (Eggleton 1996; Hurley et al. 2000; Agrawal et al. 2020). Unlike fitting formulae, stellar parameters from the given set of detailed tracks are calculated in real time with this method. Hence, one just needs to change the input stellar tracks to generate a new set of stellar parameters. It has been claimed that this approach is the most flexible, robust and efficient today when combining detailed stellar evolution with stellar dynamics (Agrawal et al. 2020).

Maeder and Meynet (1989); Schaller et al. (1992); Alongi et al. (1993); Bressan et al. (1993); Fagotto et al. (1994a, 1994b); Claret (1995); Claret and Gimenez (1995) constructed such tables, which were later then expanded upon and refined by Pols et al. (1998). In the aforementioned works, the convective mixing or overshooting length $l_{\rm OV}$ presents another hurdle, which describes the average distance by which convective cells push into stable regions (or radiative regions from Schwarzschild condition, Biermann 1932; Gabriel et al. 2014) beyond the convective boundary (Schaller et al. 1992; Pols et al. 1998; Joyce and Chaboyer 2018). This treatment was modified by Pols et al. (1998) and replaced with a "∇ prescription", which is based on the stability criterion itself ($\delta_{OV} = 0.12$ was found to best reproduce observations, Schroder et al. 1997; Pols et al. 1997, 1998; Hurley et al. 2000). This new criterion avoids physical discontinuities for disappearing classical convective cores. Further quantities that will influence the calibration of the luminosity L of a stellar evolution model are the nuclear reaction rates and the core Helium abundance Y. Another source of large uncertainty was left largely unchanged by Pols et al. (1998). This uncertainty has been described by Pols et al. (1998) as the "Achilles heel" in stellar evolution codes. This uncertainty is in the mixing length of $\alpha_{\rm MLT}$, which is derived from mixing-length theory (Böhm-Vitense 1958) to describe heat transport in the convective regions of stars (Joyce and Chaboyer 2018; Pasetto

et al. 2018) (see also Sect. 6.1). Pols et al. (1998) set α_{MLT}=2.0 (based on the Solar model). But not all stars with convective regions exhibit identical convective properties and α_{MLT} can show large variations from star to star (Joyce and Chaboyer 2018).

Even today, methods stellar evolution by interpolation between tables are being developed with increasing success as hardware memory capabilities also improve:

- SEVN Spera et al. (2015); Spera and Mapelli (2017); Spera et al. (2019), which has been completed for binary evolution (Sicilia et al. 2022) has been used extensively to study the evolution gravitational-wave source progenitor stars. Additionally, it is not available as SEVN2.0, which is integrated in PETAR Wang et al. (2020a).
- and COMBINE (Kruckow et al. 2018) codes, which also has binary evolution implemented (Kruckow 2020; Kruckow et al. 2021) has also been used extensively to study the evolution gravitational-wave source progenitor stars.
- METISSE code (Agrawal et al. 2020), which is based on the STARS (Eggleton 1971, 1972, 1973; Eggleton et al. 1973; Pols et al. 1995, 1997; Schroder et al. 1997), MESA (Paxton et al. 2011, 2013, 2015, 2016, 2018, 2019) and BEC (Yoon et al. 2006, 2012; Brott et al. 2011; Köhler et al. 2015; Szécsi et al. 2015, 2022). Unlike SEVN or COMBINE, this code does not yet account for binary stars. In general, METISSE will be another promising candidate for combining full stellar dynamics with detailed stellar evolution.

6.3.2 Interpolation/fitting formulae

A first attempt to incorporate simple stellar evolution fitting formulae in a direct *N*-body code was done by Aarseth (1996) on the basis of Eggleton et al. (1989). Later, as a successor to Eggleton et al. (1989) was created using the method developed by Pols et al. (1998). They based their code on the original Cambridge STARS stellar evolution program by Eggleton (1971, 1972, 1973); Eggleton et al. (1973); Pols et al. (1995, 1997); Schroder et al. (1997). The result are the famous SINGLE STELLAR EVOLUTION (SSE) fitting formulae, which for the first time included metallicity as a free parameter (Hurley et al. 2000; Hurley 2008b; Hurley et al. 2013a). Figure 10 shows the complex discretization of stellar phases and the possible evolutionary pathways between them in the SSE package. The figure has been included, because this fundamental structure still remains in many stellar evolution production codes today (see below).

In general, such fitting formulae take much more care and thus time to set up than method of interpolating between tables (Church et al. 2009), because the movement of a star in the Hertzsprung–Russell diagram (HRD) is highly non-uniform and erratic. Furthermore, they are also less adaptable to changes in stellar tracks, for example, when they need to be adjusted due to some new development in astrophysics. On the other hand, the SSE provides us with rapid, robust and analytic formulae, which can be easily modified and integrated into an *N*-body code along the lines of Aarseth (1996) and give stellar luminosity, radius and core mass of the stars

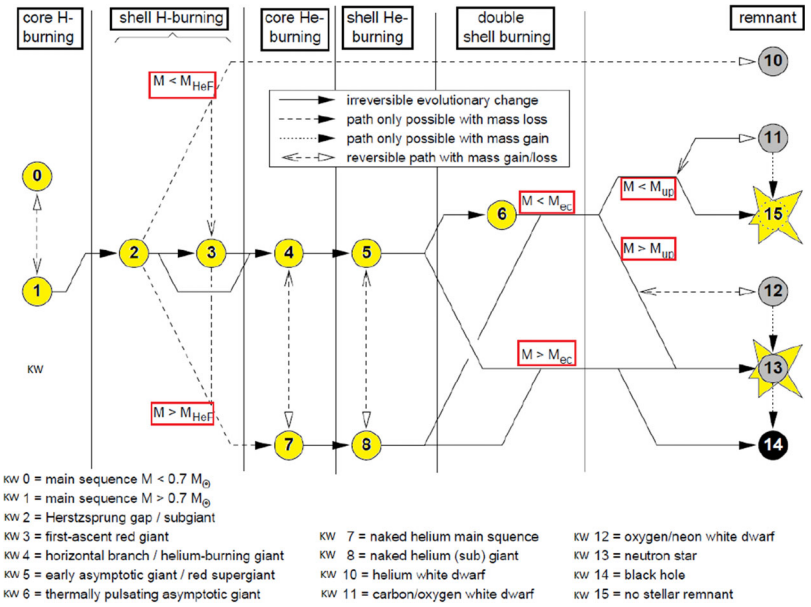

Fig. 10 Diagram showing the complete stellar evolution for the SSE code. It shows the possible paths of evolution through the various single stellar evolution phases. The paths between the individual stellar types are marked as general *irreversible* paths and *irreversible* paths only possible with *mass loss* or *mass gain*. Furthermore, there are also *reversible* paths with *mass gain or mass loss*. The meaning of the masses is as follows: $m_{\rm HeF}$ is the mass of the star to constitute the development of a degenerate He core on the GB and ignite He in a degenerate He flash at the top of the GB. $m_{\rm ec}$ and $m_{\rm up}$ deal with the remnant masses and pathways of Supernovae (SNe), when the AGB evolution is terminated, which is after the CO-core mass reaches a limiting value and undergoes SNe. $m_{\rm up} = 1.6\,M_\odot$ and $m_{\rm ec} = 2.25\,M_\odot$ depend on metallicity of the star and refers to the mass-range, where C burning leads to the formation of a degenerate ONe-core. This might collapse due to electron-capture (EC) of ^{24}Mg and result in NS production, see Sect. 6.1.5. However, in almost all stars, mass loss in the TPAGB phase leads to a shedding of the envelope, so that the final remnant is a WD. If this mass is extreme, then we get might get a mass-less remnant. If the mass of the core $M_{\rm c,BAGB} < 1.6\,M_\odot$, then the result is a COWD. With $M_{\rm c,BAGB} \geq 1.6$, then we will get a ONeWD. If $M_{\rm c,BAGB} > 2.25\,M_\odot$, then the star is massive enough to form Fe core, which result in SNes, which end up either in a NS or a BH. If mass loss comes into the equation, then we might get NS production from stars within $m_{\rm up} < M_{\rm c,BAGB} < m_{\rm ec}$. Image adapted from Hurley et al. (2000)

as functions of mass, metallicity and age for all stellar evolutionary phases (Hurley et al. 2000; Railton et al. 2014).

However, these formulae necessarily also discard a lot of crucial stellar evolution information (Hurley 2008b). For example, stellar mixing depends on several timescales and internal stellar structure parameters (Olejak et al. 2020) and so these cannot be modelled directly by the fitting formulae. Only the outcomes can be parameterised for stellar types of the individual stars along the lines of Hurley et al. (2002).

Despite these fundamental complications in stellar evolution modelling that persist to this day (see, e.g., Joyce and Chaboyer 2018; Pasetto et al. 2018; Tang and Joyce

2021; Agrawal et al. 2022) and which translate directly into the continuous and differentiable fitting formulae (polynomial form from least square fitting, Hurley et al. 2000), the SSE code has successfully, for the first time, provided us with a method by which we can evolve stars from ZAMS masses (0.1–100) $M_\odot$ (the models from Pols et al. 1998 only reach $50\,M_\odot$, but the SSE formulae can be safely extrapolated to $100\,M_\odot$, Hurley 2008b) rapidly and accurately (within 5% of detailed stellar evolution models over all phases of the evolution, Hurley et al. 2000) in N-body simulations throughout all evolutionary phases taking into account all of the astrophysical processes outlined in Sect. 6.1 and offering a metallicity range from 0.0001 to 0.03 with $Z_\odot \simeq 0.02$ being Solar metallicity as an input parameter.

However, for a complete picture we also need to model the binary evolution processes outlined in Sect. 6.2. For the fitting formulae this is provided by the BINARY STELLAR EVOLUTION (BSE) code (Hurley et al. 2002; Hurley 2008a; Hurley et al. 2013b), which is an add-on of the SSE package. This has been a huge success story and many full dynamical cluster simulations have utilised SSE & BSE to evolve the stars, e.g., Wang et al. (2016); Askar et al. (2017c); Di Carlo et al. (2019, 2020a, 2020b, 2021); Rizzuto et al. (2021, 2022); Kamlah et al. (2022a). The SSE & BSE codes have been the foundation for many other BPS codes:

- COMPAS (Team COMPAS et al. 2022)
- MSE (Hamers and Safarzadeh 2020)
- MOBSE (Giacobbo and Mapelli 2018, 2019; Mapelli et al. 2020) and related code called ASPS also used in Li et al. (2023),
- STARTRACK (Belczynski et al. 2002, 2008, 2020)
- COSMIC (Breivik et al. 2020) and its implementations in CMC (Kremer et al. 2019; Rodriguez et al. 2022)
- BSE-LEVELC (Kamlah et al. 2022a) and its implementation in MCLUSTER Kuepper et al. (2011); Kamlah et al. (2022a).

The fitting formulae from the SSE code are also implemented in BPS code BINARY_C (Izzard et al. 2004, 2006, 2009).

New fitting formulae have recently been constructed, which are derived from fitting to 1D HOSHI stellar evolution models (Takahashi et al. 2016, 2018, 2019; Yoshida et al. 2019) to extremely massive low metallicity (EMP; Pop-III) stars (Tanikawa et al. 2020, 2021a, b; Hijikawa et al. 2021). These are constructed such that they can be implemented into any of the BSE variants mentioned above in a straightforward fashion and therefore also into stellar dynamics codes such as N0BODY6++GPU (Wang et al. 2015).

6.4 Initial conditions for star cluster simulations

6.4.1 Global star cluster initial conditions

Defining appropriate global initial conditions for star cluster simulations is highly non-trivial as the formation of a star cluster and the stars within it depend on a large number of parameters that are very uncertain due to a lack of better theoretical understanding and or observations. In the following, we give an overview of the most important parameters in this context for N-body simulation of star clusters.

6.4.2 Initial 6D phase space distribution

In order to initialise an N-body star cluster simulation, we need to distribute the N particles in 6D phase space. A statistical approach as described in Sect. 3.1 is taken to realize a star cluster, which follows the probability density distribution $f(\vec{r}, \vec{v}, t)$. The full 6D distribution function is rarely known explicitly; under the assumption of steady state, such that f does not depend on time, the Jeans's theorem (Binney and Tremaine 2008) allows us to express f as a function of integrals of motion of a single star moving in the gravitational potential $\Phi(r)$. For now we assume spherical symmetry, so we have for example specific energy and specific angular momentum: $f = f(\vec{r}, \vec{v}) = f(E, L)$, which are defined as $E = v^2/2 + \Phi(r)$ and $L = |\vec{r} \times \vec{v}|$ (cf. Section 4.2). Deviations from spherical symmetry can be taken into account as well, see for example Sect. 6.4.6 for the importance of initial bulk rotation.

Examples of such self-consistent distribution functions are given by

$$f(E) = F_n E^{n-3/2}, \tag{48}$$

where n is an integer index and F_n a normalization factor to make sure that $f(E)$ is properly normalized as a probability density function. For $n = 5$ this results in the famous Plummer model (Plummer 1915), and for $n = 7/4$ another famous solution, a density cusp (Bahcall and Wolf 1976; Frank and Rees 1976) around supermassive black holes is found (Preto et al. 2004). In Binney and Tremaine (2008) these models are also called stellar polytropes, because their density distribution is the same as a gaseous polytrope (Chandrasekhar 1939) of the same index n. Analytical density distributions exist for $n = 0$, $n = 1$, and $n = 5$ (Kippenhahn et al. 2012), but for stellar systems only $n = 5$ is physically useful.

The theory of gaseous spheres also knows the isothermal solution, which is obtained for $n = \infty$; in stellar dynamics the equivalent is the isothermal sphere

$$f(E) = F_\infty \exp(-E/\sigma^2). \tag{49}$$

Here σ^2 is the r.m.s. stellar velocity dispersion, analogous to the temperature in a gaseous sphere. These models have some problem, because their radial extent is unlimited (Plummer and isothermal) or even their mass is infinite (isothermal). Therefore, and since real star clusters are often subject to a tidal cutoff due to the host galaxy, a cutoff radius is introduced (connected to a cutoff energy). If at the cutoff

radius the gravitational potential of an isolated star cluster would be Φ_0, then a relative potential Ψ and a relative energy ε are defined by

$$\Psi = \Phi - \Phi_0 \quad ; \quad \varepsilon = E - \Phi_0. \tag{50}$$

In that way the cluster extends from the center out to $\varepsilon = 0$ (and $\Psi = 0$), and lowered isothermal or Plummer distribution is defined as follows:

$$f(\varepsilon) = \begin{cases} f_\infty \exp(-\varepsilon/\sigma^2) & \varepsilon < 0 (E < \Phi_0) \\ 0 & \varepsilon \geq 0 (E \geq \Phi_0), \end{cases} \tag{51}$$

$$f(\varepsilon) = \begin{cases} f_5 \epsilon^{7/2} & \varepsilon < 0 (E < \Phi_0) \\ 0 & \varepsilon \geq 0 (E \geq \Phi_0), \end{cases} \tag{52}$$

Again f_5 and f_∞ have to be properly chosen normalization factors. The model Eq. (51) is the widely used King model (King 1966) ("lowered isothermal"). Note that some papers and books also prefer to change the sign of E (or ε), such that bound objects have a positive value. We do not follow this here to avoid confusion.

Even in spherical symmetry the distribution function could be 2D, since we have E and $|L|$ as constants of motion; it corresponds to the possibility that in spherical star clusters still at any given radius r the radial and tangential velocity dispersion may be different. So, a more general approach for the distribution function in case of an isothermal is

$$f(\varepsilon) = \begin{cases} f_\infty \exp(-L^2/L_0^2) \exp(-\varepsilon/\sigma^2) & \varepsilon < 0 (E < \Phi_0) \\ 0 & \varepsilon \geq 0 (E \geq \Phi_0), \end{cases} \tag{53}$$

which is also known as Michie (Michie 1963) distribution. Numerical solutions of the Fokker–Planck equations in 2D are based on such 2D distribution functions and Michie models could serve as potential initial models (see Sect. 3.3). It is interesting to note that the most well known 1D King distribution is actually based on the older, even more general (since 2D) Michie model; Ivan King himself gives an account of this King (1981).

1D King models are extensively used for initialising star cluster simulations (e.g., Rizzuto et al. 2021, 2022; Kamlah et al. 2022a). While the Plummer model needs two parameters (mass M and scale radius $r_\mathrm{h} \simeq 1.305 r_\mathrm{pl}$), the King model needs three parameters (mass M, scale radius r_pl and dimensionless central potential W_0). For intermediate King models ($2.5 \leq W_0 \leq 7.5$), the Plummer models are very similar ($r_\mathrm{h,Plummer} = 0.366 r_\mathrm{h,King}$) (King 2008). We note that Gieles and Zocchi (2015) developed a new family of lowered isothermal models called the LIMEPY models. Based on the 1D models of King a generalization in 2D for rotating star clusters is now being used and often described as rotating King models (see Sect. 6.4.6 and citations there).

Note that from $f(E)$ or $f(E, L)$ directly a numerical star cluster cannot be constructed, because E depends explicitly on r and implicitly through the gravitational potential (Eq. (30)). Therefore, in order to be self-consistent, the gravitational potential has to be determined by a velocity space integration over the

distribution function and then Poisson's equation solved to obtain the stellar density as function of radius (see e.g., the textbook by Binney and Tremaine 2008 for examples). In a final step a random procedure has to be used to obtain stellar positions and velocities. If density or gravitational potential are analytically known functions (like in case of a Plummer model) the entire self-consistent model can be constructed in one loop using random numbers (Aarseth et al. 1974).

6.4.3 Initial stellar mass function

In order to initialise star cluster simulations, we need to draw the ZAMS masses from an assumed distribution. For this purpose, we use an initial stellar mass function (IMF), a "Hilfskonstrukt" (Kroupa et al. 2013; Kroupa and Jerabkova 2018), as a mathematical formulation of an idealised stellar population that has formed from a singular star formation event. We will discuss in Sect. 6.4.5 that this is not the case in nature. An excellent review on the IMF and its construction has been provided by Hopkins (2018) (and sources therein) and it also explores the universality of the IMF ("unchanging distribution regardless of environment and over the entirety of cosmic history") and concludes that general the IMF is not universal. This has consequences for the initial conditions of star cluster simulations across cosmic time and we need to model the IMF of different stellar populations individually.

The IMF was established as a concept in a pioneering work by Salpeter (1955) as a quantisation of stellar masses in the Universe (Kroupa and Jerabkova 2019). In general, the number of stars in the IMF is given by

$$\xi_*(m) = \frac{\mathrm{dN}}{\mathrm{dm}}, \tag{54}$$

where dN is the number of stars formed in a small region, i.e. an embedded-cluster-forming molecular cloud core, in the mass interval m to $m + \mathrm{dm}$ (Jeřábková et al. 2018). The IMF is expressed as a (multi-)power law (powers are typically denoted by "α") depending on the stellar population to be modelled. For example, for Population I (Pop-I) an IMF from Kroupa (2001, 2002), Chabrier (2003) or Maschberger (2013) is chosen; they are quite similar. The standard NBODY-codes, such as NBODY6++GPU or NBODY7 provide tools to initialize a star cluster model with generalized Salpeter or Kroupa (Kroupa 2001) IMF's, in a mass range from 0.08 to 100 or 150 $M_\odot$. Note that also the initialization of lower mass objects has been prepared in the codes by Pavel Kroupa. Despite many observations over the last decades, the IMF for Pop-I stars is still quite uncertain, see Hopkins (2018) and sources therein.

For Pop-III stars, the IMF is very different. It becomes increasingly top-heavy for decreasing metallicity (Bromm et al. 2002; Bromm and Larson 2004; Marks et al. 2012; Bromm 2013; Stacy et al. 2016; Jeřábková et al. 2018; Kroupa et al. 2020). However, we do not have observations of Pop-III stars (yet; although even with the JWST it will be a difficult or impossible undertaking (Rydberg et al. 2013). On the other hand, de Souza et al. (2013) claim that some hundred SNe detections by JWST may be enough to constrain the IMF of Pop-III stars (see also Schauer et al. 2020 for a further discussion) and therefore, we do not have statistics from which to conclude an IMF. A flat IMF with $\alpha \simeq -1.0$ between $8\,M_\odot$ and $300\,M_\odot$ for Pop-III stars has

been proposed by Lazar and Bromm (2021). However, Fraser et al. (2017) use a Salpeter IMF (Salpeter 1955) of slope $\alpha \simeq -2.35$ with a maximum mass of around $87\,M_\odot$ instead. We will have to wait for observations of Pop-III stars or their remnants before we can reliably constrain their IMF.

6.4.4 Initial binary population

Almost all stars form in binary systems and some in higher order multiple systems (Goodwin and Kroupa 2005; Kroupa 2008; Milone et al. 2012). As with the IMF in Sect. 6.4.3, there is some debate on the universality of an initial binary population (IBP). In other words, it is contentious that the IBP is independent of environment, in which binaries form (Marks et al. 2015; Belloni et al. 2017). This is typically quietly assumed in the initialisation of star cluster simulations, at least in simulations of clusters made up of Pop-I stars (e.g., Askar et al. 2017c; Kamlah et al. 2022a). Although, we would expect this to vary for decreasing metallicity and higher redshift, because the environments and also the primordial gas from which the stars form have very different properties from Pop-I stars (e.g., Stacy et al. 2012; Stacy and Bromm 2013).

In any way, the IBP evolves on a cluster crossing timescale $t_{\rm cr}$. The widest binaries that form are dynamically disrupted, while in star clusters the hardest binaries harden further (Heggie 1975; Hills 1975b). This leads to a pronounced SN-Ia rate in star clusters (Shara and Hurley 2002). Binaries generally dominate the global, dynamical evolution of the star cluster by close Newtonian few-body interactions (binary-single and binary-binary encounters) Heggie and Hut (2003); Mapelli (2019).

A distinction is made following Kroupa (1995, 2008); Belloni et al. (2017) between a birth stellar population, where all protostars are embedded in circum-protostellar material, and an initial stellar population, which consists of pre-main-sequence stars and which are not embedded in circum-protostellar material.

The process from an initial to a fully formed main-sequence binary star population is called pre-main-sequence eigenevolution. Eigenevolution is the sum of all dissipative physical processes that transfer mass, energy and angular momentum between the companions when they are still very young and accreting (sentence directly cited from Kroupa 2008). Most obvious is the process of tidal circularization (e.g., Mardling and Aarseth 2001) of tight and initially highly eccentric binaries, which leads to a depletion of high eccentricities for small semi-major axes. In Kroupa (2008) there is a comprehensive description of eigenevolution and the relation between binary parameters at birth and after the pre-main sequence evolution, when typically N-body simulations start (see also further citations in Kroupa 2008 about observational binary data therein, and also Kroupa et al. 2013; Kuepper et al. 2011; Railton et al. 2014; Belloni et al. 2017). We present this as an example here, but it is not clear whether under all astrophysical circumstances such universal binary parameters are realized.

Dynamically, a binary star depends on four parameters: its system mass $m_{\rm sys} = m_1 + m_2$, its period P and correspondingly its semi-major axis a (via Kepler's third law), its mass ratio $q = m_2/m_1 \leq 1$ and its eccentricity

e=$(r_{\rm apo} - r_{\rm peri})/(r_{\rm apo} + r_{\rm peri})$ (Kroupa 2008), where $r_{\rm apo}$ and $r_{\rm peri}$ are the apocentric and pericentric distances, respectively. Thus, a complete initial binary population in a star cluster depends on the stellar IMF $\xi_*(m)$ (see Sect. 6.4.3), the period distribution $f_{\rm P}(\log P)$, the mass ratio distribution $f_{\rm q}(q)$ and the eccentricity distribution $f_{\rm e}(e)$ (Kroupa 2008; Moe and Di Stefano 2017; Belloni et al. 2017):

1. $f_{\rm P}(\log P)$: Kroupa (1995) show that

$$f_{\rm P}(\log P) = \eta \cdot \frac{\log(P) - \log(P_{\rm min})}{\delta + \left(\log(P) - \log(P_{\rm min})\right)^2} \tag{55}$$

   where $P_{\rm min} = 10$ days, $\delta = 45$, $\eta = 2.5$ and $P_{\rm max} = 2.188 \times 10^8$ days, because the initial binary fractions $f_{\rm b}$ is 100% (Goodwin and Kroupa 2005). Adjustments to this distribution were later made for high-mass stars with $m > 5\,M_\odot$ following Sana et al. (2012); Oh et al. (2015), where for these stars $f_{\rm P} \propto (\log(P))^{-0.55}$ with $P_{\rm min} = 1.412$ days and $P_{\rm max} = 3.162 \times 10^3$ days.
2. $f_{\rm e}$: typically, we distribute the binaries thermally, meaning angular momenta are distributed equally $f_{\rm e} = 2e$ (Kroupa 1995), although this might greatly overpredict observed merger rates according to Geller et al. (2019).
3. $f_{\rm q}$: the binary stars with members below $5\,M_\odot$ are distributed randomly and for masses above $5\,M_\odot$, the binary mass ratios are distributed uniformly ($0.1 < q < 1.0$) (Kiminki et al. 2012; Sana and Evans 2011; Sana et al. 2012; Kobulnicky et al. 2014).

Many direct N-body simulations usually start at a time when the star cluster is gas-free, when eigenevolution has terminated. Also dynamical interactions of binaries with each other and with single stars cause a further dynamical evolution of binary properties during the cluster formation phase. The "Kroupa" (Kroupa 1995) period distribution includes many wide binaries. They are dynamically ionized (disrupted) in a time scale very short compared to the relaxation time scale. Monte Carlo simulations (some of them start with binary fractions close to unity, Leigh et al. 2015) and direct N-body models, starting with lower binary fraction (but most of them tightly bound) converge quickly, as can be seen in Kamlah et al. (2022a). Therefore, one uses typically rather small binary fractions in initial models for long-term evolution of star clusters (order of 5–20%; Wang et al. 2016; Arca Sedda et al. 2023a, b, c). Also for the same reason simpler power laws for the initial distributions of $\log P$, e, and q are used (see e.g., Wang et al. 2022; Torniamenti et al. 2022). Note that in case of rotating star clusters the initial inclination of binaries with respect to the rotation axis of the cluster is a new possibly important parameter, which has not yet been examined.

It is sometimes quoted that small binary fractions are chosen in direct N-body simulations, because tightly bound binaries are computationally expensive; this may not be a problem in the near future. Already the PETAR code (Wang et al. 2020b, c) can use efficiently a very large number of binaries in the simulations (see Fig. 5). Also NBODY6++GPU potentially allows a good KS binary parallelization, which is work in progress. Since the treatment of interacting and relativistic binaries in PETAR is not

equivalent to the one used in NBODY6++GPU, tests and comparisons of both codes with respect to binary evolution are ongoing.

In summary of what we discussed so far in Sect. 6.4.1 to Sect. 6.4.4, during the initialisation of *N*-body simulations we need to distribute the stars in 6D phase space, draw their masses from some IMF, and distribute primordial binaries according to IBP (Kroupa 2008; Kuepper et al. 2011; Küpper et al. 2011). Furthermore, we generally need to make a decision if our star cluster is mass segregated at the beginning of the simulation (Fregeau et al. 2002; Šubr et al. 2008; Baumgardt et al. 2008), shows fractality (Goodwin and Whitworth 2004) and if it is or is not in virial equilibrium. Below, we highlight two more areas of active research when it comes to simulations of star clusters and their initialisation: multiple stellar populations in Sect. 6.4.5 and initial bulk rotation of the star cluster in Sect. 6.4.6, respectively.

6.4.5 Multiple stellar populations

Modern observational methods have made it possible to resolve multiple stellar populations (MSPs) in globular clusters, which can mostly be inferred from photometric diagrams such as colour-magnitude diagrams (CMDs) from multi-band HST photometry (e.g., Anderson and King 2000; Anderson et al. 2008; Gratton et al. 2012; Milone et al. 2012, 2013; Milone 2020; Milone and Marino 2022), as well as from abundance variations in integrated light (Bastian et al. 2019, 2020). Nowadays, MSPs have been confirmed in around 70 Galactic and extragalactic clusters (Milone et al. 2017a, b, 2018a, b, 2020a, b, c; Milone 2020; Milone and Marino 2022).

MSPs can have very diverse origins, see e.g., the review by Bastian and Lardo (2018). Recently, kinematic differences between multiple populations have been found in Galactic globular clusters (Martens et al. 2023). Dynamical simulations of different populations can be useful to unravel the origin of MSP and the relation between initial states and currently observed dynamics. Our direct NBODY6++GPU code allows for the distinction between different populations by defining a corresponding label for each star; this has been used by Hong et al. (2017b) to constrain the dynamical origin of multiple populations in intermediate-age clusters in the Magellanic Clouds. Another rarely used feature of NBODY6++GPU (but see Bialas et al. 2015) is that it can start with individual population data for every star (age, metallicity, population index). Also MOCCA simulations have been published Hypki et al. (2022) hosting two generations of stars as above in tidally filling and underfilling star clusters. They are able to reproduce the observed fractions and properties of second generation stars in the GCs of the Milky Way. For the time being there is no good way known to handle encounters and mixing of material from different populations in stellar collisions and binary mass overflow interactions in any of the codes.

We are still at the beginning of deciphering the complex picture of MSPs and their dynamical evolution using computational methods for collisional stellar systems. Nevertheless, the studies above are encouraging.

6.4.6 Rotation

The inclusion of initial bulk rotation in direct NBODY simulations of collisional stellar systems is still unusual (e.g., Hong et al. 2013; Wang et al. 2016; Askar et al. 2017c; Di Carlo et al. 2019, 2020a, b, 2021; Rizzuto et al. 2021, 2022; Arca-Sedda et al. 2021; Kamlah et al. 2022a), although it has been known for over a century that star clusters even today show significant imprints of rotation, which can, for example, be observed in deviations in the shapes of star clusters from sphericity (Pease and Shapley 1917; Shapley and Sawyer 1927; Shapley 1930; Kopal and Slouka 1936; King 1961; Frenk and Fall 1982; Harris 1976, 1996; Kormendy 1985; White and Shawl 1987; Lupton et al. 1987; Chen and Chen 2010; Bianchini et al. 2013). Moreover, present-day detectors and data processing methods have made it possible to resolve the photometry and kinematics of individual stars all the way down to the cluster centre revealing that rotational kinematic features vary between multiple stellar populations (Bianchini et al. 2016, 2018, 2019; Ferraro et al. 2018; Giesers et al. 2018, 2019; Lanzoni et al. 2018a, b; Kamann et al. 2016, 2018a, b, 2019; Sollima et al. 2019; Tiongco et al. 2019, 2021). Additionally, both observations and simulations support these results and find that star clusters show significant fractality (Ballone et al. 2020; Pang et al. 2021), and internal rotation at birth in general (Lahén et al. 2020; Ballone et al. 2021). Velocity anisotropy has been observed in star clusters with detected elongated structures (Pang et al. 2020, 2021), which might be induced by rotation.

So, how do we initialise rotating collisional stellar systems? Sometimes it is assumed that there exists a kind of "Maxwell's demon" that simply switches the direction of initial particle velocities to induce angular momentum to a N-body system and assuming the preservation of the spherical distribution function (e.g., Plummer 1911; King 1962; Wilson 1975) and angular momentum in the process (e.g., Lynden-Bell 1960; Lingam 2018). This procedure is not physical. We instead need distribution functions that at least depend on two integrals of motion, such as the total energy E and and the total angular momentum in the z-direction L_z (assuming that the system rotates around the z-axis initially and ignoring a third integral, which in some cases can be approximated by the total angular momentum of a star L^2 (Lupton and Gunn 1987), because a third integral is generally not analytically known). Such rotating equilibrium models were developed by Goodman (1983b); Einsel and Spurzem (1999); Longaretti and Lagoute (1996); Varri and Bertin (2012). They can be considered as generalizations of standard King models (King 1966), because their energy dependence is a lowered isothermal, and the additional term for the second independent variable is $\exp(-L_z/L_{z0})$ (analogous to Michie 1962). L_{z0} is a scaling constant; usually a dimensionless rotation parameter ω_0 is used (derived from L_{z0}, see e.g., Einsel and Spurzem 1999). The models are axisymmetric, with a rigid rotation of the inner parts of the cluster, a maximum of the rotation curve close to the half-mass radius, and a differentially decreasing rotation curve outside in the halo. Rotation supports only a fraction of the total kinetic energy (see Table 1 in Einsel and Spurzem (1999), and note that the 2nd column is erroneously labeled, it contains the percentage contained in rotational energy; i.e., for

$\omega_0 = 0.6$ we have 20% of the total kinetic energy in form of ordered rotational motion). Evolved star clusters obtained from these initial models agree quite well with observed clusters (Fiestas et al. 2006).

Due to the 2D velocity distribution function an anisotropy is possible between the velocity dispersions in radial direction (in cylindrical coordinates) and in rotational $\varphi-$ direction; the models are isotropic between radial and vertical direction (parallel to the rotation axis). Such models have been used as initial models in 2D Fokker–Planck (FP) modelling and direct N-body simulation (Kim et al. 2002, 2004, 2008; Fiestas et al. 2006; Fiestas and Spurzem 2010; Fiestas et al. 2012; Ernst et al. 2007; Hong et al. 2013; Kamlah et al. 2022b). Note that the models by Varri and Bertin (2012) are using a different form of the distribution function based on the Jacobian of

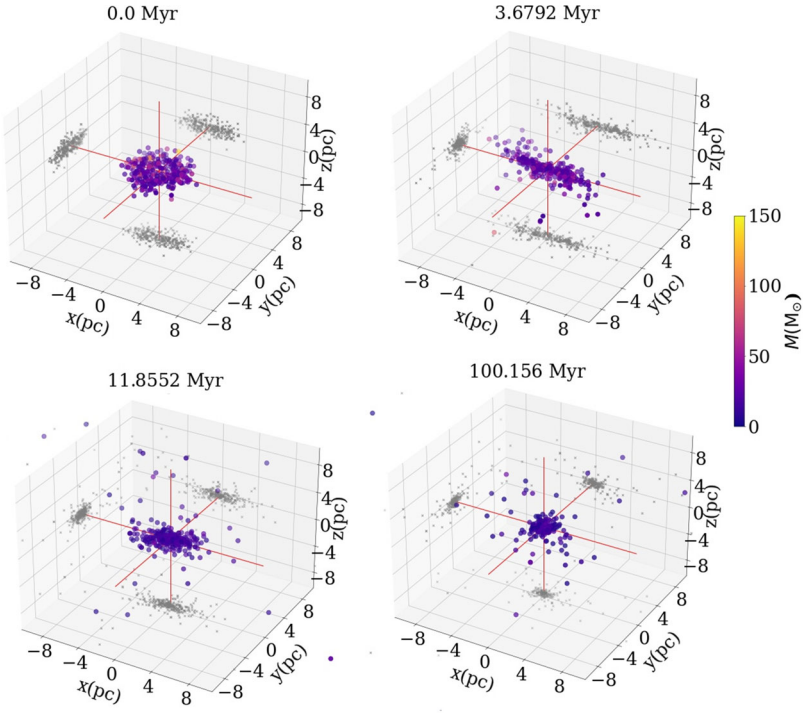

Fig. 11 3D scatter plots in showing the spatial distribution of the ZAMS of high-mass stars (and the BHs they quickly form) from the simulations that rotate extremely quickly initially ($(W_0 = 6.0, \omega_0 = 1.8)$, i.e., rotating King models by Einsel and Spurzem 1999) and have stellar evolution (`level C` by Kamlah et al. 2022a) at around 0.0 Myr, 3.68 Myr, 11.86 Myr and 100.00 Myr, respectively; The stars and compact objects are color-coded by their mass between $0.0\,M_\odot$ and $150.0\,M_\odot$. The stars and BHs are also projected onto the three dimensional axes, which can be seen from the light-grey dots. We can clearly see the (rotating) triaxial structure, a bar of the BHs and their progenitor stars, at $t = 3.68$ Myr and the spatial reconfiguration of the high-mass objects (mostly BHs) to axisymmetric structures already after 11.86 Myr. At 100.00 Myr a practically spherical system of BHs remains that is much more concentrated than the system of their progenitor stars at 0.0 Myr. Images adapted from simulations by Kamlah et al. (2022b)

a cluster rotating around the galaxy, but they are as well generalizations of King models for rotation with similar properties. They also have been used as initial models for direct NBODY models (Tiongco et al. 2016a, b, 2017, 2018, 2019, 2021, 2022; Livernois et al. 2022). Furthermore, semi-analytic models exist that (Szölgyen and Kocsis 2018; Szölgyen et al. 2019, 2021; Panamarev and Kocsis 2022) used to study the formation and evolution of rotating stellar or black hole disks in nuclear star clusters. Most of the aforementioned studies find evidence for the gravogyro catastrophe and its coupling to the gravothermal catastrophe (Inagaki and Hachisu 1978; Hachisu 1979, 1982; Akiyama and Sugimoto 1989). It is important to note that both of these effects are entirely gravitational and disappear in the absence of gravity (Lynden-Bell 1999). The gravogyro catastrophe happens on all astrophysical scales from rotating stars, to the formation of the Solar system and the dynamics of spiral galaxies. A recent study on the impact of stellar evolution on rotating star clusters, finds that the initial bulk rotation leads to a rotating triaxial structure, a bar, of black holes and their progenitor stars in early star cluster evolution that then takes the shape of an axisymmetric structure, a disk, over time (Kamlah et al. 2022b). For one of the simulations from Kamlah et al. (2022b) the results are shown in Fig. 11. This bar formation and dissolution was already found by Akiyama and Sugimoto (1989) in their pioneer low particle number N-body simulations ($N = 1024$) of rotating star clusters. However, the simulation set-up was very different and naturally less advanced. Since rotation is fundamental to star cluster dynamics and since these environments are typically very dense (Krumholz et al. 2019), it will be important to understand how this process can influence the growth of intermediate mass black holes (see Sect. 6.5) and their progenitor stars going forward. Recently, a study on extremely massive and rotating star Pop-III star clusters does indicate a trend that the larger the initial bulk rotation, the more stellar and BH-BH mergers there are (Kamlah et al. 2023). This might be due to the extremely efficient angular momentum transport in early star cluster evolution (0–2 Myr) and the resulting contraction of of the central region before stellar evolution begins to dominate the pre-core collapse evolution. However, more simulations are needed here to reach a conclusion.

Lastly, we note that due to the assumption of spherical symmetry most of the current Monte Carlo methods for collisional dynamics are currently unable to evolve initially rotation star cluster models, such as those described above (e.g., Hénon 1975; Cohn 1979; Stodołkiewicz 1982, 1986; Giersz 1998; Giersz et al. 2015; Merritt 2015; Askar et al. 2017c; Kremer et al. 2020, 2021). A restricted Monte Carlo method for rotating, axisymmetric star clusters (usable even for general geometry, but see problem below) has been presented by Vasiliev (2015). It uses Spitzer's Monte Carlo method (see Sect. 4.1), which distinguishes it from currently common Monte Carlo codes. But it has some more serious approximations, because the random relaxation scatterings are applied only in $v_{\parallel}$ and $v_{\perp}$ obtained from a fully isotropic spherically symmetric background. In 2D Fokker–Planck models of axisymmetric rotating star clusters (Einsel and Spurzem 1999) the background distribution function used for the computation of diffusion coefficients is fully self-consistent and there are five different diffusion coefficients obtained (instead of only two).

6.5 Formation of massive objects

The formation of massive objects from collisions of massive stars and mergers involving black holes is a subject with long history and in full detail beyond the scope of this review. The first detection of a massive black hole merger from LIGO-Virgo (coalescence of two black holes with 85 and 66 $M_\odot$ (Abbott et al. 2020b) has led to new interest into dynamical paths of formation of massive objects (intermediate mass black holes, IMBH) in star clusters. Numerical and theoretical works on IMBH formation in dense star clusters suggests that IMBH formation may occur through differet channels (multiple stellar mergers, accretion of stellar matter onto a stellar mass black hole, or multiple generations of relativistic black hole coalesciences (and mixtures of these processes). The idea that this may happen is not new (cf., e.g., Phinney and Sigurdsson 1991; Gerhard 2001; Portegies Zwart and McMillan 2002; Portegies Zwart et al. 2004). On the observational side IMBHs remain elusive, a recent review about the issue can be found in Greene et al. (2020).

Here we just want to highlight a few recent results obtained with N-body and MOCCA codes, showing the feasibility to grow an IMBH within a suitably initialized star cluster (e.g., Arca-Sedda 2016; Arca-Sedda et al. 2021; Arca Sedda et al. 2021, 2019; Arca-Sedda and Capuzzo-Dolcetta 2019; Morawski et al. 2018, 2019; Di Carlo et al. 2021; Rizzuto et al. 2021, 2022; Kamlah et al. 2023; Arca Sedda et al. 2023b). Star cluster environments (particularly young massive or Pop-III clusters) can precipitate the birth and growth of IMBHs in two of the main proposed mechanisms as listed in Greene et al. (2020): firstly, stellar mergers in star cluster evolution and subsequent core collapse into an IMBH of the progenitor star or secondly, gravitational runaway mergers of (IM)BHs to form (even more) massive IMBHs.

The mergers of (IM)BHs are associated with the emission of a GWs (see Sect. 6.2.7 and sources therein) and GR merger recoil kicks (see Sect. 6.2.5 and sources therein). The emitted gravitational radiation can be detected (Arca Sedda et al. 2020, 2021). (a)LIGO (Aasi et al. 2015; Abbott et al. 2018, 2019), (a)Virgo (Acernese et al. 2015; Abbott et al. 2018, 2019) and KAGRA (e.g., Abbott et al. 2018, 2020a; Kagra Collaboration et al. 2019) currently detect stellar mass black hole inspirals and mergers during their last seconds or fractions of seconds. With improved ground based detectors (Einstein Telescope Branchesi et al. (2023) or Cosmic Explorer (Reitze et al. 2019) or space-based instruments (LISA or its Chinese counterparts, see below) inspiralling stellar mass black hole binaries could be detected months and years before their final coalescence (cf. e.g., Jani et al. 2020), because they are sensitive at lower frequencies. Planned space based gravitational-wave detectors are the European-American LISA (Amaro-Seoane et al. 2017; Bayle et al. 2022) project and the Chinese projects TianQin (Luo et al. 2016) and Taiji (Ruan et al. 2018; Chen et al. 2021). Also these instruments will be more suitable for detection of other black holes inspiralling and merging with IMBHs. Here we present an example from our N-body simulations, which shows that from them one can very well predict GW signal patterns and the abundances of GW events related to IMBHs (in the lower mass regime as discussed above) originating from star clusters (e.g., Arca-Sedda and Gualandris 2018; Arca Sedda and Benacquista 2019). Figure 12

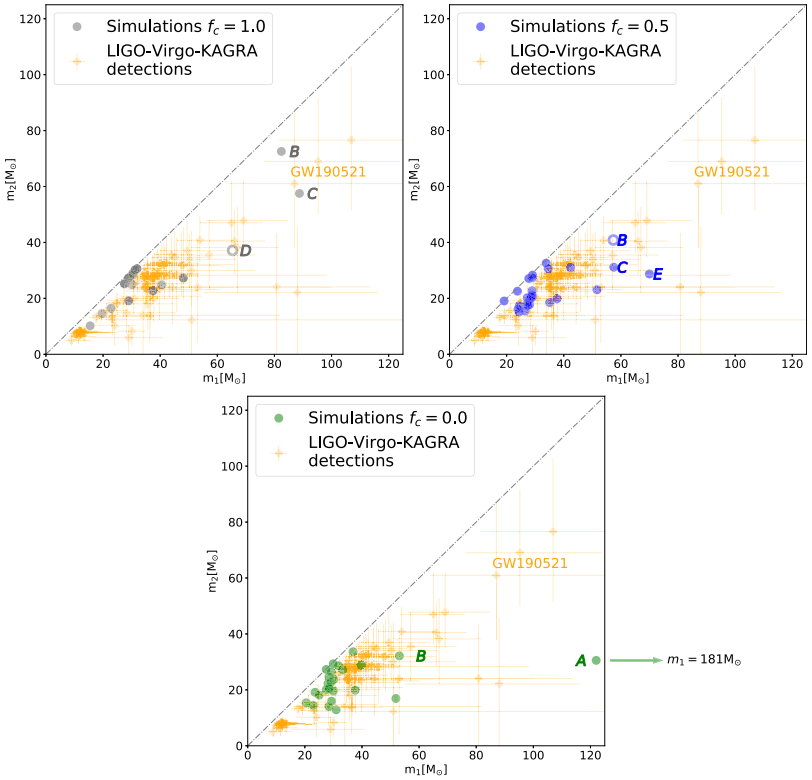

Fig. 12 The panels show the primary (m_1) and secondary (m_2) masses of all BH mergers in the simulations for an accretion fraction of $f_c = 1.0$ (left, grey circles), $f_c = 0.5$, (center, blue circles) and $f_c = 0.0$, (bottom, green circles). The currently available LIGO-Virgo-KAGRA gravitational-wave detections including error bars are indicated in orange. BH merger events that might be excluded due to gravitational recoil kicks are indicated with open circles. In general, the simulated events cover a similar parameter space as all currently available observations. The $f_c = 1.0$, simulations provide two possible formation paths for GW190521. Path C is a second-generation event and has a low probability due to a first-generation BH merger. Path B is more likely as the event itself is a first-generation BH merger. One of the $f_c = 0.0$, realizations generated an intermediate-mass ratio in-spiral of two black holes with 31 and 181 $M_\odot$, respectively, as shown in the bottom panel. Image reproduced with permission from Rizzuto et al. (2022), copyright by the author(s)

shows data from direct N-body simulations of Rizzuto et al. (2022); many BH-BH merger events found in the models fit in almost perfectly with the LIGO-Virgo-KAGRA detections. In these models a new parameter f_c is used, describing how much mass is lost in the collision of a black hole with a main sequence star, $f_c = 0$ means no black hole growth in the process, $f_c = 1$ means that all the mass of the main sequence star is added to the black hole; this parameter is now present in current NBODY6++GPU, and was introduced by Rizzuto et al. (2022).

7 Simulations of nuclear star clusters

7.1 Star-accreting supermassive black holes

As it became clear that the energy emission of quasars and active galactic nuclei originates from a supermassive central black hole (SMBH) the question became interesting, what the equilibrium stellar distribution around it is. First results by Frank and Rees (1976); Shapiro and Lightman (1976); Lightman and Shapiro (1977) found the characteristic cusp, where the stellar density would vary as $\rho \propto r^{-7/4}$. Their analysis is comparable to what we would call later a stationary gaseous or momentum model of a stellar cluster. Also already by Frank and Rees (1976); Hills (1975a) it was noticed that in such a system stars would be tidally disrupted near the SMBH, leading to its growth by mass accretion. Tidally disrupted stars would be preferentially on elongated radial orbits, with low angular momentum. The accretion process would take these stars out of the stellar distribution and create a "loss cone" in phase space. In a spherically symmetric cluster the loss cone would be refilled by diffusion of angular momenta due to two-body relaxation (Amaro-Seoane and Spurzem 2001; Amaro-Seoane et al. 2004). In axisymmetric or triaxial nuclear star clusters angular momentum diffusion can be much faster and lead to higher star accretion rates (Magorrian and Tremaine 1999; Merritt and Poon 2004; Poon and Merritt 2004; Wang and Merritt 2004; Merritt and Wang 2005). Also orbit-averaged FP models have been used for this problem (Cohn and Kulsrud 1978; Bahcall and Wolf 1976, 1977; David et al. 1987a, b). More recently, a first direct *N*-body model using NBODY6++GPU has been published (Panamarev et al. 2019) (DRAGON simulation of the Galactic Center—it led to the conclusion that the central cusp areas near the SMBH are dominated by stellar mass black holes, which will be accreted to the SMBH under gravitational-wave emission.

7.2 Tidal disruption events

If a star is tidally disrupted by the SMBH on a parabolic orbit only half of its mass should be accreted while the other half has enough energy to escape from the SMBH (Rees' conjecture, Rees 1988). The characteristic light curve of such events decays with $t^{-3/5}$; under realistic conditions, however, tidally disrupted stars will arrive on bound (eccentric) and unbound (hyperbolic) orbits, not just parabolic ones; and that will cause deviations from the standard light curve as well as change the accreted mass fraction. in Hayasaki et al. (2018); Zhong et al. (2022) large direct *N*-body simulations were done to find out the distribution of accreted stars. Furthermore, a partial tidal disruption of giant stars was implemented, where the envelope is removed early and a core similar to a white dwarf survives and gets tidally disrupted later (Zhong et al. 2022). Detailed stellar models were also used to determine the mass fraction of a star which is accreted to the SMBH after tidal disruption (Law-Smith et al. 2020). In future work this will be used in conjunction with the detailed mass function, single and binary stellar evolution as in the globular cluster simulations.

8 Practical tools

Here we want to highlight some software tools that have been developed and successfully applied in the context of collisional dynamics.

8.1 Multiscale and multiphysics simulation with AMUSE

The Astrophysical Multipurpose Software Environment (AMUSE) aims to provide a framework by which to simulate multiscale and multiphysics in a hierarchical fashion (Portegies Zwart 2011; Portegies Zwart et al. 2013, 2018; Portegies Zwart and McMillan 2018). It does so by constructing new applications from the combination of known codes (solvers). For example, for gravitational dynamics the user may choose from a selection of 18 *N*-body codes (Portegies Zwart et al. 2018). The AMUSE framework successfully connects gravitational dynamics, radiative transport, stellar evolution and hydrodynamics (Portegies Zwart and McMillan 2018), which results in incredibly diverse research: gas expulsion in early star cluster evolution (Leveque et al. 2022b; Lewis et al. 2021), star cluster collisions and massive star cluster formation (Beilis et al. 2021), the interaction of binary stars in gaseous filaments (Morales and Fellhauer 2020), the evolution of star clusters in a cosmological tidal field (Rieder et al. 2013), evolution of triple stellar systems with Roche-lobe filling binaries (de Vries et al. 2014) and many more.

Particle data and relevant quantities are shared between the constituent codes through the AMUSE framework and unit conversion and other data manipulation can be done in this process (Portegies Zwart et al. 2018). AMUSE is capable of taking care of all sorts of technical problems, such as communication between codes, boundary conditions etc.. However, AMUSE is naturally limited by algorithmic complexity of the software it combines and the astrophysical research objective itself. For example, if we wanted to simulate a globular cluster of realistic size with NBODY6++ (Stiefel and Kustaanheimo 1965; Ahmad and Cohen 1973; Aarseth 1985b; Spurzem 1999; Aarseth 1999a, b, 2003, 2008; Hut and McMillan 1986; Hut et al. 1995; Makino 1991b, 1999; Spurzem 1999; Nitadori and Aarseth 2012) and evolve the stars in the cluster with MESA (Paxton et al. 2011, 2013, 2015, 2016, 2018, 2019), it would take an enormous amount of time. This is not a problem of AMUSE, but rather a statement on the plausibility of certain simulations themselves. However, we note that the operations by AMUSE and communication between codes also costs computing time.

8.2 Simulation data processing and analysis

AMUSE (introduced in Sect. 8.1) provides a large number of in-built data analysis tools simulation data, such as the HOP (Eisenstein and Hut 1998) or the KEPLER packages (Portegies Zwart et al. 2018). These packages can be used by AMUSE users to comfortably analyse data from their simulations without having to write their own scripts.

Many *N*-body codes are now supported by built-in simulation data post-processing analysis packages mostly written in `python`. The direct *N*-body code

PETAR (Wang et al. 2020b, c) also provides built-in data analysis tools, such as movie generators from particle data and HR diagrams. Likewise, the CMC code (Joshi et al. 2000; Pattabiraman et al. 2013; Breivik et al. 2020; Rodriguez et al. 2022) uses the `cmctoolkit` package (Rui et al. 2021) for converting the simulation output into, e. g., velocity dispersion and surface brightness profiles.

Another extremely useful tool for distributed data analysis is provided by BEANS (Hypki 2018), which can in principle be used for simulation output data format—e. g., `csv`, `HDF5`, or `FITS` (Hypki 2018; Hypki et al. 2022). Therefore, this tool can be used for the data analysis of output from all previously mentioned codes. It uses the industry-standard, the Apache Hadoop platform (Dean and Ghemawat 2004), for data analysis. This platform is highly optimized for processing huge amounts of (continuously generated) data and is therefore ideal not only in the "Internet of Things" and the live communication between machines, but also on-the-fly data processing and analysis from *N*-body simulations. BEANS is currently heavily used in data processing and analysis of MOCCA simulations (e.g., Hypki et al. 2022). Recently, BEANS has also been configured to easily process the output data from NBODY6++GPU simulations.

8.3 Photometric mock observations from star cluster simulations

It is oftentimes desirable and useful to create photometric mock observations (CMDs or spectra of star clusters) from star cluster simulations. For this purpose various codes have been written. They mostly rely on the same principle: stellar masses, temperatures, luminosities and metallicities from the *N*-body output data are converted into observational magnitudes in various filter systems (e.g. HST, SDSS, 2MASS and it is typically easy to systems of new observing instruments) and into spectra in a certain wavelength range (e.g., Pang et al. 2016). Therefore, these mock observations are heavily influenced by the stellar evolution models that the respective simulations evolve the stars with. In the following paragraph, we summarise a number of codes for the creation of the observations outlined above.

The Cluster simulatiOn Comparison with ObservAtions (COCCA) code by Askar et al. (2017b, 2018) has been used extensively in the creation of mock observations from *N*-body and Monte Carlo simulations (e.g., Askar et al. 2017c; Wang et al. 2016; Askar et al. 2017a; Belloni et al. 2017). COCCA has also been extensively used in MOCCA studies concerning the evolution and detectability of IMBHs in star clusters (de Vita et al. 2017; Aros et al. 2020, 2021). In Fig. 13 a CMD constructed with COCCA is shown taken from Wang et al. (2016). They then compared this CMD with HST data of NGC 4372 (the target cluster of this study) from Piotto et al. (2002) and found that the CMDs are mostly very similar. Differences between actual and mock observations were attributed to the intrinsic observational photometry error or the presence of MSPs (see Sect. 6.4.5) in NGC 4372 that were not resolved by the simulation. Inaccurate stellar evolution modelling will have further influenced the results (in Wang et al. 2016, the so-called `level A` was used, see Kamlah et al. 2022a). This is a practical example of how photometric mock observations and the codes that produce these can be extremely useful in constraining both observation and theory.

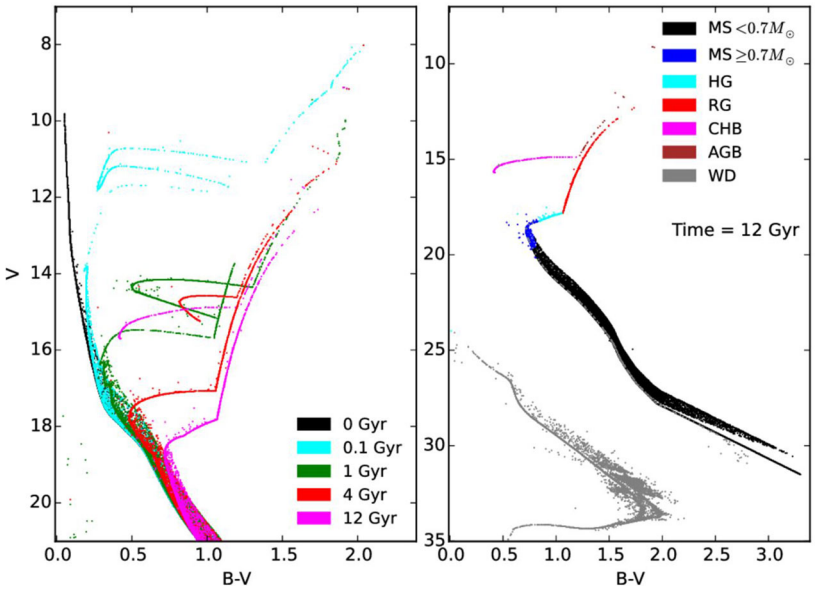

Fig. 13 Color (B-V)—magnitude (apparent V) diagram (CMD) of one of the Dragon simulations: D1-R7-IMF93. The distance modulus 13.82 (5800 pc) is used here. Left: the evolution of CMD for luminous parts. Black dots show the initial distribution. After 100 Myr the MS turnoff becomes visible already (cyan). The horizontal branch is populated after 1 Gyr (green). The MS turnoff moves down to $V \sim 17.5$ mag after 4 Gyr (red) and $V \sim 18.5$ mag after 12 Gyr (purple). Right: the full CMD after 12 Gyr. Different colors show different stellar types. HG: sub-giant branch (Hertzsprung gap); RG: red giant; CHB: horizontal branch (core helium burning); AGB: asymptotic giant branch; WD: white dwarf. Image reproduced with permission from Wang et al. (2016), copyright by the author(s)

The GAlaxy EVolutionary synthesis models (GALEV) (Kotulla et al. 2009) was adapted for the use creating mock observations from *N*-body simulations (mostly intended for NBODY6++GPU and codes from that family, but it can be used for any other code that provides stellar masses, temperatures, luminosities and metallicities of the stars) by Pang et al. (2016). The resulting code GALEVNB was applied to study the dynamical origin of MSPs (see Sect. 6.4.5) (Hong et al. 2017a), the dynamical evolution of planetary systems in star clusters (Kouwenhoven et al. 2020), the long-term evolution of binaries in the Dragon simulations (Wang et al. 2016; Shu et al. 2021) and PETAR simulations of open clusters and exploring their UV-excess (Pang et al. 2022).

More codes that are worth mentioning and fulfil the same underlying purpose as COCCA and GALEVNB are: Flexible Stellar Population Synthesis (FSPS) (Conroy et al. 2009; Conroy and Gunn 2010; Conroy et al. 2010), Simulating IFU Star Cluster Observations (SISCO) for integral field unit (IFU) observations of globular clusters (Bianchini et al. 2015), Make Your Own Synthetic ObservaTIonS (MYOSOTIS) for creating generic photometric observations (Khorrami et al. 2019) and Massive

Cluster Evolution and Analysis Package (MASSCLEAN), which serves the same purposes (Popescu and Hanson 2009).

9 Summary and conclusion

The gravitational N-body problem remains to be one of the oldest and most exciting problems in astrophysics. In this review, we have focused on a branch of this incredibly diverse field: the computation of *collisional* stellar N-body systems. The term collisional refers to the cumulative effect of distant elastic two-body encounters here. In nature these systems are commonly represented young and massive, globular, or nuclear star clusters. These clusters are also dense and gravothermal—stellar density are high enough that direct collisions and mergers between stars occur in certain phases, and gravothermal in the sense that two-body relaxation, through distant elastic encounters, provides heat transfer and viscous angular momentum transfer.

Despite exhaustive efforts to accurately model these systems, there is still no self-consistent theory available. This is partly because N-body systems are dynamically chaotic for a significant fraction of the phase space of initial conditions if $N > 2$. For small $N \leq 3$, there do exist some stable solutions (Chenciner and Montgomery 2000; Montgomery 2001), but these special configurations are extremely unlikely to occur in nature (Heggie 2000). For all $N > 3$, there exist no analytical solutions and we must solve the equation of motions numerically, thus with the help of computers. For increasing N, certain configurations of such systems exhibit truly remarkable physical properties. They might exhibit negative heat capacities that result in gravothermal contraction (sometimes also coined the "gravothermal catastrophe" (e.g., Lynden-Bell and Wood 1968). If the star cluster rotates, it could exhibit a negative moment of inertia leading angular momentum transport from high-mass particles to low mass particles in the system, while at the same time increasing the rotational velocity of the high-mass particles, which is known as the gravogyro catastrophe (e.g., Hachisu 1979; Kim et al. 2008). In a realistic star cluster simulations, both of these processes will happen at different timescales (convective angular momentum transport is more efficient than conductive heat transport in star clusters), but they are coupled and ultimately reinforce one another (Hachisu 1982). Importantly, these processes are entirely gravitational in nature and disappear in the absence of self-gravity.

The two astrophysical methods that have been most successfully tackling collisional gravitational N-body systems are either direct N-body simulations (using for gravitational force calculations at least at some times the summation over all $N-1$ other stars) or approximate methods, based on statistical mechanics, using the Fokker–Planck modelling with Monte Carlo methods. While the former method appears physically more accurate, less affected by approximations, and resolves any astrophysical object of interest (star clusters) better, the latter is much faster and computationally less expensive. And recent star-by-star Monte Carlo modelling delivers detailed data comparable to direct N-body simulations. It has been demonstrated repeatedly that for global quantities such as the time evolution of

binary fractions both methods yield very similar results. Therefore, these methods ultimately complement each other and many works have employed both side by side.

All fields in astrophysics have benefited from the revolutionary invention of computers and the ingenious hardware architectures that have been developed since. By the same token, new programming languages and parallelization techniques have had a significant impact on accelerating solving astrophysical problems on hardware and made certain problems possible to begin with. The collisional gravitational *N*-body problem is no exception here. When the astrophysics, the hardware and software domains are mastered, research in this field can culminate in groundbreaking results: the first million-body simulations of globular clusters across cosmic time, the `Dragon` simulations performed with NBODY6++GPU, are a product of this but more direct *N*-body models of Galactic and extragalactic globular and nuclear star clusters are needed to compare with both observational data and the wealth of data from Monte Carlo surveys. It follows that nowadays the gravitational *N*-body problem is in as much an astrophysics as it is a computer science problem. Examples here are the advent of novel simulation software such as the direct *N*-body codes PETAR and FROST, and new hybrid code approaches such as ETICS, which will make it possible to break into the 10^6–10^9 particle domain. Massive globular clusters such as 47 Tuc or ω Cen as well as most nuclear star clusters belong to this parameter range. Will a traditional workhorse such as NBODY6++GPU again keep up and compete here? The first Exaflop/s computer has been inaugurated in the US this year[5]—for the next steps we need to again adopt our codes to the new developing hardware. It is now 32 years ago that D. Sugimoto announced the million body problem as a challenge for direct *N*-body simulations—here we want to raise the question of when the billion body problem can be tackled and what codes and what hardware do we need?

Another challenge lies in the integration of astrophysics into gravitational *N*-body simulations. This involves classical single and binary stellar evolution as well as relativistic dynamics of compact objects, or proper modelling of external tidal fields. The central densities of collisional stellar systems are typically so high, that stars frequently interact with each other; they exchange mass and angular momentum or even collide and merge. In other words, the stars in the simulations do not only evolve on their own, they also interact with nearby stars (and compact objects) through diverse astrophysical processes, such as tidal interaction, dynamical mass transfer, gravitational-wave inspiral and many more. For this purpose there are two main methods that have been thoroughly tested: interpolation between tables or approximation of stellar evolution data by some interpolation (fitting) formulae as functions of mass, age and metallicity. These two approaches are also not in competition, but rather complement one another. The former has traditionally been limited by memory on hardware, since the tables are necessarily rather large. Due to advances in hardware, this problem is diminishing. Unlike the latter approach, fitting formulae, stellar parameters from the given set of detailed tracks are calculated in real time with this method. Therefore, this approach is probably the most flexible, robust and efficient today when combining detailed stellar evolution with stellar dynamics. Furthermore, fitting formulae typically take much more care and time to set up. But

[5] https://www.top500.org/

the effort is rewarded with rapid, robust and analytic formulae, which can be easily modified and integrated into an *N*-body code and that quickly give stellar luminosity, radius and core mass of the stars as functions of mass, metallicity and age for all stellar evolutionary phases.

When full stellar evolution is combined with collisional dynamics and the resulting code is used to study the dynamical evolution of dense star clusters of various make-ups, exciting research can be done. From the formation and evolution of exotic stellar and compact binaries, such as blue stragglers, Cataclysmic Variables, Algols, X-ray binaries, and many others to double-degenerate binaries, such as BH-BH and the elusive BH-NS binaries, to the abundances of compact objects and their dynamical properties an extremely diverse array of astrophysically fascinating populations can be modelled for large metallicity and mass ranges. Therefore, the simulations of collisional stellar systems with modern production codes are the ideal laboratory to study stellar evolution in dense stellar environments. From the gravitational-wave inspiral of compact objects that can be modelled nowadays up to order PN(3.5) as well as the associated general relativistic merger recoil kick with the use of fitting formulae to numerical relativity, the full compact object merger phase can be modelled. As a result, simulations can yield predictions for theoreticians and observers alike on the properties, abundances and dynamics of gravitational-wave sources from star clusters (and field) across cosmic time. Additionally, with the use of photometric mock observations from star cluster simulations, simulation data can be translated into magnitudes and fluxes for most mainstream filter systems, which has been done extensively already. In summary, simulations of collisional stellar systems are important and useful tools for unravelling our cosmic history in the age of multi-messenger astronomy. They are at the crossroads of many seemingly disparate astrophysical research fields, much like the simulation target, star clusters, are a fundamental building block in a hierarchy of cosmological structure formation (Krumholz et al. 2019).

Acknowledgements In alphabetical order of family name we thank Manuel Arca Sedda, Abbas Askar, Sambaran Banerjee, Peter Berczik, Maxwell Cai, Roberto Capuzzo-Dolcetta, Gaia Fabj, Francesco Flammini-Dotti, Mirek Giersz, Jarrod Hurley, Arek Hypki, Thijs Kouwenhoven, Shuo Li, Michela Mapelli, Thorsten Naab, Keigo Nitadori, Bastian Reinoso, Francesco Rizzuto, Xiaoying Pang, Qi Shu, Long Wang, Kai Wu, and Shiyan Zhong for helpful comments, discussions, and collaboration. AK wants to extend his deep gratitude to Nadine Neumayer for the support and mentorship in difficult times. The authors gratefully acknowledge project support by German Science Foundation (DFG), National Science Foundation of China (NSFC), Chinese Academy of Sciences (CAS), Volkswagen Foundation, and the Gauss Centre for Supercomputing e.V. (https://www.gauss-centre.eu/) for providing computing time through the John von Neumann Institute for Computing (NIC) on the GCS Supercomputer JUWELS and JUWELS-Booster at the Jülich Supercomputing Centre in Germany (JSC). AK is a fellow of the International Max Planck Research School for Astronomy and Cosmic Physics at the University of Heidelberg (IMPRS-HD). RS wants to thank Mirek Giersz for collaboration and extraordinary hospitality over the past decades during many visits at the Nicolaus Copernicus Astronomical Center in Warsaw, Poland. RS has been Alexander von Humboldt Polish Honorary Research Fellow by the Foundation for Polish Science. RS is grateful for experiencing many years of excellent, friendly, and open work environment at National Astronomical Observatories of Chinese Academy of Sciences in Beijing, China and at Kavli Institute for Astronomy and Astrophysics at Peking University. European collaborators—if you see some familiar fragments in the introduction area—I have been inspired by some of our old network application texts (RS). RS also wants to thank all team members and collaborators, who are not explicitly mentioned here, including all students, former and current, in Kiel, Heidelberg, Beijing, and across the Silk Road, for their hard work. You provided essential contributions to get to the current level described in this paper. The

GRAPE team at Tokyo University, represented first by Daiichiro Sugimoto and later by Junichiro Makino deserves sincere acknowledgment for making GRAPE hardware available early for international collaborators, including our team in Kiel and Heidelberg. RS expresses thanks and gratitude to Sverre Aarseth, Douglas Heggie, Gerhard Hensler, Roland Wielen, and Suijian Xue—without your support and encouragement I would not be here at this point writing this review. The editors of LRCA has been very patient, thank you for this!

Declarations

Conflict of interest The authors declare that they have no conflict of interest.

References

Aarseth S (1967) On a collisionless method in stellar dynamics. I. In: Les Nouvelles Méthodes de la Dynamique Stellaire. p 47

Aarseth SJ (1963) Dynamical evolution of clusters of galaxies. I. MNRAS 126:223. https://doi.org/10.1093/mnras/126.3.223

Aarseth SJ (1971) Direct integration methods of the N-body problem. Ap&SS 14(1):118–132. https://doi.org/10.1007/BF00649199

Aarseth SJ (1979) An N-body integration method in co-moving coordinates. In: Szebehely VG (ed) Instabilities in dynamical systems. Applications to celestial mechanics. NATO ASI Series C, vol 47. pp 69–80

Aarseth SJ (1985a) Direct methods for N-body simulations. In: Brackbill JU, Cohen BI (eds) Multiple time scales. Academic Press, pp 377–418. https://doi.org/10.1016/B978-0-12-123420-1.50017-3

Aarseth SJ (1985b) Direct N-body calculations. In: Goodman J, Hut P (eds) Dynamics of star clusters. IAU Symposium, vol 113. Reidel, Dordrecht, pp 251–259. https://doi.org/10.1007/978-94-009-5335-2_26

Aarseth SJ (1994) Direct methods for N-body simulations. In: Contopoulos G, Spyrou NK, Vlahos L (eds) Galactic dynamics and N-body simulations. Lecture Notes in Physics, vol 433. Springer, Berlin, pp 277–312. https://doi.org/10.1007/3-540-57983-4_22

Aarseth SJ (1996) N-body simulations of open clusters with binary evolution. In: Milone EF, Mermilliod JC (eds) The origins, evolution, and destinies of binary stars in clusters. Astronomical Society of the Pacific Conference Series, vol 90. p 423

Aarseth SJ (1999) From NBODY1 to NBODY6: the growth of an industry. PASP 111(765):1333–1346. https://doi.org/10.1086/316455

Aarseth SJ (1999) Star cluster simulations: the state of the art. Celest Mech Dyn Astron 73:127–137. https://doi.org/10.1023/A:1008390828807. arXiv:astro-ph/9901069 [astro-ph]

Aarseth SJ (2003) Gravitational N-body simulations. Cambridge University Press, Cambridge. https://doi.org/10.1017/CBO9780511535246

Aarseth SJ (2008) Direct N-body codes. In: Aarseth SJ, Tout CA, Mardling RA (eds) The Cambridge N-body lectures. Lecture notes in physics, vol 760. Springer, Berlin, p 1. https://doi.org/10.1007/978-1-4020-8431-7_1

Aarseth SJ (2012) Mergers and ejections of black holes in globular clusters. MNRAS 422(1):841–848. https://doi.org/10.1111/j.1365-2966.2012.20666.x. arXiv:1202.4688 [astro-ph.SR]

Aarseth SJ, Zare K (1974) A regularization of the three-body problem. Celest Mech 10(2):185–205. https://doi.org/10.1007/BF01227619

Aarseth SJ, Henon M, Wielen R (1974) A comparison of numerical methods for the study of star cluster dynamics. A&A 37(1):183–187

Aarseth SJ, Lin DNC, Palmer PL (1993) Evolution of planetesimals. II. Numerical simulations. ApJ 403:351. https://doi.org/10.1086/172208

Aasi J, Abadie J, Abbott BP, Abbott R, Abbott T, Abernathy MRea (2015) Characterization of the LIGO detectors during their sixth science run. Class Quantum Gravity 32(11):115012. https://doi.org/10.1088/0264-9381/32/11/115012. arXiv:1410.7764 [gr-qc]

Abbott BP, Abbott R, Abbott TD, Abernathy MR, Acernese F et al (2016) Observation of gravitational waves from a binary black hole merger. Phys Rev Lett 116(6):061102. https://doi.org/10.1103/PhysRevLett.116.061102. arXiv:1602.03837 [gr-qc]

Abbott BP, Abbott R, Abbott TD, Acernese F, Ackley K et al (2017) GW170817: observation of gravitational waves from a binary neutron star inspiral. Phys Rev Lett 119(16):161101. https://doi.org/10.1103/PhysRevLett.119.161101. arXiv:1710.05832 [gr-qc]

Abbott BP, Abbott R, Abbott TD, Abernathy MR, Acernese F et al (2018) Prospects for observing and localizing gravitational-wave transients with advanced LIGO, advanced Virgo and KAGRA. Living Rev Relativ 21:3. https://doi.org/10.1007/s41114-018-0012-9. arXiv:1304.0670 [gr-qc]

Abbott BP, Abbott R, Abbott TD, Abraham S, Acernese F et al (2019) Binary Black hole population properties inferred from the first and second observing runs of advanced LIGO and advanced virgo. ApJ 882(2):L24. https://doi.org/10.3847/2041-8213/ab3800. arXiv:1811.12940 [astro-ph.HE]

Abbott BP, Abbott R, Abbott TD, Abraham S, Acernese F et al (2020) Prospects for observing and localizing gravitational-wave transients with advanced LIGO, advanced virgo and KAGRA. Living Rev Relativ 23:3. https://doi.org/10.1007/s41114-020-00026-9

Abbott R, Abbott TD, Abraham S, Acernese F, Ackley K et al (2020) GW190521: a binary black hole merger with a total mass of 150 $M_{\odot}$. Phys Rev Lett 125(10):101102. https://doi.org/10.1103/PhysRevLett.125.101102. arXiv:2009.01075 [gr-qc]

Abbott R, Abbott TD, Abraham S, Acernese F, Ackley K et al (2020) GW190814: gravitational waves from the coalescence of a 23 solar mass black hole with a 2.6 solar mass compact object. ApJ 896(2):L44. https://doi.org/10.3847/2041-8213/ab960f. arXiv:2006.12611 [astro-ph.HE]

Acernese F, Agathos M, Agatsuma K, Aisa D, Allemandou N, Aea Allocca (2015) Advanced virgo: a second-generation interferometric gravitational wave detector. Class Quantum Gravity 32(2):024001. https://doi.org/10.1088/0264-9381/32/2/024001. arXiv:1408.3978 [gr-qc]

Agrawal P, Hurley J, Stevenson S, Szécsi D, Flynn C (2020) The fates of massive stars: exploring uncertainties in stellar evolution with METISSE. MNRAS 497(4):4549–4564. https://doi.org/10.1093/mnras/staa2264. arXiv:2005.13177 [astro-ph.SR]

Agrawal P, Stevenson S, Szécsi D, Hurley J (2022) A systematic study of super-Eddington layers in the envelopes of massive stars. A&A 668:A90. https://doi.org/10.1051/0004-6361/202244044. arXiv:2112.02801 [astro-ph.SR]

Ahmad A, Cohen L (1973) A numerical integration scheme for the N-body gravitational problem. J Comput Phys 12:389–402. https://doi.org/10.1016/0021-9991(73)90160-5

Akiyama K, Sugimoto D (1989) Evolution of a self-gravitating many-body system with rotation. PASJ 41(5):991–1003

Alongi M, Bertelli G, Bressan A, Chiosi C, Fagotto F, Greggio L, Nasi E (1993) Evolutionary sequences of stellar models with semiconvection and convective overshoot. I. Z=0.008. A&AS 97:851–871

Amaro-Seoane P, Spurzem R (2001) The loss-cone problem in dense nuclei. MNRAS 327(3):995–1003. https://doi.org/10.1046/j.1365-8711.2001.04799.x. arXiv:astro-ph/0105251 [astro-ph]

Amaro-Seoane P, Freitag M, Spurzem R (2004) Accretion of stars on to a massive black hole: a realistic diffusion model and numerical studies. MNRAS 352(2):655–672. https://doi.org/10.1111/j.1365-2966.2004.07956.x. arXiv:astro-ph/0401163 [astro-ph]

Amaro-Seoane P, Glaschke P, Spurzem R (2014) Hybrid methods in planetesimal dynamics: formation of protoplanetary systems and the mill condition. MNRAS 445(4):3755–3769. https://doi.org/10.1093/mnras/stu1734. arXiv:1301.3910 [astro-ph.EP]

Amaro-Seoane P, Audley H, Babak S, Baker J, Barausse E, et al (2017) Laser Interferometer Space Antenna. arXiv arXiv:1702.00786 [astro-ph.IM]

Anderson J, King IR (2000) Toward high-precision astrometry with WFPC2. I. Deriving an accurate point-spread function. PASP 112(776):1360–1382. https://doi.org/10.1086/316632. arXiv:astro-ph/0006325 [astro-ph]

Anderson J, Sarajedini A, Bedin LR, King IR, Piotto G et al (2008) The Acs survey of globular clusters. V. Generating a comprehensive star catalog for each cluster. AJ 135(6):2055–2073. https://doi.org/10.1088/0004-6256/135/6/2055. arXiv:0804.2025 [astro-ph]

Arca-Sedda M (2016) On the formation of compact, massive subsystems in stellar clusters and its relation with intermediate-mass black holes. MNRAS 455(1):35–50. https://doi.org/10.1093/mnras/stv2265. arXiv:1502.01242 [astro-ph.GA]

Arca Sedda M (2020) Dissecting the properties of neutron star-black hole mergers originating in dense star clusters. CmPhy 3(1):43. https://doi.org/10.1038/s42005-020-0310-x. arXiv:2003.02279 [astro-ph.GA]

Arca Sedda M, Benacquista M (2019) Using final black hole spins and masses to infer the formation history of the observed population of gravitational wave sources. MNRAS 482(3):2991–3010. https://doi.org/10.1093/mnras/sty2764. arXiv:1806.01285 [astro-ph.GA]

Arca-Sedda M, Capuzzo-Dolcetta R (2019) The MEGaN project. II. Gravitational waves from intermediate-mass and binary black holes around a supermassive black hole. MNRAS 483(1):152–171. https://doi.org/10.1093/mnras/sty3096. arXiv:1709.05567 [astro-ph.GA]

Arca-Sedda M, Gualandris A (2018) Gravitational wave sources from inspiralling globular clusters in the Galactic Centre and similar environments. MNRAS 477(4):4423–4442. https://doi.org/10.1093/mnras/sty922. arXiv:1804.06116 [astro-ph.GA]

Arca Sedda M, Askar A, Giersz M (2019) MOCCA-SURVEY Database I. Intermediate mass black holes in Milky Way globular clusters and their connection to supermassive black holes. arXiv e-prints arXiv:1905.00902 [astro-ph.GA]

Arca Sedda M, Berry CPL, Jani K, Amaro-Seoane P, Auclair P et al (2020) The missing link in gravitational-wave astronomy: discoveries waiting in the decihertz range. Class Quantum Grav 37 (21):215011. https://doi.org/10.1088/1361-6382/abb5c1. arXiv:1908.11375 [gr-qc]

Arca Sedda M, Amaro Seoane P, Chen X (2021) Merging stellar and intermediate-mass black holes in dense clusters: implications for LIGO, LISA, and the next generation of gravitational wave detectors. A&A 652:A54. https://doi.org/10.1051/0004-6361/202037785. arXiv:2007.13746 [astro-ph.GA]

Arca-Sedda M, Rizzuto FP, Naab T, Ostriker J, Giersz M, Spurzem R (2021) Breaching the limit: formation of GW190521-like and IMBH mergers in young massive clusters. ApJ 920(2):128. https://doi.org/10.3847/1538-4357/ac1419. arXiv:2105.07003 [astro-ph.GA]

Arca Sedda M, Kamlah A, Spurzem R, Giersz M, Berczik P, Rastello S, Iorio G, Mapelli M, Gatto M, Grebel E (2023a) The DRAGON-II simulations - I. Evolution of single and binary compact objects in star clusters with up to 1 million stars. MNRAS Subm. to MNRAS

Arca Sedda M, Kamlah A, Spurzem R, Rizzuto F, Giersz M, Naab T, Berczik P (2023b) The DRAGON-II simulations - II. Formation mechanisms, mass, and spins of intermediate-mass black holes in star clusters with up to 1 million stars. MNRAS Subm. to MNRAS

Arca Sedda M, Kamlah A, Spurzem R, Rizzuto F, Giersz M, Naab T, Berczik P (2023c) The DRAGON-II simulations - III. Compact binary mergers in clusters with up to 1 million stars: mass, spin, eccentricity, merger rate and pair instability supernovae rate. MNRAS Subm. to MNRAS

Aros FI, Sippel AC, Mastrobuono-Battisti A, Askar A, Bianchini P et al (2020) Dynamical modelling of globular clusters: challenges for the robust determination of IMBH candidates. MNRAS 499 (4):4646–4665. https://doi.org/10.1093/mnras/staa2821. arXiv:2009.07275 [astro-ph.GA]

Aros FI, Sippel AC, Mastrobuono-Battisti A, Bianchini P, Askar A et al (2021) Using binaries in globular clusters to catch sight of intermediate-mass black holes. MNRAS 508(3):4385–4398. https://doi.org/10.1093/mnras/stab2872. arXiv:2110.00590 [astro-ph.GA]

Askar A, Bianchini P, de Vita R, Giersz M, Hypki A et al (2017) MOCCA-SURVEY database I: Is NGC 6535 a dark star cluster harbouring an IMBH? MNRAS 464(3):3090–3100. https://doi.org/10.1093/mnras/stw2573. arXiv:1607.08275 [astro-ph.GA]

Askar A, Giersz M, Pych W, Dalessandro E (2017b) COCOA: simulating observations of star cluster simulations. Astrophysics Source Code Library, ascl:1703.002. https://ascl.net/1703.002

Askar A, Szkudlarek M, Gondek-Rosińska D, Giersz M, Bulik T (2017) MOCCA-SURVEY database - I. Coalescing binary black holes originating from globular clusters. MNRAS 464(1):L36–L40. https://doi.org/10.1093/mnrasl/slw177. arXiv:1608.02520 [astro-ph.HE]

Askar A, Giersz M, Pych W, Dalessandro E (2018) COCOA code for creating mock observations of star cluster models. MNRAS 475(3):4170–4185. https://doi.org/10.1093/mnras/sty101. arXiv:1703.09160 [astro-ph.GA]

Avramov B, Berczik P, Meiron Y, Acharya A, Just A (2021) Properties of loss cone stars in a cosmological galaxy merger remnant. A&A 649:A41. https://doi.org/10.1051/0004-6361/202039698. arXiv:2011.08216 [astro-ph.GA]

Bahcall JN, Wolf RA (1976) Star distribution around a massive black hole in a globular cluster. ApJ 209:214–232. https://doi.org/10.1086/154711

Bahcall JN, Wolf RA (1977) The star distribution around a massive black hole in a globular cluster. II. Unequal star masses. ApJ 216:883–907. https://doi.org/10.1086/155534

Baker JG, Boggs WD, Centrella J, Kelly BJ, McWilliams ST et al (2007) Modeling kicks from the merger of nonprecessing black hole binaries. ApJ 668(2):1140–1144. https://doi.org/10.1086/521330. arXiv:astro-ph/0702390 [astro-ph]

Baker JG, Boggs WD, Centrella J, Kelly BJ, McWilliams ST et al (2008) Mergers of nonspinning black-hole binaries: gravitational radiation characteristics. Phys Rev D 78(4):044046. https://doi.org/10.1103/PhysRevD.78.044046. arXiv:0805.1428 [gr-qc]

Ballone A, Mapelli M, Di Carlo UN, Torniamenti S, Spera M et al (2020) Evolution of fractality and rotation in embedded star clusters. MNRAS 496(1):49–59. https://doi.org/10.1093/mnras/staa1383. arXiv:2001.10003 [astro-ph.GA]

Ballone A, Torniamenti S, Mapelli M, Di Carlo UN, Spera M et al (2021) From hydrodynamics to N-body simulations of star clusters: mergers and rotation. MNRAS 501(2):2920–2933. https://doi.org/10.1093/mnras/staa3763. arXiv:2012.00767 [astro-ph.GA]

Ballone A, Costa G, Mapelli M, MacLeod M, Torniamenti S, Pacheco-Arias JM (2023) Formation of black holes in the pair-instability mass gap: hydrodynamical simulations of a head-on massive star collision. MNRAS 519(4):5191–5201. https://doi.org/10.1093/mnras/stac3752. arXiv:2204.03493 [astro-ph.SR]

Banerjee S (2021) Stellar-mass black holes in young massive and open stellar clusters - IV. Updated stellar-evolutionary and black hole spin models and comparisons with the LIGO-Virgo O1/O2 merger-event data. MNRAS 500(3):3002–3026. https://doi.org/10.1093/mnras/staa2392. arXiv:2004.07382 [astro-ph.HE]

Banerjee S (2022) Binary black hole mergers from young massive clusters in the pair-instability supernova mass gap. A&A 665:A20. https://doi.org/10.1051/0004-6361/202142331. arXiv:2109.14612 [astro-ph.HE]

Banerjee S, Belczynski K, Fryer CL, Berczik P, Hurley JR et al (2020) BSE versus StarTrack: implementations of new wind, remnant-formation, and natal-kick schemes in NBODY7 and their astrophysical consequences. A&A 639:A41. https://doi.org/10.1051/0004-6361/201935332. arXiv:1902.07718 [astro-ph.SR]

Bastian N, Lardo C (2018) Multiple stellar populations in globular clusters. ARA&A 56:83–136. https://doi.org/10.1146/annurev-astro-081817-051839. arXiv:1712.01286 [astro-ph.SR]

Bastian N, Usher C, Kamann S, Lardo C, Larsen SS, Cabrera-Ziri I, Chantereau W, Martocchia S, Salaris M, Schiavon RP, Asa'd R, Hilker M (2019) Multiple populations in integrated light spectroscopy of intermediate-age clusters. MNRAS 489(1):L80–L85. https://doi.org/10.1093/mnrasl/slz130. arXiv:1909.01404 [astro-ph.GA]

Bastian N, Lardo C, Usher C, Kamann S, Larsen SS, Cabrera-Ziri I, Chantereau W, Martocchia S, Salaris M, Asa'd R, Hilker M (2020) Searching for multiple populations in the integrated light of the young and extremely massive clusters in the merger remnant NGC 7252. MNRAS 494(1):332–337. https://doi.org/10.1093/mnras/staa716. arXiv:2003.03428 [astro-ph.SR]

Baumgardt H, Hilker M (2018) A catalogue of masses, structural parameters, and velocity dispersion profiles of 112 Milky Way globular clusters. MNRAS 478(2):1520–1557. https://doi.org/10.1093/mnras/sty1057. arXiv:1804.08359 [astro-ph.GA]

Baumgardt H, De Marchi G, Kroupa P (2008) Evidence for primordial mass segregation in globular clusters. ApJ 685(1):247–253. https://doi.org/10.1086/590488. arXiv:0806.0622 [astro-ph]

Bayle JB, Bonga B, Caprini C, Doneva D, Muratore M, Petiteau A, Rossi E, Shao L (2022) Overview and progress on the laser interferometer space antenna mission. Nat Astron 6:1334–1338. https://doi.org/10.1038/s41550-022-01847-0

Bédorf J, Gaburov E, Portegies Zwart S (2012) Bonsai: N-body GPU tree-code. Astrophysics Source Code Library. https://ascl.net/1212.001

Beilis D, Beck S, Lacy J (2021) Super star cluster formation via cluster collisions: N-body/SPH simulations of SSC-N in II Zw 40. In: American Astronomical Society Meeting Abstracts. American astronomical society meeting abstracts, vol 53. p 150.01

Belczynski K, Banerjee S (2020) Formation of low-spinning 100 $M_{\odot}$ black holes. A&A 640:L20. https://doi.org/10.1051/0004-6361/202038427. arXiv:2002.08050 [astro-ph.HE]
Belczynski K, Kalogera V, Bulik T (2002) A comprehensive study of binary compact objects as gravitational wave sources: evolutionary channels, rates, and physical properties. ApJ 572(1):407–431. https://doi.org/10.1086/340304. arXiv:astro-ph/0111452 [astro-ph]
Belczynski K, Kalogera V, Rasio FA, Taam RE, Zezas A, et al (2008) Compact object modeling with the StarTrack population synthesis code. ApJS 174(1):223–260. https://doi.org/10.1086/521026. arXiv:astro-ph/0511811 [astro-ph]
Belczynski K, Bulik T, Fryer CL, Ruiter A, Valsecchi F et al (2010) On the maximum mass of stellar black holes. ApJ 714(2):1217–1226. https://doi.org/10.1088/0004-637X/714/2/1217. arXiv:0904.2784 [astro-ph.SR]
Belczynski K, Heger A, Gladysz W, Ruiter AJ, Woosley S et al (2016) The effect of pair-instability mass loss on black-hole mergers. A&A 594:A97. https://doi.org/10.1051/0004-6361/201628980. arXiv:1607.03116 [astro-ph.HE]
Belczynski K, Ryu T, Perna R, Berti E, Tanaka TL et al (2017) On the likelihood of detecting gravitational waves from population III compact object binaries. MNRAS 471(4):4702–4721. https://doi.org/10.1093/mnras/stx1759. arXiv:1612.01524 [astro-ph.HE]
Belczynski K, Klencki J, Fields CE, Olejak A, Berti E et al (2020) Evolutionary roads leading to low effective spins, high black hole masses, and O1/O2 rates for LIGO/Virgo binary black holes. A&A 636:A104. https://doi.org/10.1051/0004-6361/201936528. arXiv:1706.07053 [astro-ph.HE]
Belleman R, Bédorf J, Portegies Zwart SF (2014) Kirin: N-body simulation library for GPUs. Astrophysics Source Code Library. https://ascl.net/1401.001
Belleman RG, Bédorf J, Portegies Zwart SF (2008) High performance direct gravitational N-body simulations on graphics processing units II: an implementation in CUDA. New A 13(2):103–112. https://doi.org/10.1016/j.newast.2007.07.004. arXiv:0707.0438 [astro-ph]
Belloni D, Askar A, Giersz M, Kroupa P, Rocha-Pinto HJ (2017) On the initial binary population for star cluster simulations. MNRAS 471(3):2812–2828. https://doi.org/10.1093/mnras/stx1763. arXiv:1707.04271 [astro-ph.GA]
Belloni D, Kroupa P, Rocha-Pinto HJ, Giersz M (2018) Dynamical equivalence, the origin of the Galactic field stellar and binary population, and the initial radius-mass relation of embedded clusters. MNRAS 474(3):3740–3745. https://doi.org/10.1093/mnras/stx3034. arXiv:1711.07987 [astro-ph.GA]
Berczik P, Spurzem R, Zhong S, Wang L, Nitadori K, Hamada T, Veles A (2013) Up to 700k GPU cores, Kepler, and the Exascale future for simulations of star clusters around black holes. In: Kunkel JM, Ludwig T, Meuer H (eds) Supercomputing. ISC 2013. Lecture Notes in Computer Science, vol 7905. Springer, Berlin Heidelberg, pp 13–25. https://doi.org/10.1007/978-3-642-38750-0_2
Bettwieser E (1983) A numerical method for the study of the gravothermal instability in star clusters. MNRAS 203:811–831. https://doi.org/10.1093/mnras/203.3.811
Bettwieser E, Spurzem R (1986) Anisotropy in stellar dynamics. A&A 161(1):102–112
Bettwieser E, Sugimoto D (1984) Post-collapse evolution and gravothermal oscillation of globular clusters. MNRAS 208:493–509. https://doi.org/10.1093/mnras/208.3.493
Bialas D, Lisker T, Olczak C, Spurzem R, Kotulla R (2015) On the occurrence of galaxy harassment. A&A 576:A103. https://doi.org/10.1051/0004-6361/201425235. arXiv:1503.01965 [astro-ph.GA]
Bianchini P, Varri AL, Bertin G, Zocchi A (2013) Rotating globular clusters. ApJ 772(1):67. https://doi.org/10.1088/0004-637X/772/1/67. arXiv:1305.6025 [astro-ph.GA]
Bianchini P, Norris MA, van de Ven G, Schinnerer E (2015) Understanding the central kinematics of globular clusters with simulated integrated-light IFU observations. MNRAS 453(1):365–376. https://doi.org/10.1093/mnras/stv1651. arXiv:1507.05632 [astro-ph.GA]
Bianchini P, van de Ven G, Norris MA, Schinnerer E, Varri AL (2016) A novel look at energy equipartition in globular clusters. MNRAS 458(4):3644–3654. https://doi.org/10.1093/mnras/stw552. arXiv:1603.00878 [astro-ph.GA]
Bianchini P, van der Marel RP, del Pino A, Watkins LL, Bellini A, Fardal MA, Libralato M, Sills A (2018) The internal rotation of globular clusters revealed by Gaia DR2. MNRAS 481(2):2125–2139. https://doi.org/10.1093/mnras/sty2365. arXiv:1806.02580 [astro-ph.GA]
Bianchini P, Ibata R, Famaey B (2019) Exploring the outskirts of globular clusters: the peculiar kinematics of NGC 3201. ApJ 887(1):L12. https://doi.org/10.3847/2041-8213/ab58d1. arXiv:1912.02195 [astro-ph.GA]
Biermann L (1932) Untersuchungen über den inneren Aufbau der Sterne. IV. Konvektionszonen im Innern der Sterne. ZAp 5:117. (Veröffentlichungen der Universitäts-Sternwarte Göttingen, Nr. 27.)

Binney J, Tremaine S (2008) Galactic dynamics, 2nd edn. Princeton University Press, Princeton
Böhm-Vitense E (1958) Über die Wasserstoffkonvektionszone in Sternen verschiedener Effektivtemperaturen und Leuchtkräfte. ZAp 46:108
Bondi H, Hoyle F (1944) On the mechanism of accretion by stars. MNRAS 104:273. https://doi.org/10.1093/mnras/104.5.273
Bortolas E, Mapelli M, Spera M (2018) Star cluster disruption by a massive black hole binary. MNRAS 474(1):1054–1064. https://doi.org/10.1093/mnras/stx2795. arXiv:1710.09418 [astro-ph.GA]
Boylan-Kolchin M (2018) The little engines that could? Globular clusters contribute significantly to reionization-era star formation. MNRAS 479(1):332–340. https://doi.org/10.1093/mnras/sty1490. arXiv:1711.00009 [astro-ph.GA]
Branchesi M, Maggiore M, Alonso D, Badger C, Banerjee B, Beirnaert F, Bhagwat S, Boileau G, Borhanian S, Brown DD, Chan ML, Cusin G, Danilishin SL, Degallaix J, De Luca V, Dhani A, Dietrich T, Dupletsa U, Foffa S, Franciolini G, Freise A, Gemme G, Goncharov B, Ghosh A, Gulminelli F, Gupta I, Gupta PK, Harms J, Hazra N, Hild S, Hinderer T, Heng IS, Iacovelli F, Janquart J, Janssens K, Jenkins AC, Kalaghatgi C, Koroveshi X, Li TGF, Li Y, Loffredo E, Maggio E, Mancarella M, Mapelli M, Martinovic K, Maselli A, Meyers P, Miller AL, Mondal C, Muttoni N, Narola H, Oertel M, Oganesyan G, Pacilio C, Palomba C, Pani P, Pasqualetti A, Perego A, Pèrigois C, Pieroni M, Juliana Piccinni O, Puecher A, Puppo P, Ricciardone A, Riotto A, Ronchini S, Sakellariadou M, Samajdar A, Santoliquido F, Sathyaprakash BS, Steinlechner J, Steinlechner S, Utina A, Van Den Broeck C, Zhang T (2023) Science with the Einstein Telescope: a comparison of different designs. arXiv e-prints arXiv:2303.15923 [gr-qc]
Breivik K, Coughlin S, Zevin M, Rodriguez CL, Kremer K et al (2020) COSMIC variance in binary population synthesis. ApJ 898(1):71. https://doi.org/10.3847/1538-4357/ab9d85. arXiv:1911.00903 [astro-ph.HE]
Brem P, Amaro-Seoane P, Spurzem R (2013) Relativistic mergers of compact binaries in clusters: the fingerprint of the spin. MNRAS 434(4):2999–3007. https://doi.org/10.1093/mnras/stt1220. arXiv:1302.3135 [astro-ph.CO]
Bressan A, Fagotto F, Bertelli G, Chiosi C (1993) Evolutionary sequences of stellar models with new radiative opacities. II. Z = 0.02. A&AS 100:647
Bromm V (2013) Formation of the first stars. Rep Progr Phys 76(11):112901. https://doi.org/10.1088/0034-4885/76/11/112901. arXiv:1305.5178 [astro-ph.CO]
Bromm V, Larson RB (2004) The first stars. ARA&A 42(1):79–118. https://doi.org/10.1146/annurev.astro.42.053102.134034. arXiv:astro-ph/0311019 [astro-ph]
Bromm V, Coppi PS, Larson RB (2002) The formation of the first stars. I. The primordial star-forming cloud. ApJ 564(1):23–51. https://doi.org/10.1086/323947. arXiv:astro-ph/0102503 [astro-ph]
Brott I, Evans CJ, Hunter I, de Koter A, Langer N, Dufton PL, Cantiello M, Trundle C, Lennon DJ, de Mink SE, Yoon SC, Anders P (2011) Rotating massive main-sequence stars. II. Simulating a population of LMC early B-type stars as a test of rotational mixing. A&A 530:A116. https://doi.org/10.1051/0004-6361/201016114. arXiv:1102.0766 [astro-ph.SR]
Burrows A, Hayes J (1996) Pulsar recoil and gravitational radiation due to asymmetrical stellar collapse and explosion. Phys Rev Lett 76(3):352–355. https://doi.org/10.1103/PhysRevLett.76.352. arXiv:astro-ph/9511106 [astro-ph]
Campanelli M, Lousto C, Zlochower Y, Merritt D (2007) Large merger recoils and spin flips from generic black hole binaries. ApJ 659(1):L5–L8. https://doi.org/10.1086/516712. arXiv:gr-qc/0701164 [gr-qc]
Campbell CG (1984) Tidal effects in twin-degenerate binaries. MNRAS 207:433–443. https://doi.org/10.1093/mnras/207.3.433
Capuzzo-Dolcetta R, Spera M, Punzo D (2013) A fully parallel, high precision, N-body code running on hybrid computing platforms. J Comput Phys 236:580–593. https://doi.org/10.1016/j.jcp.2012.11.013
Chabrier G (2003) Galactic stellar and substellar initial mass function. PASP 115(809):763–795. https://doi.org/10.1086/376392. arXiv:astro-ph/0304382 [astro-ph]
Chandrasekhar S (1939) An introduction to the study of stellar structure. The University of Chicago Press
Chandrasekhar S (1942) Principles of stellar dynamics. The University of Chicago Press
Charbonnel C, Schaerer D, Prantzos N, Ramírez-Galeano L, Fragos T, Kuruvandothi A, Marques-Chaves R, Gieles M (2023) N-enhancement in GN-z11: First evidence for supermassive stars nucleosynthesis in proto-globular clusters-like conditions at high redshift? 673:L7. https://doi.org/10.1051/0004-6361/202346410. arXiv:2303.07955 [astro-ph.GA]

Chattopadhyay D, Stevenson S, Hurley JR, Bailes M, Broekgaarden F (2021) Modelling neutron star-black hole binaries: future pulsar surveys and gravitational wave detectors. MNRAS 504(3):3682–3710. https://doi.org/10.1093/mnras/stab973. arXiv:2011.13503 [astro-ph.HE]

Chen CW, Chen WP (2010) Morphological distortion of galactic globular clusters. ApJ 721(2):1790–1819. https://doi.org/10.1088/0004-637X/721/2/1790

Chen J, Yan CS, Lu YJ, Zhao YT, Ge JQ (2021) On detecting stellar binary black holes via the LISA-Taiji network. Res Astron Astrophys 21(11):285. https://doi.org/10.1088/1674-4527/21/11/285. arXiv:2201.12516 [astro-ph.HE]

Chenciner A, Montgomery R (2000) A remarkable periodic solution of the three-body problem in the case of equal masses. Ann Math 152(3):881–901. http://www.jstor.org/stable/2661357. arXiv:math/0011268 [math.DS]

Chin SA (1997) Symplectic integrators from composite operator factorizations. Phys Lett A 226(6):344–348. https://doi.org/10.1016/S0375-9601(97)00003-0

Chin SA (2007) Physics of symplectic integrators: perihelion advances and symplectic corrector algorithms. Phys Rev E 75(3):036701. https://doi.org/10.1103/PhysRevE.75.036701. arXiv:math-ph/0608012 [math-ph]

Chin SA, Chen CR (2005) Forward symplectic integrators for solving gravitational few-body problems. Celest Mech Dyn Astron 91(3–4):301–322. https://doi.org/10.1007/s10569-004-4622-z

Church RP, Tout CA, Hurley JR (2009) N-body simulations with live stellar evolution. PASA 26(1):92–102. https://doi.org/10.1071/AS08062. arXiv:0902.0846 [astro-ph.SR]

Claeys JSW, Pols OR, Izzard RG, Vink J, Verbunt FWM (2014) Theoretical uncertainties of the Type Ia supernova rate. A&A 563:A83. https://doi.org/10.1051/0004-6361/201322714. arXiv:1401.2895 [astro-ph.SR]

Claeyssens A, Adamo A, Richard J, Mahler G, Messa M, Dessauges-Zavadsky M (2023) Star formation at the smallest scales: a JWST study of the clump populations in SMACS0723. MNRAS 520(2):2180–2203. https://doi.org/10.1093/mnras/stac3791. arXiv:2208.10450 [astro-ph.GA]

Claret A (1995) Stellar models for a wide range of initial chemical compositions until helium burning. I. From X=0.60 to X=0.80 for Z=0.02. A&AS 109:441–446

Claret A, Gimenez A (1995) Stellar models for a wide range of initial chemical compositions until helium burning. II. From X=0.63 to X=0.80, for Z=0.01. A&AS 114:549

Clark GW (1975) X-ray binaries in globular clusters. ApJ 199:L143–L145. https://doi.org/10.1086/181869

Cohn H (1979) Numerical integration of the Fokker–Planck equation and the evolution of star clusters. ApJ 234:1036–1053. https://doi.org/10.1086/157587

Cohn H (1980) Late core collapse in star clusters and the gravothermal instability. ApJ 242:765–771. https://doi.org/10.1086/158511

Cohn H, Kulsrud RM (1978) The stellar distribution around a black hole: numerical integration of the Fokker–Planck equation. ApJ 226:1087–1108. https://doi.org/10.1086/156685

Cohn H, Hut P, Wise M (1989) Gravothermal oscillations after core collapse in globular cluster evolution. ApJ 342:814. https://doi.org/10.1086/167638

Collaboration Kagra, Akutsu T, Ando M, Arai K, Arai Y et al (2019) KAGRA: 2.5 generation interferometric gravitational wave detector. Nat Astron 3:35–40. https://doi.org/10.1038/s41550-018-0658-y. arXiv:1811.08079 [gr-qc]

Conroy C, Gunn JE (2010) The propagation of uncertainties in stellar population synthesis modeling. III. Model calibration, comparison, and evaluation. ApJ 712(2):833–857. https://doi.org/10.1088/0004-637X/712/2/833. arXiv:0911.3151 [astro-ph.CO]

Conroy C, Gunn JE, White M (2009) The propagation of uncertainties in stellar population synthesis modeling. I. The relevance of uncertain aspects of stellar evolution and the initial mass function to the derived physical properties of galaxies. ApJ 699(1):486–506. https://doi.org/10.1088/0004-637X/699/1/486. arXiv:0809.4261 [astro-ph]

Conroy C, White M, Gunn JE (2010) The propagation of uncertainties in stellar population synthesis modeling. II. The challenge of comparing galaxy evolution models to observations. ApJ 708(1):58–70. https://doi.org/10.1088/0004-637X/708/1/58. arXiv:0904.0002 [astro-ph.CO]

Costa G, Ballone A, Mapelli M, Bressan A (2022) Formation of black holes in the pair-instability mass gap: evolution of a post-collision star. MNRAS 516(1):1072–1080. https://doi.org/10.1093/mnras/stac2222. arXiv:2204.03492 [astro-ph.SR]

David LP, Durisen RH, Cohn HN (1987) The evolution of active galactic nuclei. I. Models without stellar evolution. ApJ 313:556. https://doi.org/10.1086/164997

David LP, Durisen RH, Cohn HN (1987) The evolution of active galactic nuclei. II. Models with stellar evolution. ApJ 316:505. https://doi.org/10.1086/165222
de Souza RS, Ciardi B, Maio U, Ferrara A (2013) Dark matter halo environment for primordial star formation. MNRAS 428(3):2109–2117. https://doi.org/10.1093/mnras/sts181. arXiv:1209.0825 [astro-ph.CO]
de Vita R, Trenti M, Bianchini P, Askar A, Giersz M et al (2017) Prospects for detection of intermediate-mass black holes in globular clusters using integrated-light spectroscopy. MNRAS 467(4):4057–4066. https://doi.org/10.1093/mnras/stx325. arXiv:1702.01741 [astro-ph.GA]
de Vries N, Portegies Zwart S, Figueira J (2014) The evolution of triples with a Roche lobe filling outer star. MNRAS 438(3):1909–1921. https://doi.org/10.1093/mnras/stt1688. arXiv:1309.1475 [astro-ph.SR]
Dean J, Ghemawat S (2004) Mapreduce: simplified data processing on large clusters. Commun ACM 51:137–150. https://doi.org/10.1145/1327452.1327492
Decin L (2020) Evolution and mass loss of cool ageing stars: a Daedalean story. arXiv e-prints arXiv:2011.13472 [astro-ph.SR]
Dehnen W, Hernandez DM (2017) Symplectic fourth-order maps for the collisional N -body problem. MNRAS 465(1):1201–1217. https://doi.org/10.1093/mnras/stw2758. arXiv:1609.09375 [math.NA]
Dewi JDM, Tauris TM (2000) On the energy equation and efficiency parameter of the common envelope evolution. A&A 360:1043–1051 arXiv:astro-ph/0007034 [astro-ph]
Di Carlo UN, Giacobbo N, Mapelli M, Pasquato M, Spera M et al (2019) Merging black holes in young star clusters. MNRAS 487(2):2947–2960. https://doi.org/10.1093/mnras/stz1453. arXiv:1901.00863 [astro-ph.HE]
Di Carlo UN, Mapelli M, Bouffanais Y, Giacobbo N, Santoliquido F et al (2020) Binary black holes in the pair instability mass gap. MNRAS 497(1):1043–1049. https://doi.org/10.1093/mnras/staa1997. arXiv:1911.01434 [astro-ph.HE]
Di Carlo UN, Mapelli M, Giacobbo N, Spera M, Bouffanais Y et al (2020) Binary black holes in young star clusters: the impact of metallicity. MNRAS 498(1):495–506. https://doi.org/10.1093/mnras/staa2286. arXiv:2004.09525 [astro-ph.HE]
Di Carlo UN, Mapelli M, Pasquato M, Rastello S, Ballone A, Dall'Amico M, Giacobbo N, Iorio G, Spera M, Torniamenti S, Haardt F (2021) Intermediate-mass black holes from stellar mergers in young star clusters. MNRAS 507(4):5132–5143. https://doi.org/10.1093/mnras/stab2390. arXiv:2105.01085 [astro-ph.GA]
Dorband EN, Hemsendorf M, Merritt D (2003) Systolic and hyper-systolic algorithms for the gravitational N-body problem, with an application to Brownian motion. J Comput Phys 185(2):484–511. https://doi.org/10.1016/S0021-9991(02)00067-0. arXiv:astro-ph/0112092 [astro-ph]
Eggenberger P, Meynet G, Maeder A, Hirschi R, Charbonnel C et al (2008) The Geneva stellar evolution code. Ap&SS 316(1–4):43–54. https://doi.org/10.1007/s10509-007-9511-y
Eggleton P (2006) Evolutionary processes in binary and multiple stars. Cambridge University Press, Cambridge
Eggleton PP (1971) The evolution of low mass stars. MNRAS 151:351. https://doi.org/10.1093/mnras/151.3.351
Eggleton PP (1972) Composition changes during stellar evolution. MNRAS 156:361. https://doi.org/10.1093/mnras/w156.3.361
Eggleton PP (1973) A numerical treatment of double shell source stars. MNRAS 163:279. https://doi.org/10.1093/mnras/163.3.279
Eggleton PP (1983) Aproximations to the radii of Roche lobes. ApJ 268:368–369. https://doi.org/10.1086/160960
Eggleton PP (1996) Combining Stellar evolution and stellar dynamics. In: Hut P, Makino J (eds) Dynamical evolution of star clusters: confrontation of theory and observations. vol 174. p 213
Eggleton PP, Faulkner J, Flannery BP (1973) An approximate equation of state for stellar material. A&A 23:325
Eggleton PP, Fitchett MJ, Tout CA (1989) The distribution of visual binaries with two bright components. ApJ 347:998. https://doi.org/10.1086/168190
Eggleton PP, Kiseleva LG, Hut P (1998) The equilibrium tide model for tidal friction. ApJ 499(2):853–870. https://doi.org/10.1086/305670. arXiv:astro-ph/9801246 [astro-ph]
Einsel C, Spurzem R (1999) Dynamical evolution of rotating stellar systems—I. Pre-collapse, equal-mass system. MNRAS 302(1):81–95. https://doi.org/10.1046/j.1365-8711.1999.02083.x

Eisenstein DJ, Hut P (1998) HOP: a new group-finding algorithm for N-body simulations. ApJ 498 (1):137–142. https://doi.org/10.1086/305535. arXiv:astro-ph/9712200 [astro-ph]
Ekström S, Georgy C, Eggenberger P, Meynet G, Mowlavi N et al (2012) Grids of stellar models with rotation. I. Models from 0.8 to 120 $M_{\odot}$ at solar metallicity (Z = 0.014). A&A 537:A146. https://doi.org/10.1051/0004-6361/201117751. arXiv:1110.5049 [astro-ph.SR]
Eldridge JJ, Tout CA (2004) The progenitors of core-collapse supernovae. MNRAS 353(1):87–97. https://doi.org/10.1111/j.1365-2966.2004.08041.x. arXiv:astro-ph/0405408 [astro-ph]
Eldridge JJ, Stanway ER, Xiao L, McClelland LAS, Taylor G, Ng M, Greis SML, Bray JC (2017) Binary population and spectral synthesis version 2.1: construction, observational verification, and new results. PASA 34:e058. https://doi.org/10.1017/pasa.2017.51. arXiv:1710.02154 [astro-ph.SR]
Elson R, Hut P, Inagaki S (1987) Dynamical evolution of globular clusters. ARA&A 25:565–601. https://doi.org/10.1146/annurev.aa.25.090187.003025
Ernst A, Glaschke P, Fiestas J, Just A, Spurzem R (2007) N-body models of rotating globular clusters. MNRAS 377(2):465–479. https://doi.org/10.1111/j.1365-2966.2007.11602.x. arXiv:astro-ph/0702206 [astro-ph]
Fagotto F, Bressan A, Bertelli G, Chiosi C (1994) Evolutionary sequences of stellar models with new radiative opacities. III. Z=0.0004 and Z=0.05. A&AS 104:365–376
Fagotto F, Bressan A, Bertelli G, Chiosi C (1994) Evolutionary sequences of stellar models with new radiative opacities. IV. Z=0.004 and Z=0.008. A&AS 105:29–38
Fellhauer M, Lin DNC, Bolte M, Aarseth SJ, Williams KA (2003) The white dwarf deficit in open clusters: dynamical processes. ApJ 595(1):L53–L56. https://doi.org/10.1086/379005. arXiv:astro-ph/0308261 [astro-ph]
Ferraro FR, Mucciarelli A, Lanzoni B, Pallanca C, Lapenna E, Origlia L, Dalessandro E, Valenti E, Beccari G, Bellazzini M, Vesperini E, Varri A, Sollima A (2018) MIKiS: the multi-instrument kinematic survey of galactic globular clusters. I. Velocity dispersion profiles and rotation signals of 11 globular clusters. ApJ 860(1):50. https://doi.org/10.3847/1538-4357/aabe2f. arXiv:1804.08618 [astro-ph.GA]
Fiestas J, Spurzem R (2010) Dynamical evolution of rotating dense stellar systems with embedded black holes. MNRAS 405(1):194–208. https://doi.org/10.1111/j.1365-2966.2010.16479.x
Fiestas J, Spurzem R, Kim E (2006) 2D Fokker–Planck models of rotating clusters. MNRAS 373(2):677–686. https://doi.org/10.1111/j.1365-2966.2006.11036.x. arXiv:astro-ph/0609056 [astro-ph]
Fiestas J, Porth O, Berczik P, Spurzem R (2012) Evolution of growing black holes in axisymmetric galaxy cores. MNRAS 419(1):57–69. https://doi.org/10.1111/j.1365-2966.2011.19670.x. arXiv:1108.3993 [astro-ph.GA]
Fragos T, Willems B, Kalogera V, Ivanova N, Rockefeller G, Fryer CL, Young PA (2009) Understanding compact object formation and Natal Kicks. II. The case of XTE J1118 + 480. ApJ 697(2):1057–1070. https://doi.org/10.1088/0004-637X/697/2/1057. arXiv:0809.1588 [astro-ph]
Fragos T, Andrews JJ, Ramirez-Ruiz E, Meynet G, Kalogera V, Taam RE, Zezas A (2019) The complete evolution of a neutron-star binary through a common envelope phase using 1d hydrodynamic simulations. ApJ 883(2):L45. https://doi.org/10.3847/2041-8213/ab40d1
Frank J, Rees MJ (1976) Effects of massive black holes on dense stellar systems. MNRAS 176:633–647. https://doi.org/10.1093/mnras/176.3.633
Fraser M, Casey AR, Gilmore G, Heger A, Chan C (2017) The mass distribution of population III stars. MNRAS 468(1):418–425. https://doi.org/10.1093/mnras/stx480. arXiv:1511.03428 [astro-ph.SR]
Fregeau JM, Joshi KJ, Portegies Zwart SF, Rasio FA (2002) Mass segregation in globular clusters. ApJ 570 (1):171–183. https://doi.org/10.1086/339576. arXiv:astro-ph/0111057 [astro-ph]
Frenk CS, Fall SM (1982) An ellipticity-age relation for globular clusters in the Large Magellanic Cloud—I. Measurements. MNRAS 199:565–580. https://doi.org/10.1093/mnras/199.3.565
Fryer CL (2004) Neutron star kicks from asymmetric collapse. ApJ 601(2):L175–L178. https://doi.org/10.1086/382044. arXiv:astro-ph/0312265 [astro-ph]
Fryer CL, Kusenko A (2006) Effects of neutrino-driven kicks on the supernova explosion mechanism. ApJS 163(2):335–343. https://doi.org/10.1086/500933. arXiv:astro-ph/0512033 [astro-ph]
Fryer CL, Young PA (2007) Late-time convection in the collapse of a 23 M_{solar} star. ApJ 659(2):1438–1448. https://doi.org/10.1086/513003. arXiv:astro-ph/0612154 [astro-ph]
Fryer CL, Woosley SE, Heger A (2001) Pair-instability supernovae, gravity waves, and gamma-ray transients. ApJ 550(1):372–382. https://doi.org/10.1086/319719. arXiv:astro-ph/0007176 [astro-ph]
Fryer CL, Belczynski K, Wiktorowicz G, Dominik M, Kalogera V et al (2012) Compact remnant mass function: dependence on the explosion mechanism and metallicity. ApJ 749(1):91. https://doi.org/10.1088/0004-637X/749/1/91. arXiv:1110.1726 [astro-ph.SR]

Fuller GM, Kusenko A, Mocioiu I, Pascoli S (2003) Pulsar kicks from a dark-matter sterile neutrino. Phys Rev D 68(10):103002. https://doi.org/10.1103/PhysRevD.68.103002. arXiv:astro-ph/0307267 [astro-ph]

Fuller J, Ma L (2019) Most black holes are born very slowly rotating. ApJ 881(1):L1. https://doi.org/10.3847/2041-8213/ab339b. arXiv:1907.03714 [astro-ph.SR]

Fuller J, Piro AL, Jermyn AS (2019) Slowing the spins of stellar cores. MNRAS 485(3):3661–3680. https://doi.org/10.1093/mnras/stz514. arXiv:1902.08227 [astro-ph.SR]

Funato Y, Hut P, McMillan S, Makino J (1996) Time-symmetrized Kustaanheimo–Stiefel regularization. AJ 112:1697. https://doi.org/10.1086/118136. arXiv:astro-ph/9604025 [astro-ph]

Gabriel M, Noels A, Montalbán J, Miglio A (2014) Proper use of Schwarzschild Ledoux criteria in stellar evolution computations. A&A 569:A63. https://doi.org/10.1051/0004-6361/201423442. arXiv:1405.0128 [astro-ph.SR]

Gaburov E, Harfst S, Portegies Zwart S (2009) SAPPORO: a way to turn your graphics cards into a GRAPE-6. New A 14(7):630–637. https://doi.org/10.1016/j.newast.2009.03.002. arXiv:0902.4463 [astro-ph.IM]

Geller AM, Leigh NWC, Giersz M, Kremer K, Rasio FA (2019) In search of the thermal eccentricity distribution. ApJ 872(2):165. https://doi.org/10.3847/1538-4357/ab0214. arXiv:1902.00019 [astro-ph.SR]

Gerhard O (2001) The galactic center HE I stars: remains of a dissolved young cluster? ApJ 546(1):L39–L42. https://doi.org/10.1086/318054. arXiv:astro-ph/0005096 [astro-ph]

Gessner A, Janka HT (2018) Hydrodynamical neutron-star kicks in electron-capture supernovae and implications for the CRAB supernova. ApJ 865(1):61. https://doi.org/10.3847/1538-4357/aadbae. arXiv:1802.05274 [astro-ph.HE]

Giacobbo N, Mapelli M (2018) The progenitors of compact-object binaries: impact of metallicity, common envelope and natal kicks. MNRAS 480(2):2011–2030. https://doi.org/10.1093/mnras/sty1999. arXiv:1806.00001 [astro-ph.HE]

Giacobbo N, Mapelli M (2019) Erratum: The progenitors of compact-object binaries: impact of metallicity, common envelope and natal kicks. MNRAS 486(2):2494–2495. https://doi.org/10.1093/mnras/stz892

Gieles M, Zocchi A (2015) A family of lowered isothermal models. MNRAS 454(1):576–592. https://doi.org/10.1093/mnras/stv1848. arXiv:1508.02120 [astro-ph.IM]

Giersz M (1998) Monte Carlo simulations of star clusters—I. First results. MNRAS 298(4):1239–1248. https://doi.org/10.1046/j.1365-8711.1998.01734.x. arXiv:astro-ph/9804127 [astro-ph]

Giersz M, Heggie DC (1994) Statistics of N-body simulations—part one—equal masses before core collapse. MNRAS 268:257. https://doi.org/10.1093/mnras/268.1.257. arXiv:astro-ph/9305008 [astro-ph]

Giersz M, Heggie DC (1994) Statistics of N-body simulations—part two—equal masses after core collapse. MNRAS 270:298. https://doi.org/10.1093/mnras/270.2.298. arXiv:astro-ph/9403024 [astro-ph]

Giersz M, Heggie DC (1996) Statistics of N-body simulations - III. Unequal masses. MNRAS 279 (3):1037–1056. https://doi.org/10.1093/mnras/279.3.1037

Giersz M, Heggie DC (1997) Statistics of N-body simulations—IV. Unequal masses with a tidal field. MNRAS 286(3):709–731. https://doi.org/10.1093/mnras/286.3.709

Giersz M, Spurzem R (1994) Comparing direct N-body integration with anisotropic gaseous models of star clusters. MNRAS 269:241. https://doi.org/10.1093/mnras/269.2.241. arXiv:astro-ph/9305033 [astro-ph]

Giersz M, Heggie DC, Hurley JR, Hypki A (2013) MOCCA code for star cluster simulations—II. Comparison with N-body simulations. MNRAS 431(3):2184–2199. https://doi.org/10.1093/mnras/stt307. arXiv:1112.6246 [astro-ph.GA]

Giersz M, Leigh N, Hypki A, Lützgendorf N, Askar A (2015) MOCCA code for star cluster simulations—IV. A new scenario for intermediate mass black hole formation in globular clusters. MNRAS 454 (3):3150–3165. https://doi.org/10.1093/mnras/stv2162. arXiv:1506.05234 [astro-ph.GA]

Giesers B, Dreizler S, Husser TO, Kamann S, Anglada Escudé G, Brinchmann J, Carollo CM, Roth MM, Weilbacher PM, Wisotzki L (2018) A detached stellar-mass black hole candidate in the globular cluster NGC 3201. MNRAS 475(1):L15–L19. https://doi.org/10.1093/mnrasl/slx203. arXiv:1801.05642 [astro-ph.SR]

Giesers B, Kamann S, Dreizler S, Husser TO, Askar A, Göttgens F, Brinchmann J, Latour M, Weilbacher PM, Wendt M, Roth MM (2019) A stellar census in globular clusters with MUSE: binaries in NGC 3201. A&A 632:A3. https://doi.org/10.1051/0004-6361/201936203. arXiv:1909.04050 [astro-ph.SR]

Glaschke P, Amaro-Seoane P, Spurzem R (2014) Hybrid methods in planetesimal dynamics: description of a new composite algorithm. MNRAS 445(4):3620–3649. https://doi.org/10.1093/mnras/stu1558. arXiv:1105.6094 [astro-ph.EP]
Goodman J (1983) Core collapse with strong encounters. ApJ 270:700–710. https://doi.org/10.1086/161161
Goodman J, Heggie DC, Hut P (1993) On the exponential instability of N-body systems. ApJ 415:715. https://doi.org/10.1086/173196
Goodman JJ (1983b) Dynamical relaxation in stellar systems. Ph.D. thesis, Princeton University Press
Goodwin SP, Kroupa P (2005) Limits on the primordial stellar multiplicity. A&A 439(2):565–569. https://doi.org/10.1051/0004-6361:20052654. arXiv:astro-ph/0505470 [astro-ph]
Goodwin SP, Whitworth AP (2004) The dynamical evolution of fractal star clusters: the survival of substructure. A&A 413:929–937. https://doi.org/10.1051/0004-6361:20031529. arXiv:astro-ph/0310333 [astro-ph]
Gratton RG, Carretta E, Bragaglia A (2012) Multiple populations in globular clusters. Lessons learned from the Milky Way globular clusters. AAPR 20:50. https://doi.org/10.1007/s00159-012-0050-3. arXiv:1201.6526 [astro-ph.SR]
Greene JE, Strader J, Ho LC (2020) Intermediate-mass black holes. ARA&A 58:257–312. https://doi.org/10.1146/annurev-astro-032620-021835. arXiv:1911.09678 [astro-ph.GA]
Hachisu I (1979) Gravogyro catastrophe of self-gravitating and rotating systems. PASJ 31:523–540
Hachisu I (1982) Gravothermal and Gravogyro catastrophes of rotating and self-gravitating gaseous disks. PASJ 34:313
Hachisu I, Nakada Y, Nomoto K, Sugimoto D (1978) Gravothermal catastrophe of finite amplitude. Prog Theor Phys 60(2):393–402. https://doi.org/10.1143/PTP.60.393
Hamers AS, Safarzadeh M (2020) Was GW190412 born from a hierarchical 3 + 1 quadruple configuration? ApJ 898(2):99. https://doi.org/10.3847/1538-4357/ab9b27. arXiv:2005.03045 [astro-ph.HE]
Hansen BMS, Phinney ES (1997) The pulsar kick velocity distribution. MNRAS 291(3):569–577. https://doi.org/10.1093/mnras/291.3.569. arXiv:astro-ph/9708071 [astro-ph]
Harfst S, Gualandris A, Merritt D, Spurzem R, Portegies Zwart S, Berczik P (2007) Performance analysis of direct N-body algorithms on special-purpose supercomputers. New A 12(5):357–377. https://doi.org/10.1016/j.newast.2006.11.003. arXiv:astro-ph/0608125 [astro-ph]
Harris WE (1976) Spatial structure of the globular cluster system and the distance to the galactic center. AJ 81:1095–1116. https://doi.org/10.1086/111991
Harris WE (1996) A catalog of parameters for globular clusters in the milky way. AJ 112:1487. https://doi.org/10.1086/118116
Harris WE, Blakeslee JP, Harris GLH (2017) Galactic Dark matter halos and globular cluster populations. III. Extension to extreme environments. ApJ 836(1):67. https://doi.org/10.3847/1538-4357/836/1/67. arXiv:1701.04845 [astro-ph.GA]
Hayasaki K, Zhong S, Li S, Berczik P, Spurzem R (2018) Classification of tidal disruption events based on stellar orbital properties. ApJ 855(2):129. https://doi.org/10.3847/1538-4357/aab0a5. arXiv:1802.06798 [astro-ph.HE]
Heggie D, Hut P (2003) The gravitational million-body problem: a multidisciplinary approach to star cluster dynamics. Cambridge University Press, Cambridge
Heggie DC (1974) A global regularisation of the gravitational N-body problem. CeMec 10(2):217–241. https://doi.org/10.1007/BF01227621
Heggie DC (1975) Binary evolution in stellar dynamics. MNRAS 173:729–787. https://doi.org/10.1093/mnras/173.3.729
Heggie DC (1984) Post-collapse evolution of a gaseous cluster model. MNRAS 206:179–195. https://doi.org/10.1093/mnras/206.1.179
Heggie DC (2000) A new outcome of binary-binary scattering. MNRAS 318(4):L61–L63. https://doi.org/10.1046/j.1365-8711.2000.04027.x. arXiv:astro-ph/9604016 [astro-ph]
Hellström C, Mikkola S (2010) Explicit algorithmic regularization in the few-body problem for velocity-dependent perturbations. Celest Mech Dyn Astron 106(2):143–156. https://doi.org/10.1007/s10569-009-9248-8
Hemsendorf M, Sigurdsson S, Spurzem R (2002) Collisional dynamics around binary black holes in galactic centers. ApJ 581(2):1256–1270. https://doi.org/10.1086/344255. arXiv:astro-ph/0103410 [astro-ph]
Hénon M (1961) Sur l'évolution dynamique des amas globulaires. AnAp 24:369

Hénon M (1971) Monte Carlo models of star clusters (Part of the Proceedings of the IAU Colloquium No. 10, held in Cambridge, England, August 12–15, 1970.). Ap&SS 13(2):284–299. https://doi.org/10.1007/BF00649159

Hénon M (1975) Two recent developments concerning the monte carlo method. In: Hayli A (ed) Dynamics of the solar systems, vol 69. p 133

Hernquist L, Ostriker JP (1992) A self-consistent field method for galactic dynamics. ApJ 386:375. https://doi.org/10.1086/171025

Hijikawa K, Tanikawa A, Kinugawa T, Yoshida T, Umeda H (2021) On the population III binary black hole mergers beyond the pair-instability mass gap. MNRAStmp. https://doi.org/10.1093/mnrasl/slab052. arXiv:2104.13384 [astro-ph.HE]

Hills JG (1975) Encounters between binary and single stars and their effect on the dynamical evolution of stellar systems. AJ 80:809–825. https://doi.org/10.1086/111815

Hills JG (1975) Possible power source of Seyfert galaxies and QSOs. Nature 254(5498):295–298. https://doi.org/10.1038/254295a0

Hobbs G, Lorimer DR, Lyne AG, Kramer M (2005) A statistical study of 233 pulsar proper motions. MNRAS 360(3):974–992. https://doi.org/10.1111/j.1365-2966.2005.09087.x. arXiv:astro-ph/0504584 [astro-ph]

Hoffman L, Loeb A (2007) Dynamics of triple black hole systems in hierarchically merging massive galaxies. MNRAS 377(3):957–976. https://doi.org/10.1111/j.1365-2966.2007.11694.x. arXiv:astro-ph/0612517 [astro-ph]

Hong J, Kim E, Lee HM, Spurzem R (2013) Comparative study between N-body and Fokker–Planck simulations for rotating star clusters—II. Two-component models. MNRAS 430(4):2960–2972. https://doi.org/10.1093/mnras/stt099. arXiv:1211.6527 [astro-ph.SR]

Hong J, de Grijs R, Askar A, Berczik P, Li C et al (2017) The dynamical origin of multiple populations in intermediate-age clusters in the Magellanic Clouds. MNRAS 472(1):67–77. https://doi.org/10.1093/mnras/stx1954. arXiv:1707.09153 [astro-ph.GA]

Hong J, Vesperini E, Belloni D, Giersz M (2017) Dynamical formation of cataclysmic variables in globular clusters. MNRAS 464(2):2511–2516. https://doi.org/10.1093/mnras/stw2595. arXiv:1611.00779 [astro-ph.GA]

Hong J, Askar A, Giersz M, Hypki A, Yoon SJ (2020) MOCCA survey database I: Binary black hole mergers from globular clusters with intermediate mass black holes. MNRAS 498(3):4287–4294. https://doi.org/10.1093/mnras/staa2677. arXiv:2008.10823 [astro-ph.HE]

Hopkins AM (2018) The Dawes Review 8: measuring the stellar initial mass function. PASA 35:e039. https://doi.org/10.1017/pasa.2018.29. arXiv:1807.09949 [astro-ph.GA]

Huang SY, Spurzem R, Berczik P (2016) Performance analysis of parallel gravitational N-body codes on large GPU clusters. Res Astron Astrophys 16(1):11. https://doi.org/10.1088/1674-4527/16/1/011. arXiv:1508.02510 [astro-ph.IM]

Hughes SA (2009) Gravitational waves from merging compact binaries. ARA&A 47(1):107–157. https://doi.org/10.1146/annurev-astro-082708-101711. arXiv:0903.4877 [astro-ph.CO]

Hurley JR (2008a) N-body binary evolution. In: Aarseth SJ, Tout CA, Mardling RA (eds) The Cambridge N-body lectures. Lecture notes in physics, vol. 760. Springer, Berlin, p 321. https://doi.org/10.1007/978-1-4020-8431-7_12

Hurley JR (2008b) N-body stellar evolution. In: Aarseth SJ, Tout CA, Mardling RA (eds) The Cambridge N-body lectures. Lecture notes in physics, vol 760. Springer, Berlin, p 283. https://doi.org/10.1007/978-1-4020-8431-7_10

Hurley JR, Shara MM (2003) White Dwarf sequences in dense star clusters. ApJ 589(1):179–198. https://doi.org/10.1086/374637. arXiv:astro-ph/0302119 [astro-ph]

Hurley JR, Pols OR, Tout CA (2000) Comprehensive analytic formulae for stellar evolution as a function of mass and metallicity. MNRAS 315(3):543–569. https://doi.org/10.1046/j.1365-8711.2000.03426.x. arXiv:astro-ph/0001295 [astro-ph]

Hurley JR, Tout CA, Pols OR (2002) Evolution of binary stars and the effect of tides on binary populations. MNRAS 329(4):897–928. https://doi.org/10.1046/j.1365-8711.2002.05038.x. arXiv:astro-ph/0201220 [astro-ph]

Hurley JR, Pols OR, Aarseth SJ, Tout CA (2005) A complete N-body model of the old open cluster M67. MNRAS 363(1):293–314. https://doi.org/10.1111/j.1365-2966.2005.09448.x. arXiv:astro-ph/0507239 [astro-ph]

Hurley JR, Pols OR, Tout CA (2013a) SSE: Single Star Evolution. Astrophysics Source Code Library, ascl:1303.015. https://ascl.net/1303.015

Hurley JR, Tout CA, Pols OR (2013b) BSE: Binary Star Evolution. Astrophysics Source Code Library, ascl:1303.014. https://ascl.net/1303.014
Hut P (1980) Stability of tidal equilibrium. A&A 92(1–2):167–170
Hut P (1981) Tidal evolution in close binary systems. A&A 99:126–140
Hut P, McMillan SLW (1986) The use of supercomputers in stellar dynamics, lecture notes in physics, vol 267. Springer, Berlin. https://doi.org/10.1007/BFb0116387
Hut P, Makino J, McMillan S (1995) Building a Better Leapfrog. ApJ 443:L93. https://doi.org/10.1086/187844
Hypki A (2018) BEANS: a software package for distributed Big Data analysis. MNRAS 477(3):3076–3090. https://doi.org/10.1093/mnras/sty803
Hypki A, Giersz M, Hong J, Leveque A, Askar A, Belloni D, Otulakowska-Hypka M (2022) MOCCA: dynamics and evolution of single and binary stars of multiple stellar populations in tidally filling and underfilling globular star clusters. MNRAS 517(4):4768–4787. https://doi.org/10.1093/mnras/stac2815. arXiv:2205.05397 [astro-ph.GA]
Inagaki S, Hachisu I (1978) Thermodynamic stability of rotating gaseous cylinders. I. Stability analysis by linear series. PASJ 30:39–56
Inagaki S, Lynden-Bell D (1983) Self-similar solutions for post-collapse evolution of globular clusters. MNRAS 205:913–930. https://doi.org/10.1093/mnras/205.4.913
Ivanova N (2016) Evolution of binaries with compact objects in globular clusters. In: Meiron Y, Li S, Liu FK, Spurzem R (eds) Star clusters and black holes in galaxies across cosmic time. IAU Symposium, vol 312. pp 203–212. https://doi.org/10.1017/S1743921315007826. arXiv:1706.07578 [astro-ph.SR]
Ivanova N (2018) On the use of hydrogen recombination energy during common envelope events. ApJ 858 (2):L24. https://doi.org/10.3847/2041-8213/aac101. arXiv:1804.10681 [astro-ph.SR]
Ivanova N (2019) Common envelope physics. In: KITP conference: merging visions: exploring compact-object binaries with gravity and light. p 7
Ivanova N, Nandez JLA (2016) Common envelope events with low-mass giants: understanding the transition to the slow spiral-in. MNRAS 462(1):362–381. https://doi.org/10.1093/mnras/stw1676. arXiv:1606.04923 [astro-ph.SR]
Ivanova N, Heinke CO, Rasio FA, Belczynski K, Fregeau JM (2008) Formation and evolution of compact binaries in globular clusters - II. Binaries with neutron stars. MNRAS 386(1):553–576. https://doi.org/10.1111/j.1365-2966.2008.13064.x. arXiv:0706.4096 [astro-ph]
Ivanova N, Justham S, Chen X, De Marco O, Fryer CL et al (2013) Common envelope evolution: where we stand and how we can move forward. A&ARv 21:59. https://doi.org/10.1007/s00159-013-0059-2. arXiv:1209.4302 [astro-ph.HE]
Ivanova N, Justham S, Ricker P (2020) Common envelope evolution. 2514–3433, IOP Publishing. https://doi.org/10.1088/2514-3433/abb6f0
Iwasawa M, Portegies Zwart S, Makino J (2015) GPU-enabled particle–particle particle-tree scheme for simulating dense stellar cluster system. Comput Astrophys Cosmol 2:6. https://doi.org/10.1186/s40668-015-0010-1. arXiv:1506.04553 [astro-ph.IM]
Iwasawa M, Tanikawa A, Hosono N, Nitadori K, Muranushi T, Makino J (2016) Implementation and performance of FDPS: a framework for developing parallel particle simulation codes. PASJ 68(4):54. https://doi.org/10.1093/pasj/psw053. arXiv:1601.03138 [astro-ph.IM]
Iwasawa M, Oshino S, Fujii MS, Hori Y (2017) PENTACLE: parallelized particle-particle particle-tree code for planet formation. PASJ 69(5):81. https://doi.org/10.1093/pasj/psx073. arXiv:1810.11970 [astro-ph.EP]
Iwasawa M, Namekata D, Nitadori K, Nomura K, Wang L, Tsubouchi M, Makino J (2020) Accelerated FDPS: algorithms to use accelerators with FDPS. PASJ 72(1):13. https://doi.org/10.1093/pasj/psz133. arXiv:1907.02290 [astro-ph.IM]
Izzard RG, Tout CA, Karakas AI, Pols OR (2004) A new synthetic model for asymptotic giant branch stars. MNRAS 350(2):407–426. https://doi.org/10.1111/j.1365-2966.2004.07446.x. arXiv:astro-ph/0402403 [astro-ph]
Izzard RG, Dray LM, Karakas AI, Lugaro M, Tout CA (2006) Population nucleosynthesis in single and binary stars. I. Model. A&A 460(2):565–572. https://doi.org/10.1051/0004-6361:20066129
Izzard RG, Glebbeek E, Stancliffe RJ, Pols OR (2009) Population synthesis of binary carbon-enhanced metal-poor stars. A&A 508(3):1359–1374. https://doi.org/10.1051/0004-6361/200912827. arXiv:0910.2158 [astro-ph.SR]

Jani K, Shoemaker D, Cutler C (2020) Detectability of intermediate-mass black holes in multiband gravitational wave astronomy. Nat Astronomy 4:260–265. https://doi.org/10.1038/s41550-019-0932-7. arXiv:1908.04985 [gr-qc]

Jeřábková T, Hasani Zonoozi A, Kroupa P, Beccari G, Yan Z, Vazdekis A, Zhang ZY (2018) Impact of metallicity and star formation rate on the time-dependent, galaxy-wide stellar initial mass function. A&A 620:A39. https://doi.org/10.1051/0004-6361/201833055. arXiv:1809.04603 [astro-ph.GA]

Jiménez-Forteza X, Keitel D, Husa S, Hannam M, Khan S et al (2017) Hierarchical data-driven approach to fitting numerical relativity data for nonprecessing binary black holes with an application to final spin and radiated energy. Phys Rev D 95(6):064024. https://doi.org/10.1103/PhysRevD.95.064024. arXiv:1611.00332 [gr-qc]

Joshi KJ, Rasio FA, Portegies Zwart S (2000) Monte Carlo simulations of globular cluster evolution. I. Method and test calculations. ApJ 540(2):969–982. https://doi.org/10.1086/309350. arXiv:astro-ph/9909115 [astro-ph]

Joyce M, Chaboyer B (2018) Not All stars are the sun: empirical calibration of the mixing length for metal-poor stars using one-dimensional stellar evolution models. ApJ 856(1):10. https://doi.org/10.3847/1538-4357/aab200. arXiv:1712.05082 [astro-ph.SR]

Jülich Supercomputing Centre (2021) JUWELS Cluster and Booster: Exascale pathfinder with modular supercomputing architecture at Juelich Supercomputing Centre. J Large-scale Res Facilit 7(A138). https://doi.org/10.17815/jlsrf-7-183

Kamann S, Husser TO, Brinchmann J, Emsellem E, Weilbacher PM et al (2016) MUSE crowded field 3D spectroscopy of over 12 000 stars in the globular cluster NGC 6397. II. Probing the internal dynamics and the presence of a central black hole. A&A 588:A149. https://doi.org/10.1051/0004-6361/201527065. arXiv:1602.01643 [astro-ph.SR]

Kamann S, Bastian N, Husser TO, Martocchia S, Usher C et al (2018) Cluster kinematics and stellar rotation in NGC 419 with MUSE and adaptive optics. MNRAS 480(2):1689–1695. https://doi.org/10.1093/mnras/sty1958. arXiv:1807.10612 [astro-ph.GA]

Kamann S, Husser TO, Dreizler S, Emsellem E, Weilbacher PM et al (2018) A stellar census in globular clusters with MUSE: the contribution of rotation to cluster dynamics studied with 200 000 stars. MNRAS 473(4):5591–5616. https://doi.org/10.1093/mnras/stx2719. arXiv:1710.07257 [astro-ph.GA]

Kamann S, Bastian NJ, Gieles M, Balbinot E, Hénault-Brunet V (2019) Linking the rotation of a cluster to the spins of its stars: the kinematics of NGC 6791 and NGC 6819 in 3D. MNRAS 483(2):2197–2206. https://doi.org/10.1093/mnras/sty3144. arXiv:1811.08476 [astro-ph.GA]

Kamann S, Giesers B, Bastian N, Brinchmann J, Dreizler S et al (2020) The binary content of multiple populations in NGC 3201. A&A 635:A65. https://doi.org/10.1051/0004-6361/201936843. arXiv:1912.01627 [astro-ph.SR]

Kamlah AWH, Leveque A, Spurzem R, Arca Sedda M, Askar A, Banerjee S, Berczik P, Giersz M, Hurley J, Belloni D, Kühmichel L, Wang L (2022) Preparing the next gravitational million-body simulations: evolution of single and binary stars in NBODY6++GPU, MOCCA, and MCLUSTER. MNRAS 511(3):4060–4089. https://doi.org/10.1093/mnras/stab3748. arXiv:2105.08067 [astro-ph.GA]

Kamlah AWH, Spurzem R, Berczik P, Arca Sedda M, Flammini Dotti F, Neumayer N, Pang X, Shu Q, Tanikawa A, Giersz M (2022) The impact of stellar evolution on rotating star clusters: the gravothermal-gravogyro catastrophe and the formation of a bar of black holes. MNRAS 516(3):3266–3283. https://doi.org/10.1093/mnras/stac2281. arXiv:2205.04470 [astro-ph.GA]

Kamlah AWH, Tanikawa A, Arca Sedda M, Giersz M, Neumayer N, Spurzem R (2023) Direct N-body simulations of extremely massive and initially rotating Population III star clusters. MNRAS In prep

Kandrup HE, Mahon ME, Haywood Smith J (1994) On the sensitivity of the N-body problem toward small changes in initial conditions. IV. ApJ 428:458. https://doi.org/10.1086/174259

Kerr RP (1963) Gravitational field of a spinning mass as an example of algebraically special metrics. Phys Rev Lett 11(5):237–238. https://doi.org/10.1103/PhysRevLett.11.237

Khorrami Z, Khalaj P, Buckner ASM, Clark PC, Moraux E et al (2019) A code to make your own synthetic ObservaTIonS (MYOSOTIS). MNRAS 485(3):3124–3133. https://doi.org/10.1093/mnras/stz490. arXiv:1902.05525 [astro-ph.SR]

Kiel PD, Hurley JR (2006) Populating the Galaxy with low-mass X-ray binaries. MNRAS 369(3):1152–1166. https://doi.org/10.1111/j.1365-2966.2006.10400.x. arXiv:astro-ph/0605080 [astro-ph]

Kiel PD, Hurley JR (2009) Populating the Galaxy with pulsars—II. Galactic dynamics. MNRAS 395(4):2326–2346. https://doi.org/10.1111/j.1365-2966.2009.14711.x. arXiv:0903.1905 [astro-ph.GA]

Kiel PD, Hurley JR, Bailes M, Murray JR (2008) Populating the Galaxy with pulsars—I. Stellar and binary evolution. MNRAS 388(1):393–415. https://doi.org/10.1111/j.1365-2966.2008.13402.x. arXiv:0805.0059 [astro-ph]

Kim E, Einsel C, Lee HM, Spurzem R, Lee MG (2002) Dynamical evolution of rotating stellar systems—II. Post-collapse, equal-mass system. MNRAS 334(2):310–322. https://doi.org/10.1046/j.1365-8711.2002.05420.x. arXiv:astro-ph/0109062 [astro-ph]

Kim E, Lee HM, Spurzem R (2004) Dynamical evolution of rotating stellar systems—III. The effect of the mass spectrum. MNRAS 351(1):220–236. https://doi.org/10.1111/j.1365-2966.2004.07776.x. arXiv:astro-ph/0402478 [astro-ph]

Kim E, Yoon I, Lee HM, Spurzem R (2008) Comparative study between N-body and Fokker–Planck simulations for rotating star clusters—I. Equal-mass system. MNRAS 383(1):2–10. https://doi.org/10.1111/j.1365-2966.2007.12524.x. arXiv:0709.4318 [astro-ph]

Kiminki DC, Kobulnicky HA, Ewing I, Bagley Kiminki MM, Lundquist M et al (2012) Additional massive binaries in the Cygnus OB2 association. ApJ 747(1):41. https://doi.org/10.1088/0004-637X/747/1/41. arXiv:1112.3383 [astro-ph.SR]

King I (1961) The shape of a rotating star cluster. AJ 66:68. https://doi.org/10.1086/108376

King I (1962) The structure of star clusters. I. An empirical density law. AJ 67:471. https://doi.org/10.1086/108756

King IR (1966) The structure of star clusters. III. Some simple dynamical models. AJ 71:64. https://doi.org/10.1086/109857

King IR (1981) The dynamics of globular clusters. QJRAS 22:227

King IR (2008) The simple underlying dynamics of globular clusters. In: Vesperini E, Giersz M, Sills A (eds) Dynamical evolution of dense stellar systems. Proceedings of the IAU, vol S246. pp 131–140. https://doi.org/10.1017/S1743921308015470

Kippenhahn R, Weigert A, Weiss A (2012) Stellar structure and evolution, 2nd edn. Springer, Berlin. https://doi.org/10.1007/978-3-642-30304-3

Kobulnicky HA, Kiminki DC, Lundquist MJ, Burke J, Chapman J et al (2014) Toward complete statistics of massive binary stars: penultimate results from the cygnus OB2 radial velocity survey. ApJS 213(2):34. https://doi.org/10.1088/0067-0049/213/2/34. arXiv:1406.6655 [astro-ph.SR]

Köhler K, Langer N, de Koter A, de Mink SE, Crowther PA, Evans CJ, Gräfener G, Sana H, Sanyal D, Schneider FRN, Vink JS (2015) The evolution of rotating very massive stars with LMC composition. A&A 573:A71. https://doi.org/10.1051/0004-6361/201424356. arXiv:1501.03794 [astro-ph.SR]

Kokubo E, Yoshinaga K, Makino J (1998) On a time-symmetric Hermite integrator for planetary N-body simulation. MNRAS 297(4):1067–1072. https://doi.org/10.1046/j.1365-8711.1998.01581.x

Kopal Z (1978) Dynamics of close binary systems. Reidel, Dordrecht. https://doi.org/10.1007/978-94-009-9780-6

Kopal Z, Slouka H (1936) Axial rotation of globular star clusters. Nature 137(3467):621. https://doi.org/10.1038/137621a0

Kormendy J (1985) Families of ellipsoidal stellar systems and the formation of dwarf elliptical galaxies. ApJ 295:73–79. https://doi.org/10.1086/163350

Kotulla R, Fritze U, Weilbacher P, Anders P (2009) GALEV evolutionary synthesis models—I. Code, input physics and web interface. MNRAS 396(1):462–484. https://doi.org/10.1111/j.1365-2966.2009.14717.x. arXiv:0903.0378 [astro-ph.CO]

Kouwenhoven MBN, Flammini Dotti F, Shu Q, Xu X, Wu K et al (2020) Planetary systems in dense stellar environments. J Phys Conf Ser 1523:012011. https://doi.org/10.1088/1742-6596/1523/1/012011

Kremer K, Rodriguez CL, Amaro-Seoane P, Breivik K, Chatterjee S et al (2019) Post-Newtonian dynamics in dense star clusters: binary black holes in the LISA band. Phys Rev D 99(6):063003. https://doi.org/10.1103/PhysRevD.99.063003. arXiv:1811.11812 [astro-ph.HE]

Kremer K, Ye CS, Rui NZ, Weatherford NC, Chatterjee S et al (2020) Modeling Dense Star clusters in the milky way and beyond with the CMC cluster catalog. ApJS 247(2):48. https://doi.org/10.3847/1538-4365/ab7919. arXiv:1911.00018 [astro-ph.HE]

Kremer K, Rui NZ, Weatherford NC, Chatterjee S, Fragione G, Rasio FA, Rodriguez CL, Ye CS (2021) White Dwarf subsystems in core-collapsed globular clusters. ApJ 917(1):28. https://doi.org/10.3847/1538-4357/ac06d4. arXiv:2104.11751 [astro-ph.GA]

Kroupa P (1995) The dynamical properties of stellar systems in the Galactic disc. MNRAS 277:1507. https://doi.org/10.1093/mnras/277.4.1507. arXiv:astro-ph/9508084 [astro-ph]

Kroupa P (2001) On the variation of the initial mass function. MNRAS 322(2):231–246. https://doi.org/10.1046/j.1365-8711.2001.04022.x. arXiv:astro-ph/0009005 [astro-ph]

Kroupa P (2002) The initial mass function of stars: evidence for uniformity in variable systems. Sci 295 (5552):82–91. https://doi.org/10.1126/science.1067524. arXiv:astro-ph/0201098 [astro-ph]
Kroupa P (2008) Initial conditions for star clusters. In: Aarseth SJ, Tout CA, Mardling RA (eds) The Cambridge N-body lectures. Lecture notes in physics, vol 760. Springer, Berlin, p 181. https://doi.org/10.1007/978-1-4020-8431-7_8
Kroupa P, Jerabkova T (2018) The impact of binaries on the stellar initial mass function. arXiv e-prints arXiv:1806.10605 [astro-ph.GA]
Kroupa P, Jerabkova T (2019) The Salpeter IMF and its descendants. NatAs 3:482–484. https://doi.org/10.1038/s41550-019-0793-0. arXiv:1910.01126 [astro-ph.SR]
Kroupa P, Weidner C, Pflamm-Altenburg J, Thies I, Dabringhausen J, Marks M, Maschberger T (2013) The Stellar and sub-stellar initial mass function of simple and composite populations. In: Oswalt TD, Gilmore G (eds) Planets, stars and stellar systems. Volume 5: galactic structure and stellar populations. Springer, Dordrecht, pp 115–242. https://doi.org/10.1007/978-94-007-5612-0_4
Kroupa P, Subr L, Jerabkova T, Wang L (2020) Very high redshift quasars and the rapid emergence of supermassive black holes. MNRAS 498(4):5652–5683. https://doi.org/10.1093/mnras/staa2276. arXiv:2007.14402 [astro-ph.GA]
Kruckow MU (2020) Masses of double neutron star mergers. A&A 639:A123. https://doi.org/10.1051/0004-6361/202037519. arXiv:2002.08011 [astro-ph.SR]
Kruckow MU, Tauris TM, Langer N, Kramer M, Izzard RG (2018) Progenitors of gravitational wave mergers: binary evolution with the stellar grid-based code COMBINE. MNRAS 481(2):1908–1949. https://doi.org/10.1093/mnras/sty2190. arXiv:1801.05433 [astro-ph.SR]
Kruckow MU, Neunteufel PG, Di Stefano R, Gao Y, Kobayashi C (2021) A catalog of potential post-common envelope binaries. ApJ 920(2):86. https://doi.org/10.3847/1538-4357/ac13ac. arXiv:2107.05221 [astro-ph.SR]
Krumholz MR, McKee CF, Bland-Hawthorn J (2019) Star clusters across cosmic time. ARA&A 57:227–303. https://doi.org/10.1146/annurev-astro-091918-104430. arXiv:1812.01615 [astro-ph.GA]
Kuepper AHW, Maschberger T, Kroupa P, Baumgardt H (2011) McLuster: a tool to make a star cluster. Astrophysics Source Code Library, ascl:1107.015. https://ascl.net/1107.015
Kupi G, Amaro-Seoane P, Spurzem R (2006) Dynamics of compact object clusters: a post-Newtonian study. MNRAS 371(1):L45–L49. https://doi.org/10.1111/j.1745-3933.2006.00205.x. arXiv:astro-ph/0602125 [astro-ph]
Küpper AHW, Maschberger T, Kroupa P, Baumgardt H (2011) Mass segregation and fractal substructure in young massive clusters - I. The McLuster code and method calibration. MNRAS 417(3):2300–2317. https://doi.org/10.1111/j.1365-2966.2011.19412.x. arXiv:1107.2395 [astro-ph.GA]
Kustaanheimo P, Stiefel E (1965) Perturbation theory of Kepler motion based on spinor regularization. J Reine Angew Math 218:204–219
Lahén N, Naab T, Johansson PH, Elmegreen B, Hu CY et al (2020) Structure and rotation of young massive star clusters in a simulated dwarf starburst. ApJ 904(1):71. https://doi.org/10.3847/1538-4357/abc001. arXiv:2008.04320 [astro-ph.GA]
Lanzoni B, Ferraro FR, Mucciarelli A, Pallanca C, Lapenna E, Origlia L, Dalessandro E, Valenti E, Bellazzini M, Tiongco MA, Varri AL, Vesperini E, Beccari G (2018) The strong rotation of M5 (NGC 5904) as seen from the MIKiS survey of galactic globular clusters. ApJ 861(1):16. https://doi.org/10.3847/1538-4357/aac26a. arXiv:1804.10509 [astro-ph.GA]
Lanzoni B, Ferraro FR, Mucciarelli A, Pallanca C, Tiongco MA, Varri A, Vesperini E, Bellazzini M, Dalessandro E, Origlia L, Valenti E, Sollima A, Lapenna E, Beccari G (2018) The ESO multi-instrument kinematic survey (MIKiS) of Galactic globular clusters: solid-body rotation and anomalous velocity dispersion profile in NGC 5986. ApJ 865(1):11. https://doi.org/10.3847/1538-4357/aad810. arXiv:1808.01194 [astro-ph.GA]
Larson RB (1970) A method for Computing the evolution of star clusters. MNRAS 147:323. https://doi.org/10.1093/mnras/147.4.323
Lattimer JM (2012) The nuclear equation of state and neutron star masses. ARNPS 62(1):485–515. https://doi.org/10.1146/annurev-nucl-102711-095018. arXiv:1305.3510 [nucl-th]
Lattimer JM, Prakash M (2004) The physics of neutron stars. Sci 304(5670):536–542. https://doi.org/10.1126/science.1090720. arXiv:astro-ph/0405262 [astro-ph]
Law-Smith JAP, Coulter DA, Guillochon J, Mockler B, Ramirez-Ruiz E (2020) Stellar tidal disruption events with abundances and realistic structures (STARS): library of fallback rates. ApJ 905(2):141. https://doi.org/10.3847/1538-4357/abc489. arXiv:2007.10996 [astro-ph.HE]

Lazar A, Bromm V (2021) Probing the initial mass function of the first stars with transients. arXiv e-prints arXiv:2110.11956 [astro-ph.HE]
Lecar M, Aarseth SJ (1986) A numerical simulation of the formation of the terrestrial planets. ApJ 305:564. https://doi.org/10.1086/164269
Leigh NWC, Giersz M, Marks M, Webb JJ, Hypki A et al (2015) The state of globular clusters at birth—II. Primordial binaries. MNRAS 446(1):226–239. https://doi.org/10.1093/mnras/stu2110. arXiv:1410.2248 [astro-ph.SR]
Leung SC, Nomoto K, Blinnikov S (2019) Pulsational pair-instability supernovae. I. Pre-collapse evolution and Pulsational mass ejection. ApJ 887(1):72. https://doi.org/10.3847/1538-4357/ab4fe5. arXiv:1901.11136 [astro-ph.HE]
Leung SC, Blinnikov S, Ishidoshiro K, Kozlov A, Nomoto K (2020) Pulsational pair-instability supernovae. II. Neutrino signals from pulsations and their detection by terrestrial neutrino detectors. ApJ 889(2):75. https://doi.org/10.3847/1538-4357/ab6211. arXiv:2007.08470 [astro-ph.HE]
Leung SC, Nomoto K, Suzuki T (2020) Electron-capture supernovae of super-AGP stars: sensitivity on input physics. ApJ 889(1):34. https://doi.org/10.3847/1538-4357/ab5d2f. arXiv:1901.11438 [astro-ph.HE]
Leveque A, Giersz M, Paolillo M (2021) MOCCA survey database: extra galactic globular clusters. I. Method and first results. MNRAS 501(4):5212–5228. https://doi.org/10.1093/mnras/staa4027. arXiv:2006.05887 [astro-ph.GA]
Leveque A, Giersz M, Arca-Sedda M, Askar A (2022) MOCCA-survey data base: extra galactic globular clusters - II. Milky Way and Andromeda. MNRAS 514(4):5751–5766. https://doi.org/10.1093/mnras/stac1694. arXiv:2206.03967 [astro-ph.GA]
Leveque A, Giersz M, Banerjee S, Vesperini E, Hong J, Portegies Zwart S (2022) A Monte Carlo study of early gas expulsion and evolution of star clusters: new simulations with the MOCCA code in the AMUSE framework. MNRAS 514(4):5739–5750. https://doi.org/10.1093/mnras/stac1690. arXiv:2206.03404 [astro-ph.GA]
Leveque A, Giersz M, Askar A, Arca-Sedda M, Olejak A (2023) MOCCA-survey database: extra galactic globular clusters - III. The population of black holes in Milky Way and Andromeda-like galaxies. MNRAS 520(2):2593–2610. https://doi.org/10.1093/mnras/stad240. arXiv:2209.01564 [astro-ph.GA]
Levi-Civita T (1916) Sur la régularisation du probléme des trois corps. C R Hebd Acad Sci Paris 162:625–628. Reprinted in Levi–Civita, 1954–1973, vol. III, pp 589–593
Lewis S, Cournoyer-Cloutier C, Tran A, Farner W, McMillan S, Low MM, Portegies Zwart S, Toonen S, Wall J (2021) The effects of early massive star formation: gas expulsion and cluster dynamics. BAAS 53(6). https://baas.aas.org/pub/2021n6i232p08
Li S, Liu FK, Berczik P, Spurzem R (2017) Boosted tidal disruption by massive black hole binaries during galaxy mergers from the view of N-body simulation. ApJ 834(2):195. https://doi.org/10.3847/1538-4357/834/2/195. arXiv:1509.00158 [astro-ph.GA]
Li S, Berczik P, Chen X, Liu FK, Spurzem R, Qiu Y (2019) Direct N-body simulations of tidal disruption rate evolution in unequal-mass galaxy mergers. ApJ 883(2):132. https://doi.org/10.3847/1538-4357/ab3e4a. arXiv:1909.08280 [astro-ph.GA]
Li ZM, Kayastha B, Kamlah A, Berczik P, Deng YY, Spurzem R (2023) Fractions of compact object binaries in star clusters: theoretical predictions. Res Astron Astrophys 23(2):025019. https://doi.org/10.1088/1674-4527/aca94f
Lightman AP, Shapiro SL (1977) The distribution and consumption rate of stars around a massive, collapsed object. ApJ 211:244–262. https://doi.org/10.1086/154925
Linares M (2018) Compact binary pulsar search (COBIPULSE): first results. In: 42nd COSPAR scientific assembly. vol 42. pp E1.3–27–18
Linares M (2020) Super-massive neutron stars and compact binary millisecond pulsars. In: Multifrequency behaviour of high energy cosmic sources—XIII. 3–8 June 2019. Palermo. p 23. arXiv:1910.09572 [astro-ph.HE]
Lingam M (2018) Black hole Brownian motion in a rotating environment. MNRAS 473(2):1719–1735. https://doi.org/10.1093/mnras/stx2531
Lippert T, Ritzenhöfer G, Glaessner U, Hoeber H, Seyfried A, Schilling K (1996) Hyper-systolic processing on APE100/QUADRICS:. n^2-LOOP computations. Int J Mod Phys C 7(4):485–501. https://doi.org/10.1142/S0129183196000430. arXiv:hep-lat/9512020 [hep-lat]

Lippert T, Petkov N, Palazzari P, Schilling K (1998) Hyper-systolic matrix multiplication. arXiv e-prints cs/9809105. https://doi.org/10.48550/arXiv.cs/9809105. arXiv:cs/9809105 [cs.MS]
Livernois AR, Vesperini E, Varri AL, Hong J, Tiongco M (2022) Long-term evolution of multimass rotating star clusters. MNRAS 512(2):2584–2593. https://doi.org/10.1093/mnras/stac651
Longaretti PY, Lagoute C (1996) Rotating globular clusters. II. Relaxation and evaporation. A&A 308:453–464
Louis PD, Spurzem R (1991) Anisotropic gaseous models for the evolution of star clusters. MNRAS 251:408–426. https://doi.org/10.1093/mnras/251.3.408
Lousto CO, Zlochower Y, Dotti M, Volonteri M (2012) Gravitational recoil from accretion-aligned black-hole binaries. Phys Rev D 85(8):084015. https://doi.org/10.1103/PhysRevD.85.084015. arXiv:1201.1923 [gr-qc]
Luo J, Chen LS, Duan HZ, Gong YG, Hu S, Ji J, Liu Q, Mei J, Milyukov V, Sazhin M, Shao CG, Toth VT, Tu HB, Wang Y, Wang Y, Yeh HC, Zhan MS, Zhang Y, Zharov V, Zhou ZB (2016) TianQin: a space-borne gravitational wave detector. Classical Quantum Gravity 33(3):035010. https://doi.org/10.1088/0264-9381/33/3/035010. arXiv:1512.02076 [astro-ph.IM]
Lupton RH, Gunn JE (1987) Three-integral models of globular clusters. AJ 93:1106. https://doi.org/10.1086/114394
Lupton RH, Gunn JE, Griffin RF (1987) Dynamical studies of globular clusters based on photoelectric radial velocities of individual stars and on the observed mass function. II. M13. AJ 93:1114. https://doi.org/10.1086/114395
Lurie JC, Vyhmeister K, Hawley SL, Adilia J, Chen A, Davenport JRA, Jurić M, Puig-Holzman M, Weisenburger KL (2017) Tidal synchronization and differential rotation of Kepler eclipsing binaries. AJ 154(6):250. https://doi.org/10.3847/1538-3881/aa974d. arXiv:1710.07339 [astro-ph.SR]
Lynden-Bell D (1960) Can spherical clusters rotate? MNRAS 120:204. https://doi.org/10.1093/mnras/120.3.204
Lynden-Bell D (1999) Negative specific heat in astronomy, physics and chemistry. Physica A Stat Mech Appl 263(1–4):293–304. https://doi.org/10.1016/S0378-4371(98)00518-4. arXiv:cond-mat/9812172 [cond-mat.stat-mech]
Lynden-Bell D, Eggleton PP (1980) On the consequences of the gravothermal catastrophe. MNRAS 191:483–498. https://doi.org/10.1093/mnras/191.3.483
Lynden-Bell D, Wood R (1968) The gravo-thermal catastrophe in isothermal spheres and the onset of red-giant structure for stellar systems. MNRAS 138:495. https://doi.org/10.1093/mnras/138.4.495
Maeder A, Meynet G (1989) Grids of evolutionary models from 0.85 to 120M: observational tests and the mass limits. A&A 210:155–173
Magorrian J, Tremaine S (1999) Rates of tidal disruption of stars by massive central black holes. MNRAS 309(2):447–460. https://doi.org/10.1046/j.1365-8711.1999.02853.x. arXiv:astro-ph/9902032 [astro-ph]
Makino J (1991) A modified Aarseth code for GRAPE and vector processors. PASJ 43:859–876
Makino J (1991) Optimal order and time-step criterion for Aarseth-type N-body integrators. ApJ 369:200. https://doi.org/10.1086/169751
Makino J (1996) Postcollapse evolution of globular clusters. ApJ 471:796. https://doi.org/10.1086/178007. arXiv:astro-ph/9608160 [astro-ph]
Makino J (1999) Yet another fast multipole method without multipoles-pseudoparticle multipole method. J Comput Phys 151(2):910–920. https://doi.org/10.1006/jcph.1999.6226. arXiv:astro-ph/9806213 [astro-ph]
Makino J (2002) An efficient parallel algorithm for O(N^2) direct summation method and its variations on distributed-memory parallel machines. New A 7(7):373–384. https://doi.org/10.1016/S1384-1076(02)00143-4. arXiv:astro-ph/0108412 [astro-ph]
Makino J, Aarseth SJ (1992) On a hermite integrator with ahmad-cohen scheme for gravitational many-body problems. PASJ 44:141–151
Makino J, Hut P (1988) Performance analysis of direct N-body calculations. ApJS 68:833. https://doi.org/10.1086/191306
Makino J, Taiji M (1998) Scientific simulations with special-purpose computers-the GRAPE systems. Wiley-VCH
Makino J, Kokubo E, Taiji M (1993) HARP: a special-purpose computer for N-body problem. PASJ 45:349–360

Makino J, Taiji M, Ebisuzaki T, Sugimoto D (1997) GRAPE-4: a massively parallel special-purpose computer for collisional N-body simulations. ApJ 480(1):432–446. https://doi.org/10.1086/303972
Makino J, Fukushige T, Koga M, Namura K (2003) GRAPE-6: massively-parallel special-purpose computer for astrophysical particle simulations. PASJ 55:1163–1187. https://doi.org/10.1093/pasj/55.6.1163. arXiv:astro-ph/0310702 [astro-ph]
Manchester RN, Hobbs GB, Teoh A, Hobbs M (2005) The Australia telescope national facility pulsar catalogue. AJ 129(4):1993–2006. https://doi.org/10.1086/428488. arXiv:astro-ph/0412641 [astro-ph]
Mapelli M (2018) Astrophysics of stellar black holes. arXiv e-prints arXiv:1809.09130 [astro-ph.HE]
Mapelli M (2019) The Maxwell's demon of star clusters. In: Beccari G, Boffin H (eds) The impact of binary stars on stellar evolution. Cambridge University Press, Cambridge, pp 244–260. https://doi.org/10.1017/9781108553070.019. arXiv:1807.07944 [astro-ph.SR]
Mapelli M, Spera M, Montanari E, Limongi M, Chieffi A et al (2020) Impact of the rotation and compactness of progenitors on the mass of black holes. ApJ 888(2):76. https://doi.org/10.3847/1538-4357/ab584d. arXiv:1909.01371 [astro-ph.HE]
Mardling R, Aarseth S (1999) Dynamics and stability of three-body systems. In: Steves BA, Roy AE (eds) The dynamics of small bodies in the solar system, a major key to solar system studies. NATO ASI Series C, vol 522. p 385
Mardling RA (1995) The role of chaos in the circularization of tidal capture binaries. I. The chaos boundary. ApJ 450:722. https://doi.org/10.1086/176178
Mardling RA (1995) The role of chaos in the circularization of tidal capture binaries. II. Long-time evolution. ApJ 450:732. https://doi.org/10.1086/176179
Mardling RA, Aarseth SJ (2001) Tidal interactions in star cluster simulations. MNRAS 321(3):398–420. https://doi.org/10.1046/j.1365-8711.2001.03974.x
Marks M, Kroupa P, Dabringhausen J, Pawlowski MS (2012) Evidence for top-heavy stellar initial mass functions with increasing density and decreasing metallicity. MNRAS 422(3):2246–2254. https://doi.org/10.1111/j.1365-2966.2012.20767.x. arXiv:1202.4755 [astro-ph.GA]
Marks M, Janson M, Kroupa P, Leigh N, Thies I (2015) M-dwarf binaries as tracers of star and brown dwarf formation. MNRAS 452(1):1014–1025. https://doi.org/10.1093/mnras/stv1361. arXiv:1506.05113 [astro-ph.GA]
Martens S, Kamann S, Dreizler S, Göttgens F, Husser TO, Latour M, Balakina E, Krajnović D, Pechetti R, Weilbacher PM (2023) Kinematic differences between multiple populations in Galactic globular clusters. A&A 671:A106. https://doi.org/10.1051/0004-6361/202244787. arXiv:2301.08675 [astro-ph.GA]
Maschberger T (2013) On the function describing the stellar initial mass function. MNRAS 429(2):1725–1733. https://doi.org/10.1093/mnras/sts479. arXiv:1212.0939 [astro-ph.GA]
Mazeh T (2008) Observational evidence for tidal interaction in close binary systems. In: Goupil MJ, Zahn JP (eds) Tidal effects in stars, planets and disks. EAS Publications Series, vol 29. EDP Sciences, pp 1–65. https://doi.org/10.1051/eas:0829001. arXiv:0801.0134 [astro-ph]
McMillan SLW, Aarseth SJ (1993) An O(N N) integration scheme for collisional stellar systems. ApJ 414:200. https://doi.org/10.1086/173068
Meakin CA, Arnett D (2006) Active carbon and oxygen shell burning hydrodynamics. ApJ 637(1):L53–L56. https://doi.org/10.1086/500544. arXiv:astro-ph/0601348 [astro-ph]
Meakin CA, Arnett D (2007) Anelastic and compressible simulations of stellar oxygen burning. ApJ 665(1):690–697. https://doi.org/10.1086/519372. arXiv:astro-ph/0611317 [astro-ph]
Meibom S, Mathieu RD (2005) A robust measure of tidal circularization in coeval binary populations: the solar-type spectroscopic binary population in the open cluster M35. ApJ 620(2):970–983. https://doi.org/10.1086/427082. arXiv:astro-ph/0412147 [astro-ph]
Meiron Y, Li B, Holley-Bockelmann K, Spurzem R (2014) Expansion techniques for Collisionless stellar dynamical simulations. ApJ 792(2):98. https://doi.org/10.1088/0004-637X/792/2/98. arXiv:1406.4254 [astro-ph.IM]
Merritt D (2015) Gravitational encounters and the evolution of galactic nuclei. I. Method. ApJ 804(1):52. https://doi.org/10.1088/0004-637X/804/1/52. arXiv:1505.07516 [astro-ph.GA]
Merritt D, Poon MY (2004) Chaotic loss cones and black hole fueling. ApJ 606(2):788–798. https://doi.org/10.1086/382497. arXiv:astro-ph/0302296 [astro-ph]
Merritt D, Wang J (2005) Loss cone refilling rates in galactic nuclei. ApJ 621(2):L101–L104. https://doi.org/10.1086/429272. arXiv:astro-ph/0411210 [astro-ph]
Mestel L (1968) Magnetic braking by a stellar wind-I. MNRAS 138:359. https://doi.org/10.1093/mnras/138.3.359

Mestel L (1968) Magnetic braking by a stellar wind-II. MNRAS 140:177. https://doi.org/10.1093/mnras/140.2.177
Mestel L, Spruit HC (1987) On magnetic braking of late-type stars. MNRAS 226:57–66. https://doi.org/10.1093/mnras/226.1.57
Michie RW (1962) Dynamics of spherical stellar systems: properties of theoretical models, and comparison with clusters and elliptical galaxies. AJ 67:582. https://doi.org/10.1086/108880
Michie RW (1963) The dynamics of spherical stellar systems. III. MNRAS 126:331. https://doi.org/10.1093/mnras/126.4.331
Mikkola S (1997) Numerical treatment of small stellar systems with binaries. Celest Mech Dyn Astron 68 (1):87–104. https://doi.org/10.1023/A:1008291715719
Mikkola S (1997) Practical symplectic methods with time transformation for the few-body problem. Celest Mech Dyn Astron 67(2):145–165. https://doi.org/10.1023/A:1008217427749
Mikkola S, Aarseth SJ (1990) A chain regularization method for the few-body problem. Celest Mech Dyn Astron 47(4):375–390
Mikkola S, Aarseth SJ (1996) A slow-down treatment for close binaries. Celest Mech Dyn Astron 64 (3):197–208. https://doi.org/10.1007/BF00728347
Mikkola S, Aarseth SJ (1998) An efficient integration method for binaries in N-body simulations. NA 3 (5):309–320. https://doi.org/10.1016/S1384-1076(98)00018-9
Mikkola S, Merritt D (2008) Implementing few-body algorithmic regularization with post-Newtonian terms. AJ 135(6):2398–2405. https://doi.org/10.1088/0004-6256/135/6/2398. arXiv:0709.3367 [astro-ph]
Mikkola S, Tanikawa K (1999) Algorithmic regularization of the few-body problem. MNRAS 310(3):745–749. https://doi.org/10.1046/j.1365-8711.1999.02982.x
Mikkola S, Tanikawa K (1999) Explicit symplectic algorithms for time-transformed Hamiltonians. Celest Mech Dyn Astron 74(4):287–295. https://doi.org/10.1023/A:1008368322547
Miller RH (1964) Irreversibility in small stellar dynamical systems. ApJ 140:250. https://doi.org/10.1086/147911
Milone AP (2020) Thirteen facts that you need to know on multiple populations in globular clusters. In: Bragaglia A, Davies M, Sills A, Vesperini E (eds) Star Clusters: From the Milky Way to the Early Universe. Proceedings of the IAU, vol S351. pp 251–260. https://doi.org/10.1017/S1743921319010044. arXiv:1908.11703 [astro-ph.SR]
Milone AP, Marino AF (2022) Multiple Populations in Star Clusters. arXiv e-prints arXiv:2206.10564 [astro-ph.GA]
Milone AP, Piotto G, Bedin LR, Cassisi S, Anderson J et al (2012) Luminosity and mass functions of the three main sequences of the globular cluster NGC 2808. A&A 537:A77. https://doi.org/10.1051/0004-6361/201116539. arXiv:1108.2391 [astro-ph.SR]
Milone AP, Marino AF, Piotto G, Bedin LR, Anderson J et al (2013) A WFC3/HST view of the three stellar populations in the globular cluster NGC 6752. ApJ 767(2):120. https://doi.org/10.1088/0004-637X/767/2/120. arXiv:1301.7044 [astro-ph.SR]
Milone AP, Marino AF, Bedin LR, Anderson J, Apai D et al (2017) The HST large programme on ω Centauri—I. Multiple stellar populations at the bottom of the main sequence probed in NIR-Optical. MNRAS 469(1):800–812. https://doi.org/10.1093/mnras/stx836. arXiv:1704.00418 [astro-ph.SR]
Milone AP, Piotto G, Renzini A, Marino AF, Bedin LR et al (2017) The Hubble space telescope UV legacy survey of galactic globular clusters—IX. The atlas of multiple stellar populations. MNRAS 464 (3):3636–3656. https://doi.org/10.1093/mnras/stw2531. arXiv:1610.00451 [astro-ph.SR]
Milone AP, Marino AF, Mastrobuono-Battisti A, Lagioia EP (2018) Gaia unveils the kinematics of multiple stellar populations in 47 Tucanae. MNRAS 479(4):5005–5011. https://doi.org/10.1093/mnras/sty1873. arXiv:1807.03511 [astro-ph.SR]
Milone AP, Marino AF, Renzini A, D'Antona F, Anderson J et al (2018) The hubble space telescope UV legacy survey of galactic globular clusters—XVI. The helium abundance of multiple populations. MNRAS 481(4):5098–5122. https://doi.org/10.1093/mnras/sty2573. arXiv:1809.05006 [astro-ph.SR]
Milone AP, Marino AF, Da Costa GS, Lagioia EP, D'Antona F et al (2020) Multiple populations in globular clusters and their parent galaxies. MNRAS 491(1):515–531. https://doi.org/10.1093/mnras/stz2999. arXiv:1910.09683 [astro-ph.GA]
Milone AP, Marino AF, Renzini A, Li C, Jang S et al (2020) A chromosome map to unveil stellar populations with different magnesium abundances. The case of ω Centauri. MNRAS 497(3):3846–3859. https://doi.org/10.1093/mnras/staa2119. arXiv:2006.13101 [astro-ph.SR]

Milone AP, Vesperini E, Marino AF, Hong J, van der Marel R et al (2020) The Hubble space telescope UV legacy survey of galactic globular clusters—XXI. Binaries among multiple stellar populations. MNRAS 492(4):5457–5469. https://doi.org/10.1093/mnras/stz3629. arXiv:2002.06479 [astro-ph.SR]
Moe M, Di Stefano R (2017) Mind Your Ps and Qs: the interrelation between Period (P) and mass-ratio (Q) distributions of binary stars. ApJS 230(2):15. https://doi.org/10.3847/1538-4365/aa6fb6. arXiv:1606.05347 [astro-ph.SR]
Montgomery R (2001) A new solution to the three-body problem. Notices AMS 48(5):471
Morales MC, Fellhauer M (2020) Binary interactions in a static filament. BAAA 61C:94–94
Morawski J, Giersz M, Askar A, Belczynski K (2018) MOCCA-SURVEY database I: assessing GW kick retention fractions for BH–BH mergers in globular clusters. MNRAS 481(2):2168–2179. https://doi.org/10.1093/mnras/sty2401. arXiv:1802.01192 [astro-ph.GA]
Morawski J, Giersz M, Askar A, Belczynski K (2019) Erratum to: MOCCA-SURVEY Database I: Assessing GW kick retention fractions for BH–BH mergers in globular clusters. MNRAS 486(3):3402–3402. https://doi.org/10.1093/mnras/stz1074
Neumayer N, Seth A, Böker T (2020) Nuclear star clusters. A&ARv 28(1):4. https://doi.org/10.1007/s00159-020-00125-0. arXiv:2001.03626 [astro-ph.GA]
Neutsch W, Scherer K (1992) Celestial mechanics. Bibliographisches Institut, Mannheim
Nitadori K, Aarseth SJ (2012) Accelerating NBODY6 with graphics processing units. MNRAS 424(1):545–552. https://doi.org/10.1111/j.1365-2966.2012.21227.x. arXiv:1205.1222 [astro-ph.IM]
Nitadori K, Makino J (2008) Sixth- and eighth-order Hermite integrator for N-body simulations. New Astron 13(7):498–507. https://doi.org/10.1016/j.newast.2008.01.010. arXiv:0708.0738 [astro-ph]
Nomoto K (1984) Evolution of 8–10 solar mass stars toward electron capture supernovae. I—Formation of electron-degenerate O + NE + MG cores. ApJ 277:791–805. https://doi.org/10.1086/161749
Nomoto K (1987) Evolution of 8–10 M_{sun} stars toward electron capture supernovae. II. Collapse of an O + NE + MG Core. ApJ 322:206. https://doi.org/10.1086/165716
Oh S, Kroupa P, Pflamm-Altenburg J (2015) Dependency of dynamical ejections of O stars on the masses of very young star clusters. ApJ 805(2):92. https://doi.org/10.1088/0004-637X/805/2/92. arXiv:1503.08827 [astro-ph.GA]
Olejak A, Belczynski K, Bulik T, Sobolewska M (2020) Synthetic catalog of black holes in the Milky Way. A&A 638:A94. https://doi.org/10.1051/0004-6361/201936557. arXiv:1908.08775 [astro-ph.SR]
Olejak A, Belczynski K, Ivanova N (2021) Impact of common envelope development criteria on the formation of LIGO/Virgo sources. A&A 651:A100. https://doi.org/10.1051/0004-6361/202140520. arXiv:2102.05649 [astro-ph.HE]
Oshino S, Funato Y, Makino J (2011) Particle–particle particle-tree: a direct-tree hybrid scheme for collisional N-body simulations. PASJ 63:881. https://doi.org/10.1093/pasj/63.4.881. arXiv:1101.5504 [astro-ph.EP]
Paczynski B (1976) Common Envelope Binaries. In: Eggleton P, Mitton S, Whelan J (eds) Structure and evolution of close binary systems. IAU Symposium, vol 73. Reidel, p 75. https://doi.org/10.1017/S0074180900011864
Panamarev T, Kocsis B (2022) A numerical study of stellar discs in galactic nuclei. MNRAS 517(4):6205–6224. https://doi.org/10.1093/mnras/stac3050. arXiv:2207.06398 [astro-ph.GA]
Panamarev T, Just A, Spurzem R, Berczik P, Wang L et al (2019) Direct N-body simulation of the Galactic centre. MNRAS 484(3):3279–3290. https://doi.org/10.1093/mnras/stz208. arXiv:1805.02153 [astro-ph.GA]
Pang X, Li Y, Tang SY, Pasquato M, Kouwenhoven MBN (2020) Different fates of young star clusters after gas expulsion. ApJ 900(1):L4. https://doi.org/10.3847/2041-8213/abad28. arXiv:2008.02803 [astro-ph.GA]
Pang X, Li Y, Yu Z, Tang SY, Dinnbier F et al (2021) 3D morphology of open clusters in the solar neighborhood with Gaia EDR 3: its relation to cluster dynamics. ApJ 912(2):162. https://doi.org/10.3847/1538-4357/abeaac. arXiv:2102.10508 [astro-ph.GA]
Pang X, Shu Q, Wang L, Kouwenhoven MBN (2022) Investigating the UV-excess in star clusters with N-body simulations: predictions for future CSST observations. Res Astron Astrophys 22(9):095015. https://doi.org/10.1088/1674-4527/ac7f0f. arXiv:2207.00772 [astro-ph.GA]
Pang XY, Olczak C, Guo DF, Spurzem R, Kotulla R (2016) GalevNB: a conversion from N-body simulations to observations. RAA 16(3):37. https://doi.org/10.1088/1674-4527/16/3/037. arXiv:1509.05864 [astro-ph.GA]

Pasetto S, Chiosi C, Cropper M, Grebel E (2018) New theory of stellar convection without the mixing-length parameter: new stellar atmosphere model. J Phys Conf Ser 940:012020. https://doi.org/10.1088/1742-6596/940/1/012020

Pattabiraman B, Umbreit S, Wk Liao, Choudhary A, Kalogera V et al (2013) A parallel Monte Carlo code for simulating collisional N-body systems. ApJS 204(2):15. https://doi.org/10.1088/0067-0049/204/2/15. arXiv:1206.5878 [astro-ph.IM]

Paxton B, Bildsten L, Dotter A, Herwig F, Lesaffre P et al (2011) Modules for Experiments in Stellar Astrophysics (MESA). ApJS 192(1):3. https://doi.org/10.1088/0067-0049/192/1/3. arXiv:1009.1622 [astro-ph.SR]

Paxton B, Cantiello M, Arras P, Bildsten L, Brown EF et al (2013) Modules for Experiments in Stellar Astrophysics (MESA): planets, oscillations, rotation, and massive stars. ApJS 208(1):4. https://doi.org/10.1088/0067-0049/208/1/4. arXiv:1301.0319 [astro-ph.SR]

Paxton B, Marchant P, Schwab J, Bauer EB, Bildsten L et al (2015) Modules for Experiments in Stellar Astrophysics (MESA): binaries, pulsations, and explosions. ApJS 220(1):15. https://doi.org/10.1088/0067-0049/220/1/15. arXiv:1506.03146 [astro-ph.SR]

Paxton B, Marchant P, Schwab J, Bauer EB, Bildsten L et al (2016) Erratum: "Modules for Experiments in Stellar Astrophysics (MESA): Binaries, Pulsations, and Explosions" (2015, ApJS, 220, 15). ApJS 223(1):18. https://doi.org/10.3847/0067-0049/223/1/18

Paxton B, Schwab J, Bauer EB, Bildsten L, Blinnikov S et al (2018) Modules for Experiments in Stellar Astrophysics (MESA): convective boundaries, element diffusion, and massive star explosions. ApJS 234(2):34. https://doi.org/10.3847/1538-4365/aaa5a8. arXiv:1710.08424 [astro-ph.SR]

Paxton B, Smolec R, Schwab J, Gautschy A, Bildsten L et al (2019) Modules for Experiments in Stellar Astrophysics (MESA): pulsating variable stars, rotation, convective boundaries, and energy conservation. ApJS 243(1):10. https://doi.org/10.3847/1538-4365/ab2241. arXiv:1903.01426 [astro-ph.SR]

Pease FG, Shapley H (1917) On the distribution of stars in twelve globular clusters. ApJ 45:225–243. https://doi.org/10.1086/142324

Peters PC (1964) Gravitational radiation and the motion of two point masses. Phys Rev 136(4B):1224–1232. https://doi.org/10.1103/PhysRev.136.B1224

Peters PC, Mathews J (1963) Gravitational radiation from point masses in a Keplerian orbit. Phys Rev 131 (1):435–440. https://doi.org/10.1103/PhysRev.131.435

Phinney ES, Sigurdsson S (1991) Ejection of pulsars and binaries to the outskirts of globular clusters. Nature 349(6306):220–223. https://doi.org/10.1038/349220a0

Piotto G, King IR, Djorgovski SG, Sosin C, Zoccali M et al (2002) HST color-magnitude diagrams of 74 galactic globular clusters in the HST F439W and F555W bands. A&A 391:945–965. https://doi.org/10.1051/0004-6361:20020820. arXiv:astro-ph/0207124 [astro-ph]

Plummer HC (1911) On the problem of distribution in globular star clusters. MNRAS 71:460–470. https://doi.org/10.1093/mnras/71.5.460

Plummer HC (1915) The distribution of stars in globular clusters. MNRAS 76:107–121. https://doi.org/10.1093/mnras/76.2.107

Podsiadlowski P, Langer N, Poelarends AJT, Rappaport S, Heger A et al (2004) The effects of binary evolution on the dynamics of core collapse and neutron star kicks. ApJ 612(2):1044–1051. https://doi.org/10.1086/421713. arXiv:astro-ph/0309588 [astro-ph]

Pols OR, Tout CA, Eggleton PP, Han Z (1995) Approximate input physics for stellar modelling. MNRAS 274(3):964–974. https://doi.org/10.1093/mnras/274.3.964. arXiv:astro-ph/9504025 [astro-ph]

Pols OR, Tout CA, Schroder KP, Eggleton PP, Manners J (1997) Further critical tests of stellar evolution by means of double-lined eclipsing binaries. MNRAS 289(4):869–881. https://doi.org/10.1093/mnras/289.4.869

Pols OR, Schröder KP, Hurley JR, Tout CA, Eggleton PP (1998) Stellar evolution models for Z = 0.0001 to 0.03. MNRAS 298(2):525–536. https://doi.org/10.1046/j.1365-8711.1998.01658.x

Poon MY, Merritt D (2004) A self-consistent study of triaxial black hole nuclei. ApJ 606(2):774–787. https://doi.org/10.1086/383190. arXiv:astro-ph/0212581 [astro-ph]

Popescu B, Hanson MM (2009) MASSCLEAN–MASSive CLuster Evolution and ANalysis package: description and tests. AJ 138(6):1724–1740. https://doi.org/10.1088/0004-6256/138/6/1724. arXiv:0811.4210 [astro-ph]

Portegies Zwart S (2011) AMUSE: Astrophysical Multipurpose Software Environment. Astrophysics Source Code Library, ascl:1107.007. https://ascl.net/1107.007

Portegies Zwart S, McMillan S (2018) Astrophysical recipes: the art of AMUSE. IOP Publ. https://doi.org/10.1088/978-0-7503-1320-9

Portegies Zwart S, McMillan SLW, van Elteren E, Pelupessy I, de Vries N (2013) Multi-physics simulations using a hierarchical interchangeable software interface. CoPhC 184(3):456–468. https://doi.org/10.1016/j.cpc.2012.09.024. arXiv:1204.5522 [astro-ph.IM]

Portegies Zwart S, van Elteren A, Pelupessy I, McMillan S, Rieder S, et al (2018) Amuse: the astrophysical multipurpose software environment. https://doi.org/10.5281/zenodo.1443252

Portegies Zwart SF, McMillan SLW (2002) The runaway growth of intermediate-mass black holes in dense star clusters. ApJ 576(2):899–907. https://doi.org/10.1086/341798. arXiv:astro-ph/0201055 [astro-ph]

Portegies Zwart SF, Baumgardt H, Hut P, Makino J, McMillan SLW (2004) Formation of massive black holes through runaway collisions in dense young star clusters. Nature 428(6984):724–726. https://doi.org/10.1038/nature02448. arXiv:astro-ph/0402622 [astro-ph]

Portegies Zwart SF, Belleman RG, Geldof PM (2007) High-performance direct gravitational N-body simulations on graphics processing units. New A 12(8):641–650. https://doi.org/10.1016/j.newast.2007.05.004. arXiv:astro-ph/0702058 [astro-ph]

Portegies Zwart SF, McMillan SLW, Gieles M (2010) Young massive star clusters. ARA&A 48:431–493. https://doi.org/10.1146/annurev-astro-081309-130834. arXiv:1002.1961 [astro-ph.GA]

Preto M, Tremaine S (1999) A class of symplectic integrators with adaptive time step for separable hamiltonian systems. AJ 118(5):2532–2541. https://doi.org/10.1086/301102. arXiv:astro-ph/9906322 [astro-ph]

Preto M, Merritt D, Spurzem R (2004) N-body growth of a Bahcall-Wolf cusp around a black hole. ApJ 613(2):L109–L112. https://doi.org/10.1086/425139. arXiv:astro-ph/0406324 [astro-ph]

Quinlan GD, Tremaine S (1992) On the reliability of gravitational N-body integrations. MNRAS 259 (3):505–518. https://doi.org/10.1093/mnras/259.3.505

Railton AD, Tout CA, Aarseth SJ (2014) Pre-mainsequence stellar evolution in N-body models. PASA 31: e017. https://doi.org/10.1017/pasa.2014.10. arXiv:1402.3323 [astro-ph.SR]

Ramos-Almendares F, Sales LV, Abadi MG, Doppel JE, Muriel H, Peng EW (2020) Simulating the spatial distribution and kinematics of globular clusters within galaxy clusters in illustris. MNRAS 493 (4):5357–5368. https://doi.org/10.1093/mnras/staa551. arXiv:1906.11921 [astro-ph.GA]

Rantala A, Naab T, Springel V (2021) frost: a momentum-conserving CUDA implementation of a hierarchical fourth-order forward symplectic integrator. MNRAS 502(4):5546–5562. https://doi.org/10.1093/mnras/stab057. arXiv:2011.14984 [astro-ph.IM]

Rantala A, Naab T, Rizzuto FP, Mannerkoski M, Partmann C, Lautenschütz K (2023) BIFROST: simulating compact subsystems in star clusters using a hierarchical fourth-order forward symplectic integrator code. MNRAS 522(4):5180–5203. https://doi.org/10.1093/mnras/stad1360

Rasio FA, Tout CA, Lubow SH, Livio M (1996) Tidal decay of close planetary orbits. ApJ 470:1187. https://doi.org/10.1086/177941. arXiv:astro-ph/9605059 [astro-ph]

Rees MJ (1988) Tidal disruption of stars by black holes of 10^6-10^8 solar masses in nearby galaxies. Nature 333(6173):523–528. https://doi.org/10.1038/333523a0

Reina-Campos M, Kruijssen JMD, Pfeffer JL, Bastian N, Crain RA (2019) Formation histories of stars, clusters, and globular clusters in the E-MOSAICS simulations. MNRAS 486(4):5838–5852. https://doi.org/10.1093/mnras/stz1236. arXiv:1905.02217 [astro-ph.GA]

Reitze D, Adhikari RX, Ballmer S, Barish B, Barsotti L, Billingsley G, Brown DA, Chen Y, Coyne D, Eisenstein R, Evans M, Fritschel P, Hall ED, Lazzarini A, Lovelace G, Read J, Sathyaprakash BS, Shoemaker D, Smith J, Torrie C, Vitale S, Weiss R, Wipf C, Zucker M (2019) Cosmic explorer: The u.s. contribution to gravitational-wave astronomy beyond ligo. arXiv:1907.04833 [astro-ph.IM]

Rezzolla L, Barausse E, Dorband EN, Pollney D, Reisswig C et al (2008) Final spin from the coalescence of two black holes. Phys Rev D 78(4):044002. https://doi.org/10.1103/PhysRevD.78.044002. arXiv:0712.3541 [gr-qc]

Rieder S, Ishiyama T, Langelaan P, Makino J, McMillan SLW et al (2013) Evolution of star clusters in a cosmological tidal field. MNRAS 436(4):3695–3706. https://doi.org/10.1093/mnras/stt1848. arXiv:1309.7352 [astro-ph.CO]

Rizzuto FP, Naab T, Spurzem R, Giersz M, Ostriker JP et al (2021) Intermediate mass black hole formation in compact young massive star clusters. MNRAS 501(4):5257–5273. https://doi.org/10.1093/mnras/staa3634. arXiv:2008.09571 [astro-ph.GA]

Rizzuto FP, Naab T, Spurzem R, Arca-Sedda M, Giersz M et al (2022) Black hole mergers in compact star clusters and massive black hole formation beyond the mass gap. MNRAS 512(1):884–898. https://doi.org/10.1093/mnras/stac231. arXiv:2108.11457 [astro-ph.GA]

Rodriguez CL, Kremer K, Chatterjee S, Fragione G, Loeb A et al (2021) The observed rate of binary black hole mergers can be entirely explained by globular clusters. RNAAS 5(1):19. https://doi.org/10.3847/2515-5172/abdf54. arXiv:2101.07793 [astro-ph.HE]

Rodriguez CL, Weatherford NC, Coughlin SC, Amaro Seoane, P, Breivik K, Chatterjee S, Fragione G, Kıroğlu F, Kremer K, Rui NZ, Ye CS, Zevin M, Rasio FA (2021b) CMC-COSMIC: Cluster Monte Carlo Code. Astrophysics Source Code Library, ascl:2108.023. https://ascl.net/2108.023

Rodriguez CL, Weatherford NC, Coughlin SC, Amaro-Seoane P, Breivik K et al (2022) Modeling dense star clusters in the milky way and beyond with the Cluster Monte Carlo Code. ApJS 258(2):22. https://doi.org/10.3847/1538-4365/ac2edf. arXiv:2106.02643 [astro-ph.GA]

Rosenbluth MN, MacDonald WM, Judd DL (1957) Fokker–Planck equation for an inverse-square force. Phys Rev 107(1):1–6. https://doi.org/10.1103/PhysRev.107.1

Ruan WH, Guo ZK, Cai RG, Zhang YZ (2018) Taiji program: gravitational-wave sources. arXiv e-prints https://doi.org/10.48550/arXiv.1807.09495. arXiv:1807.09495 [gr-qc]

Rui NZ, Kremer K, Weatherford NC, Chatterjee S, Rasio FA, Rodriguez CL, Ye CS (2021) Matching globular cluster models to observations. ApJ 912(2):102. https://doi.org/10.3847/1538-4357/abed49. arXiv:2103.05033 [astro-ph.GA]

Ruiter AJ, Ferrario L, Belczynski K, Seitenzahl IR, Crocker RM, Karakas AI (2019) On the formation of neutron stars via accretion-induced collapse in binaries. MNRAS 484(1):698–711. https://doi.org/10.1093/mnras/stz001

Rydberg CE, Zackrisson E, Lundqvist P, Scott P (2013) Detection of isolated population III stars with the James Webb Space Telescope. MNRAS 429(4):3658–3664. https://doi.org/10.1093/mnras/sts653. arXiv:1206.0007 [astro-ph.CO]

Saio H, Nomoto K (1985) Evolution of a merging pair of C + O white dwarfs to form a single neutron star. A&A 150(1):L21–L23

Saio H, Nomoto K (1998) Inward propagation of nuclear-burning shells in merging C–O and He White Dwarfs. ApJ 500(1):388–397. https://doi.org/10.1086/305696. arXiv:astro-ph/9801084 [astro-ph]

Saio H, Nomoto K (2004) Off-center carbon ignition in rapidly rotating. Accreting carbon-oxygen white dwarfs. ApJ 615(1):444–449. https://doi.org/10.1086/423976. arXiv:astro-ph/0401141 [astro-ph]

Salaris M, Cassisi S (2017) Chemical element transport in stellar evolution models. R Soc Open Sci 4 (8):170192. https://doi.org/10.1098/rsos.170192. arXiv:1707.07454 [astro-ph.SR]

Salpeter EE (1955) The luminosity function and stellar evolution. ApJ 121:161. https://doi.org/10.1086/145971

Sana H, Evans CJ (2011) The multiplicity of massive stars. In: Neiner C, Wade G, Meynet G, Peters G (eds) Active OB stars: structure, evolution, mass loss, and critical limits. vol 272. pp 474–485. https://doi.org/10.1017/S1743921311011124. arXiv:1009.4197 [astro-ph.SR]

Sana H, de Mink SE, de Koter A, Langer N, Evans CJ et al (2012) Binary interaction dominates the evolution of massive stars. Sci 337(6093):444. https://doi.org/10.1126/science.1223344. arXiv:1207.6397 [astro-ph.SR]

Sander AAC, Vink JS (2020) On the nature of massive helium star winds and Wolf–Rayet-type mass-loss. MNRAS 499(1):873–892. https://doi.org/10.1093/mnras/staa2712. arXiv:2009.01849 [astro-ph.SR]

Schaller G, Schaerer D, Meynet G, Maeder A (1992) New grids of stellar models from 0.8 to 120 $M_{\odot}$ at $Z = 0.020$ and $Z = 0.001$. A&AS 96:269

Schauer ATP, Drory N, Bromm V (2020) The ultimately large telescope: what kind of facility do we need to detect population III stars? ApJ 904(2):145. https://doi.org/10.3847/1538-4357/abbc0b. arXiv:2007.02946 [astro-ph.GA]

Scheck L, Plewa T, Janka HT, Kifonidis K, Müller E (2004) Pulsar recoil by large-scale anisotropies in supernova explosions. Phys Rev Lett 92(1):011103. https://doi.org/10.1103/PhysRevLett.92.011103. arXiv:astro-ph/0307352 [astro-ph]

Scheck L, Janka HT, Foglizzo T, Kifonidis K (2008) Multidimensional supernova simulations with approximative neutrino transport. II. Convection and the advective-acoustic cycle in the supernova core. A&A 477(3):931–952. https://doi.org/10.1051/0004-6361:20077701. arXiv:0704.3001 [astro-ph]

Schive HY, Chien CH, Wong SK, Tsai YC, Chiueh T (2008) Graphic-card cluster for astrophysics (GraCCA)—performance tests. New Astron 13(6):418–435. https://doi.org/10.1016/j.newast.2007.12.005. arXiv:0707.2991 [astro-ph]

Schneider FRN, Podsiadlowski P, Müller B (2021) Pre-supernova evolution, compact-object masses, and explosion properties of stripped binary stars. A&A 645:A5. https://doi.org/10.1051/0004-6361/202039219. arXiv:2008.08599 [astro-ph.SR]

Schneider J, Amaro-Seoane P, Spurzem R (2011) Higher-order moment models of dense stellar systems: applications to the modelling of the stellar velocity distribution function. MNRAS 410(1):432–454. https://doi.org/10.1111/j.1365-2966.2010.17454.x. arXiv:1006.1365 [astro-ph.GA]

Schödel R, Feldmeier A, Neumayer N, Meyer L, Yelda S (2014) The nuclear cluster of the Milky Way: our primary testbed for the interaction of a dense star cluster with a massive black hole. Class Quantum Grav 31(24):244007. https://doi.org/10.1088/0264-9381/31/24/244007. arXiv:1411.4504 [astro-ph.GA]

Schreiber MR, Zorotovic M, Wijnen TPG (2016) Three in one go: consequential angular momentum loss can solve major problems of CV evolution. MNRAS 455(1):L16–L20. https://doi.org/10.1093/mnrasl/slv144. arXiv:1510.04294 [astro-ph.SR]

Schroder KP, Pols OR, Eggleton PP (1997) A critical test of stellar evolution and convective core 'overshooting' by means of zeta Aurigae systems. MNRAS 285(4):696–710. https://doi.org/10.1093/mnras/285.4.696

Shapiro SL, Lightman AP (1976) The distribution of stars around a massive black hole. Nature 262 (5571):743–745. https://doi.org/10.1038/262743a0

Shapley H (1930) Star clusters, harvard observatory monographs, vol 2. McGraw-Hill, New York

Shapley H, Sawyer HB (1927) Apparent diameters and ellipticities of globular clusters. Harvard College Obs Bull 852:22–26

Shara MM, Hurley JR (2002) Star clusters as type Ia supernova factories. ApJ 571(2):830–842. https://doi.org/10.1086/340062. arXiv:astro-ph/0202179 [astro-ph]

Shu Q, Pang X, Flammini Dotti F, Kouwenhoven MBN, Arca Sedda M, Spurzem R (2021) The long-term evolution of main-sequence binaries in DRAGON simulations. ApJS 253(1):14. https://doi.org/10.3847/1538-4365/abcfb8. arXiv:2011.14911 [astro-ph.SR]

Sicilia A, Lapi A, Boco L, Spera M, Di Carlo UN, Mapelli M, Shankar F, Alexander DM, Bressan A, Danese L (2022) The black hole mass function across cosmic times. I. Stellar black holes and light seed distribution. ApJ 924(2):56. https://doi.org/10.3847/1538-4357/ac34fb. arXiv:2110.15607 [astro-ph.GA]

Siess L, Izzard RG, Davis PJ, Deschamps R (2013) BINSTAR: a new binary stellar evolution code. Tidal interactions. A&A 550:A100. https://doi.org/10.1051/0004-6361/201220327

Sollima A, Baumgardt H, Hilker M (2019) The eye of Gaia on globular clusters kinematics: internal rotation. MNRAS 485(1):1460–1476. https://doi.org/10.1093/mnras/stz505. arXiv:1902.05895 [astro-ph.GA]

Spera M (2014) Using graphics processing units to solve the classical N-body problem in physics and astrophysics. arXiv e-prints arXiv:1411.5234 [astro-ph.IM]

Spera M, Mapelli M (2017) Very massive stars, pair-instability supernovae and intermediate-mass black holes with the SEVN code. MNRAS 470(4):4739–4749. https://doi.org/10.1093/mnras/stx1576. arXiv:1706.06109 [astro-ph.SR]

Spera M, Mapelli M, Bressan A (2015) The mass spectrum of compact remnants from the PARSEC stellar evolution tracks. MNRAS 451(4):4086–4103. https://doi.org/10.1093/mnras/stv1161. arXiv:1505.05201 [astro-ph.SR]

Spera M, Mapelli M, Giacobbo N, Trani AA, Bressan A et al (2019) Merging black hole binaries with the SEVN code. MNRAS 485(1):889–907. https://doi.org/10.1093/mnras/stz359. arXiv:1809.04605 [astro-ph.HE]

Spitzer L Jr, Mathieu RD (1980) Random gravitational encounters and the evolution of spherical systems. VIII—clusters with an initial distribution of binaries. ApJ 241:618–636. https://doi.org/10.1086/158376

Spitzer L Jr, Shull JM (1975) Random gravitational encounters and the evolution of spherical systems. VI. Plummer's model. ApJ 200:339–342. https://doi.org/10.1086/153793

Spitzer L Jr, Shull JM (1975) Random gravitational encounters and the evolution of spherical systems. VII. Systems with several mass groups. ApJ 201:773–782. https://doi.org/10.1086/153943

Spitzer L Jr, Chevalier RA (1973) Random gravitational encounters and the evolution of spherical systems. V. Gravitational shocks. ApJ 183:565–582. https://doi.org/10.1086/152247

Spitzer L Jr, Hart MH (1971) Random gravitational encounters and the evolution of spherical systems. I. Method. ApJ 164:399. https://doi.org/10.1086/150855

Spitzer JL, Hart MH (1971) Random gravitational encounters and the evolution of spherical systems. II. Models. ApJ 166:483. https://doi.org/10.1086/150977
Spitzer L Jr, Shapiro SL (1972) Random gravitational encounters and the evolution of spherical systems. III. Halo. ApJ 173:529. https://doi.org/10.1086/151442
Spitzer L Jr, Thuan TX (1972) Random gravitational encounters and the evolution of spherical systems. IV Isolated systems of identical stars. ApJ 175:31. https://doi.org/10.1086/151537
Spitzer L Jr (1987) Dynamical evolution of globular clusters. Princeton University Press, Princeton
Spruit HC (2002) Dynamo action by differential rotation in a stably stratified stellar interior. A&A 381:923–932. https://doi.org/10.1051/0004-6361:20011465. arXiv:astro-ph/0108207 [astro-ph]
Spurzem R (1991) Gravothermal instability of anisotropic self-gravitating gas spheres: singular equilibrium solution. MNRAS 252:177–189. https://doi.org/10.1093/mnras/252.2.177
Spurzem R (1999) Direct N-body simulations. J Comput Appl Math 109:407–432 arXiv:astro-ph/9906154 [astro-ph]
Spurzem R, Aarseth SJ (1996) Direct collisional simulation of 10,000 particles past core collapse. MNRAS 282:19. https://doi.org/10.1093/mnras/282.1.19. arXiv:astro-ph/9605003 [astro-ph]
Spurzem R, Takahashi K (1995) Comparison between Fokker–Planck and gaseous models of star clusters in the multi-mass case revisited. MNRAS 272(4):772–784. https://doi.org/10.1093/mnras/272.4.772
Spurzem R, Rizzuto F, Arca Sedda M, Kamlah A, Berczik P, Shu Q, Tanikawa A, Naab T (2022) Growth of seed black holes in galactic nuclei. In: Müller M, Peter C, Trautmann A (eds) NIC Symposium 2022. Publication Series of the John von Neumann Institute for Computing (NIC), NIC Series, vol 51, pp 159–172
Stacy A, Bromm V (2013) Constraining the statistics of population III binaries. MNRAS 433(2):1094–1107. https://doi.org/10.1093/mnras/stt789. arXiv:1211.1889 [astro-ph.CO]
Stacy A, Pawlik AH, Bromm V, Loeb A (2012) Effect of population III multiplicity on dark star formation. MNRAS 421(1):894–907. https://doi.org/10.1111/j.1365-2966.2011.20373.x. arXiv:1111.1527 [astro-ph.CO]
Stacy A, Bromm V, Lee AT (2016) Building up the population III initial mass function from cosmological initial conditions. MNRAS 462(2):1307–1328. https://doi.org/10.1093/mnras/stw1728. arXiv:1603.09475 [astro-ph.GA]
Stiefel E, Kustaanheimo P (1965) Perturbation theory of Kepler motion based on spinor regularization. J Reine und Angewandte Math 218:204–219. http://eudml.org/doc/150684
Stodołkiewicz JS (1982) Dynamical evolution of globular clusters. I. Acta Astron 32(1–2):63–91
Stodołkiewicz JS (1986) Dynamical evolution of globular clusters. II. Binaries method. Acta Astron 36 (1):19–41
Šubr L, Kroupa P, Baumgardt H (2008) A new method to create initially mass segregated star clusters in virial equilibrium. MNRAS 385(3):1673–1680. https://doi.org/10.1111/j.1365-2966.2008.12993.x. arXiv:0801.2768 [astro-ph]
Sugimoto D, Bettwieser E (1983) Post-collapse evolution of globular clusters. MNRAS 204:19P-22P. https://doi.org/10.1093/mnras/204.1.19P
Sugimoto D, Chikada Y, Makino J, Ito T, Ebisuzaki T, Umemura M (1990) A special-purpose computer for gravitational many-body problems. Nature 345(6270):33–35. https://doi.org/10.1038/345033a0
Sundman K (1907) Recherches sur le problème des trois corps. Acta Soc Sci Fennicae 34:1–34
Sundman K (1909) Nouvelles recherches sur le problème des trois corps. Acta Soc Sci Fennicae 35:1–27
Sweatman WL (1994) The development of a parallel N-body code for the edinburgh concurrent supercomputer. J Comput Phys 111(1):110–119. https://doi.org/10.1006/jcph.1994.1048
Szebehely V, Peters CF (1967) Complete solution of a general problem of three bodies. AJ 72:876. https://doi.org/10.1086/110355
Szécsi D, Langer N, Yoon SC, Sanyal D, de Mink S, Evans CJ, Dermine T (2015) Low-metallicity massive single stars with rotation. Evolutionary models applicable to I Zwicky 18. A&A 581:A15. https://doi.org/10.1051/0004-6361/201526617. arXiv:1506.09132 [astro-ph.SR]
Szécsi D, Agrawal P, Wünsch R, Langer N (2022) Bonn optimized stellar tracks (BoOST). Simulated populations of massive and very massive stars for astrophysical applications. A&A 658:A125. https://doi.org/10.1051/0004-6361/202141536. arXiv:2004.08203 [astro-ph.SR]
Szölgyen A, Kocsis B (2018) Black hole disks in galactic nuclei. Phys Rev Lett 121(10):101101. https://doi.org/10.1103/PhysRevLett.121.101101. arXiv:1803.07090 [astro-ph.GA]
Szölgyen A, Meiron Y, Kocsis B (2019) Anisotropic mass segregation in rotating globular clusters. ApJ 887(2):123. https://doi.org/10.3847/1538-4357/ab50bb. arXiv:1903.11610 [astro-ph.GA]

Szölgyen A, Máthé G, Kocsis B (2021) Resonant dynamical friction in nuclear star clusters: rapid alignment of an intermediate-mass black hole with a stellar disk. ApJ 919(2):140. https://doi.org/10.3847/1538-4357/ac13ab. arXiv:2103.14042 [astro-ph.GA]

Takahashi K (1995) Fokker–Planck models of star clusters with anisotropic velocity distributions I. Pre-collapse evolution. PASJ 47:561–573 arXiv:astro-ph/9507040 [astro-ph]

Takahashi K (1996) Fokker–Planck models of star clusters with anisotropic velocity distributions II. Post-collapse evolution. PASJ 48:691–700. https://doi.org/10.1093/pasj/48.5.691. arXiv:astro-ph/9609025 [astro-ph]

Takahashi K (1997) Fokker–Planck models of star clusters with anisotropic velocity distributions III. Multi-mass clusters. PASJ 49:547–560. https://doi.org/10.1093/pasj/49.5.547. arXiv:astro-ph/9703190 [astro-ph]

Takahashi K, Yoshida T, Umeda H, Sumiyoshi K, Yamada S (2016) Exact and approximate expressions of energy generation rates and their impact on the explosion properties of pair instability supernovae. MNRAS 456(2):1320–1331. https://doi.org/10.1093/mnras/stv2649. arXiv:1511.03040 [astro-ph.SR]

Takahashi K, Yoshida T, Umeda H (2018) Stellar yields of rotating first stars. II. Pair-instability supernovae and comparison with observations. ApJ 857(2):111. https://doi.org/10.3847/1538-4357/aab95f. arXiv:1803.06630 [astro-ph.SR]

Takahashi K, Sumiyoshi K, Yamada S, Umeda H, Yoshida T (2019) The evolution toward electron capture supernovae: the flame propagation and the pre-bounce electron-neutrino radiation. ApJ 871(2):153. https://doi.org/10.3847/1538-4357/aaf8a8

Tang J, Joyce M (2021) Revised best estimates for the age and mass of the methuselah star HD 140283 using MESA and interferometry and implications for 1D convection. RNAAS 5(5):117. https://doi.org/10.3847/2515-5172/ac01ca. arXiv:2105.11311 [astro-ph.SR]

Tanikawa A, Hut P, Makino J (2012) Unexpected formation modes of the first hard binary in core collapse. New Astron 17(3):272–280. https://doi.org/10.1016/j.newast.2011.09.001. arXiv:1107.3866 [astro-ph.GA]

Tanikawa A, Yoshida T, Kinugawa T, Takahashi K, Umeda H (2020) Fitting formulae for evolution tracks of massive stars under extreme metal-poor environments for population synthesis calculations and star cluster simulations. MNRAS 495(4):4170–4191. https://doi.org/10.1093/mnras/staa1417. arXiv:1906.06641 [astro-ph.HE]

Tanikawa A, Kinugawa T, Yoshida T, Hijikawa K, Umeda H (2021a) Population III binary black holes: effects of convective overshooting on formation of GW190521. MNRAStmp https://doi.org/10.1093/mnras/stab1421. arXiv:2010.07616 [astro-ph.HE]

Tanikawa A, Susa H, Yoshida T, Trani AA, Kinugawa T (2021) Merger rate density of population III Binary black holes below, above, and in the pair-instability mass gap. ApJ 910(1):30. https://doi.org/10.3847/1538-4357/abe40d. arXiv:2008.01890 [astro-ph.HE]

Tauris TM (2015) Maximum speed of hypervelocity stars ejected from binaries. MNRAS 448:L6–L10. https://doi.org/10.1093/mnrasl/slu189. arXiv:1412.0657 [astro-ph.SR]

Tauris TM, Langer N, Moriya TJ, Podsiadlowski P, Yoon SC et al (2013) Ultra-stripped Type Ic supernovae from close binary evolution. ApJ 778(2):L23. https://doi.org/10.1088/2041-8205/778/2/L23. arXiv:1310.6356 [astro-ph.SR]

Tauris TM, Kramer M, Freire PCC, Wex N, Janka HT et al (2017) Formation of double neutron star systems. ApJ 846(2):170. https://doi.org/10.3847/1538-4357/aa7e89. arXiv:1706.09438 [astro-ph.HE]

Team COMPAS, Riley J, Agrawal P, Barrett JW, Boyett KNK, Broekgaarden FS, Chattopadhyay D, Gaebel SM, Gittins F, Hirai R, Howitt G, Justham S, Khandelwal L, Kummer F, Lau MYM, Mandel I, de Mink SE, Neijssel C, Riley T, van Son L, Stevenson S, Vigna-Gomez A, Vinciguerra S, Wagg T, Willcox R (2022) Rapid stellar and binary population synthesis with COMPAS. ApJS 258:34. https://doi.org/10.3847/1538-4365/ac416c. arXiv:2109.10352 [astro-ph.IM]

Thorne KS, Zytkow AN (1977) Stars with degenerate neutron cores. I. Structure of equilibrium models. ApJ 212:832–858. https://doi.org/10.1086/155109

Tiongco M, Collier A, Varri AL (2021) Central dynamics of multimass rotating star clusters. MNRAS 506(3):4488–4498. https://doi.org/10.1093/mnras/stab1968. arXiv:2107.03396 [astro-ph.GA]

Tiongco MA, Vesperini E, Varri AL (2016) Kinematical evolution of tidally limited star clusters: the role of retrograde stellar orbits. MNRAS 461(1):402–411. https://doi.org/10.1093/mnras/stw1341. arXiv:1606.06743 [astro-ph.GA]

Tiongco MA, Vesperini E, Varri AL (2016) Velocity anisotropy in tidally limited star clusters. MNRAS 455(4):3693–3701. https://doi.org/10.1093/mnras/stv2574. arXiv:1511.02236 [astro-ph.GA]

Tiongco MA, Vesperini E, Varri AL (2017) Kinematical evolution of tidally limited star clusters: rotational properties. MNRAS 469(1):683–692. https://doi.org/10.1093/mnras/stx853. arXiv:1704.05918 [astro-ph.GA]

Tiongco MA, Vesperini E, Varri AL (2018) The complex kinematics of rotating star clusters in a tidal field. MNRAS 475(1):L86–L90. https://doi.org/10.1093/mnrasl/sly009. arXiv:1801.06236 [astro-ph.GA]

Tiongco MA, Vesperini E, Varri AL (2019) Kinematical evolution of multiple stellar populations in star clusters. MNRAS 487(4):5535–5548. https://doi.org/10.1093/mnras/stz1595. arXiv:1907.05901 [astro-ph.GA]

Tiongco MA, Vesperini E, Varri AL (2022) Early dynamical evolution of rotating star clusters in a tidal field. MNRAS 512(2):1584–1597. https://doi.org/10.1093/mnras/stac643. arXiv:2203.04330 [astro-ph.GA]

Torniamenti S, Bertin G, Bianchini P (2019) A simple two-component description of energy equipartition and mass segregation for anisotropic globular clusters. A&A 632:A67. https://doi.org/10.1051/0004-6361/201935878. arXiv:1909.13093 [astro-ph.GA]

Torniamenti S, Rastello S, Mapelli M, Di Carlo UN, Ballone A, Pasquato M (2022) Dynamics of binary black holes in young star clusters: the impact of cluster mass and long-term evolution. MNRAS 517 (2):2953–2965. https://doi.org/10.1093/mnras/stac2841. arXiv:2203.08163 [astro-ph.GA]

Tout CA (2008) Binary Stars. In: Aarseth SJ, Tout CA, Mardling RA (eds) The Cambridge N-body lectures. Lecture Notes in Physics, vol 760. Springer, Berlin, p 297. https://doi.org/10.1007/978-1-4020-8431-7_11

Tout CA, Aarseth SJ, Pols OR, Eggleton PP (1997) Rapid binary star evolution for N-body simulations and population synthesis. MNRAS 291(4):732–748. https://doi.org/10.1093/mnras/291.4.732

Tout CA, Wickramasinghe DT, Liebert J, Ferrario L, Pringle JE (2008) Binary star origin of high field magnetic white dwarfs. MNRAS 387(2):897–901. https://doi.org/10.1111/j.1365-2966.2008.13291.x. arXiv:0805.0115 [astro-ph]

Trabucchi M, Wood PR, Montalbán J, Marigo P, Pastorelli G, Girardi L (2019) Modelling long-period variables— I. A new grid of O-rich and C-rich pulsation models. MNRAS 482(1):929–949. https://doi.org/10.1093/mnras/sty2745. arXiv:1810.05655 [astro-ph.SR]

Trani AA, Rieder S, Tanikawa A, Iorio G, Martini R, Karelin G, Glanz H, Portegies Zwart S (2022) Revisiting the common envelope evolution in binary stars: a new semianalytic model for N -body and population synthesis codes. Phys Rev D 106(4):043014. https://doi.org/10.1103/PhysRevD.106.043014. arXiv:2205.13537 [astro-ph.SR]

van Meter JR, Miller MC, Baker JG, Boggs WD, Kelly BJ (2010) Test of a general formula for black hole gravitational wave kicks. ApJ 719(2):1427–1432. https://doi.org/10.1088/0004-637X/719/2/1427. arXiv:1003.3865 [astro-ph.HE]

Vanzella E, Calura F, Meneghetti M, Mercurio A, Castellano M, Caminha GB, Balestra I, Rosati P, Tozzi P, De Barros S, Grazian A, D'Ercole A, Ciotti L, Caputi K, Grillo C, Merlin E, Pentericci L, Fontana A, Cristiani S, Coe D (2017) Paving the way for the JWST: witnessing globular cluster formation at $z > 3$. MNRAS 467(4):4304–4321. https://doi.org/10.1093/mnras/stx351. arXiv:1612.01526 [astro-ph.GA]

Vanzella E, Calura F, Meneghetti M, Castellano M, Caminha GB, Mercurio A, Cupani G, Rosati P, Grillo C, Gilli R, Mignoli M, Fiorentino G, Arcidiacono C, Lombini M, Cortecchia F (2019) Massive star cluster formation under the microscope at $z = 6$. MNRAS 483(3):3618–3635. https://doi.org/10.1093/mnras/sty3311. arXiv:1809.02617 [astro-ph.GA]

Vanzella E, Meneghetti M, Caminha GB, Castellano M, Calura F, Rosati P, Grillo C, Dijkstra M, Gronke M, Sani E, Mercurio A, Tozzi P, Nonino M, Cristiani S, Mignoli M, Pentericci L, Gilli R, Treu T, Caputi K, Cupani G, Fontana A, Grazian A, Balestra I (2020) Candidate Population III stellar complex at $z = 6.629$ in the MUSE Deep Lensed Field. MNRAS 494(1):L81–L85. https://doi.org/10.1093/mnrasl/slaa041. arXiv:2001.03619 [astro-ph.GA]

Vanzella E, Adamo A, Annibali F, Annunziatella M, Bartosch Caminha G, Bergamini P, Calura F, Caputi K, Castellano M, Comastri A, Dickinson M, Gilli R, Grillo C, Gronke M, Gruppioni C, Meneghetti M, Mercurio A, Mignoli M, Nonino M, Ravindranath S, Ricotti M, Rosati P, Sani E (2021) Constraining the nature of the first stellar complexes: globular cluster precursors and Population III stellar clusters at $z \sim 6-7$. JWST Proposal 1908. https://www.stsci.edu/cgi-bin/get-proposal-info?observatory=JWST &id=1908

Varri AL, Bertin G (2012) Self-consistent models of quasi-relaxed rotating stellar systems. A&A 540:A94. https://doi.org/10.1051/0004-6361/201118300. arXiv:1201.1899 [astro-ph.GA]

Varri AL, Cai MX, Concha-Ramírez F, Dinnbier F, Lützgendorf N, Pavlík V, Rastello S, Sollima A, Wang L, Zocchi A (2018) A MODEST review. Comput Astrophys Cosmol 5(1):2. https://doi.org/10.1186/s40668-018-0024-6. arXiv:1810.07532 [astro-ph.GA]

Vasiliev E (2015) A new Monte Carlo method for dynamical evolution of non-spherical stellar systems. MNRAS 446(3):3150–3161. https://doi.org/10.1093/mnras/stu2360. arXiv:1411.1757 [astro-ph.GA]

Vink JS (2021) Theory and diagnostics of hot star mass loss. arXiv e-prints arXiv:2109.08164 [astro-ph.SR]

von Hoerner S (1960) Die numerische integration des n-Körper-Problemes für Sternhaufen, I. ZAp 50:184–214

von Hoerner S (1963) Die numerische integration des n-Körper-Problems für Sternhaufen, II. ZAp 57:47–82

von Hoerner S (2001) How it All started. In: Deiters S, Fuchs B, Just A, Spurzem R, Wielen R (eds) Dynamics of star clusters and the milky way. Astronomical Society of the Pacific Conference Series, vol 228. p 11

Wang J, Merritt D (2004) Revised rates of stellar disruption in galactic nuclei. ApJ 600(1):149–161. https://doi.org/10.1086/379767. arXiv:astro-ph/0305493 [astro-ph]

Wang L, Hernandez DM (2021) On the reliability of simulations of collisional stellar systems. arXiv e-prints arXiv:2104.10843 [astro-ph.SR]

Wang L, Spurzem R, Aarseth S, Nitadori K, Berczik P et al (2015) NBODY6++GPU: ready for the gravitational million-body problem. MNRAS 450(4):4070–4080. https://doi.org/10.1093/mnras/stv817. arXiv:1504.03687 [astro-ph.IM]

Wang L, Spurzem R, Aarseth S, Giersz M, Askar A et al (2016) The DRAGON simulations: globular cluster evolution with a million stars. MNRAS 458(2):1450–1465. https://doi.org/10.1093/mnras/stw274. arXiv:1602.00759 [astro-ph.SR]

Wang L, Iwasawa M, Nitadori K, Makino J (2020) PETAR: a high-performance N-body code for modelling massive collisional stellar systems. MNRAS 497(1):536–555. https://doi.org/10.1093/mnras/staa1915. arXiv:2006.16560 [astro-ph.IM]

Wang L, Kroupa P, Takahashi K, Jerabkova T (2020) The possible role of stellar mergers for the formation of multiple stellar populations in globular clusters. MNRAS 491(1):440–454. https://doi.org/10.1093/mnras/stz3033. arXiv:1910.14040 [astro-ph.SR]

Wang L, Nitadori K, Makino J (2020) A slow-down time-transformed symplectic integrator for solving the few-body problem. MNRAS 493(3):3398–3411. https://doi.org/10.1093/mnras/staa480. arXiv:2002.07938 [astro-ph.EP]

Wang L, Tanikawa A, Fujii MS (2022) The impact of primordial binary on the dynamical evolution of intermediate massive star clusters. MNRAS 509(4):4713–4722. https://doi.org/10.1093/mnras/stab3255. arXiv:2110.15555 [astro-ph.GA]

Webbink RF (1984) Double white dwarfs as progenitors of R Coronae Borealis stars and type I supernovae. ApJ 277:355–360. https://doi.org/10.1086/161701

Webbink RF (1985) Stellar evolution and binaries. In: Pringle JE, Wade RA (eds) Interacting binary stars. Cambridge University Press, p 39

Webbink RF (2003) Contact binaries. In: Turcotte S, Keller SC, Cavallo RM (eds) 3D stellar evolution. Astronomical Society of the Pacific Conference Series, vol 293. p 76. arXiv:astro-ph/0304420 [astro-ph]

White RE, Shawl SJ (1987) Axial ratios and orientations for 100 galactic globular star clusters. ApJ 317:246. https://doi.org/10.1086/165273

Willems B, Henninger M, Levin T, Ivanova N, Kalogera V, McGhee K, Timmes FX, Fryer CL (2005) Understanding compact object formation and natal Kicks. I. Calculation methods and the case of GRO J1655-40. ApJ 625(1):324–346. https://doi.org/10.1086/429557. arXiv:astro-ph/0411423 [astro-ph]

Wilson CP (1975) Dynamical models of elliptical galaxies. AJ 80:175–187. https://doi.org/10.1086/111729

Wisdom J, Holman M (1991) Symplectic maps for the N-body problem. AJ 102:1528–1538. https://doi.org/10.1086/115978

Wong TW, Valsecchi F, Fragos T, Kalogera V (2012) Understanding compact object formation and natal kicks. III. The case of Cygnus X-1. ApJ 747(2):111. https://doi.org/10.1088/0004-637X/747/2/111. arXiv:1107.5585 [astro-ph.HE]

Wong TW, Valsecchi F, Ansari A, Fragos T, Glebbeek E, Kalogera V, McClintock J (2014) Understanding compact object formation and natal kicks. IV. The case of IC 10 X-1. ApJ 790(2):119. https://doi.org/10.1088/0004-637X/790/2/119. arXiv:1304.3756 [astro-ph.HE]

Woosley SE (2017) Pulsational pair-instability supernovae. ApJ 836(2):244. https://doi.org/10.3847/1538-4357/836/2/244. arXiv:1608.08939 [astro-ph.HE]
Woosley SE, Heger A (2021) The pair-instability mass gap for black holes. ApJ 912(2):L31. https://doi.org/10.3847/2041-8213/abf2c4. arXiv:2103.07933 [astro-ph.SR]
Ye CS, Kremer K, Rodriguez CL, Rui NZ, Weatherford NC, Chatterjee S, Fragione G, Rasio FA (2022) Compact object modeling in the globular cluster 47 tucanae. ApJ 931(2):84. https://doi.org/10.3847/1538-4357/ac5b0b. arXiv:2110.05495 [astro-ph.HE]
Yoon SC, Langer N, Norman C (2006) Single star progenitors of long gamma-ray bursts. Nuovo Cimento B 121(12):1631–1632. https://doi.org/10.1393/ncb/i2007-10344-4
Yoon SC, Dierks A, Langer N (2012) Evolution of massive population III stars with rotation and magnetic fields. A&A 542:A113. https://doi.org/10.1051/0004-6361/201117769. arXiv:1201.2364 [astro-ph.SR]
Yoshida T, Umeda H, Maeda K, Ishii T (2016) Mass ejection by pulsational pair instability in very massive stars and implications for luminous supernovae. MNRAS 457(1):351–361. https://doi.org/10.1093/mnras/stv3002. arXiv:1511.01695 [astro-ph.SR]
Yoshida T, Takiwaki T, Kotake K, Takahashi K, Nakamura K et al (2019) One-, two-, and three-dimensional simulations of oxygen-shell burning just before the core collapse of massive stars. ApJ 881(1):16. https://doi.org/10.3847/1538-4357/ab2b9d. arXiv:1903.07811 [astro-ph.SR]
Zahn JP (1970) Forced oscillations in close binaries. The adiabatic approximation. A&A 4:452
Zahn JP (1974) Rotational instabilities and stellar evolution. In: Ledoux P, Noels A, Rodgers AW (eds) Stellar instability and evolution. IAU Symposium, vol 59. p 185. https://doi.org/10.1017/S0074180900237492
Zahn JP (1975) The dynamical tide in close binaries. A&A 41:329–344
Zahn JP (1977) Tidal friction in close binary stars. A&A 500:121–132
Zahn JP (1989) Tidal evolution of close binary stars. I—Revisiting the theory of the equilibrium tide. A&A 220(1–2):112–116
Zahn JP (1991) Convective penetration in stellar interiors. A&A 252:179–188
Zahn JP (1992) Circulation and turbulence in rotating stars. A&A 265:115–132
Zhong S, Berczik P, Spurzem R (2014) Super massive black hole in galactic nuclei with tidal disruption of stars. ApJ 792(2):137. https://doi.org/10.1088/0004-637X/792/2/137. arXiv:1407.3537 [astro-ph.GA]
Zhong S, Berczik P, Spurzem R (2015) Supermassive black holes in galactic nuclei with tidal disruption of stars. II. Axisymmetric nuclei. ApJ 811(1):22. https://doi.org/10.1088/0004-637X/811/1/22. arXiv:1508.02838 [astro-ph.GA]
Zhong S, Li S, Berczik P, Spurzem R (2022) Revisit the rate of tidal disruption events: the role of the partial tidal disruption event. ApJ 933(1):96. https://doi.org/10.3847/1538-4357/ac71ad. arXiv:2205.09945 [astro-ph.GA]
Zorotovic M, Schreiber MR, Parsons SG, Gänsicke BT, Hardy A et al (2016) Detached cataclysmic variables are crossing the orbital period gap. MNRAS 457(4):3867–3877. https://doi.org/10.1093/mnras/stw246. arXiv:1601.07785 [astro-ph.SR]